

Wnt Regulation in Cystic Kidney Diseases:  
Roles for Jade-1, NPHP4, and CK1 $\alpha$

Inaugural-Dissertation  
zur  
Erlangung des Doktorgrades  
der Mathematisch-Naturwissenschaftlichen Fakultät

vorgelegt von

Lori Borgal  
aus Halifax (Canada)

Berichtersteller: Prof. Dr. Michael Melkonian  
(Gutachter) Prof. Dr. Thomas Benzing

Tag der mündlichen Prüfung: 15 Jan. 2013

**TABLE OF CONTENTS**

<b>Table of Contents</b> .....	I
<b>List of Figures</b> .....	III
<b>List of Tables</b> .....	IV
<b>Abbreviations</b> .....	V
<b>1 ABSTRACT</b> .....	1
<b>2 ZUSAMMENFASSUNG</b> .....	2
<b>3 INTRODUCTION</b> .....	3
3.1 Cystic Kidney Disease.....	3
3.1.1 Nephronophthisis.....	3
3.1.2 Ciliopathies.....	6
3.2 The Primary Cilium.....	7
3.2.1 Ciliary Communication with the Cell – the “Ciliary Pore Complex”.....	9
3.2.2 Nephrocystin proteins at the ciliary pore complex.....	13
3.3 The role of primary cilia as signaling pathway platforms.....	14
3.3.1 The Wnt signaling pathway and kidney cyst formation.....	17
3.3.2 The Wnt signaling pathway and the role of cilia & NPH proteins.....	20
<b>4 THESIS AIMS</b> .....	22
<b>5 MATERIALS AND METHODS</b> .....	23
5.1 Materials.....	23
5.1.1 Chemical Reagents.....	23
5.1.2 Assays/Kits.....	25
5.1.3 Antibodies.....	25
5.1.4 Enzymes.....	26
5.1.5 Genes of Interest.....	27
5.1.6 Plasmids and their providers.....	27
5.1.7 Oligonucleotides.....	28
5.1.8 Buffers & Solutions.....	30
5.1.9 Materials.....	32
5.1.10 Equipment.....	34
5.1.11 Software.....	35
5.2 Methods.....	36
5.2.1 Plasmids & siRNA.....	36
5.2.2 Clone Selection and Plasmid Amplification.....	38
5.2.3 Cell Culture.....	41

---

5.2.4	Biochemistry/ Molecular Biology .....	43
5.2.5	Zebrafish .....	48
5.2.6	Mass Spectrometry .....	49
5.2.7	Statistics .....	49
6	<b>RESULTS</b> .....	51
6.1	Jade-1 is a dynamic protein that co-localizes with neprocystins at the transition zone.....	51
6.2	Jade-1 interacts with the neprocystin protein complex. ....	55
6.3	Overexpressed NPHP4 facilitates nuclear translocation of Jade-1 in a phosphorylation-dependent manner.....	57
6.4	NPHP4 and Jade-1 additively reduce canonical Wnt signaling .....	62
6.5	Genetic interaction of NPHP4 and Jade-1 in zebrafish embryos. ....	64
6.6	Classical $\beta$ -catenin kinase CK1 $\alpha$ phosphorylates Jade-1, abolishing negative Wnt regulation.....	65
6.7	Perspectives: CK1-mediated phosphorylation of Jade-1 by PLK1. ....	72
7	<b>DISCUSSION</b> .....	74
7.1	Jade-1 is a novel member of the neprocystin protein complex at the ciliary region .....	74
7.2	NPHP4 increases nuclear translocation of Jade-1 in a phosphorylation dependent manner .....	75
7.3	NPHP4 and Jade-1 additively regulate canonical Wnt signaling .....	77
7.4	Phosphorylation of Jade-1 by CK1 $\alpha$ abrogates negative Wnt regulation.....	78
7.4.1	CK1 $\alpha$ phosphorylates Jade-1 and $\beta$ -catenin using the same motif.....	78
7.4.2	Exogenous $\beta$ -catenin causes CK1 $\alpha$ and Jade-1 degradation at different thresholds ...	80
7.5	Requirement and regulation of Wnt/ $\beta$ -catenin signaling in the adult kidney: possible roles for Jade-1 and neprocystin proteins.....	81
7.5.1	Wnt signaling defects during development do not explain cyst formation in NPH ....	81
7.5.2	The Wnt signaling pathways are required for injury repair .....	82
7.5.3	Different mechanisms of canonical Wnt activation during injury repair and development: roles for cystoproteins at the primary cilium and cell-to-cell contacts .....	83
7.5.4	Re-establishing polarity after injury: roles for cystoproteins and the primary cilium.....	85
7.6	Conclusion.....	87
8	<b>PUBLICATIONS</b> .....	89
8.1	Publications in Academic Journals.....	89
8.2	Publications in International Academic Conferences.....	89
10	<b>ACKNOWLEDGEMENTS</b> .....	111
11	<b>ERKLÄRUNG</b> .....	112
12	<b>CURRICULUM VITAE</b> .....	113

**LIST OF FIGURES**

Figure 1. Healthy and polycystic kidneys. ....	5
Figure 2. The primary cilium. ....	10
Figure 3. Wnt signaling pathways. ....	19
Figure 4. Jade-1 is a dynamic protein that localizes to the nucleus, cytoplasm, and centrosome in ciliated RPE-1 cells. ....	52
Figure 5. Confirmation of centrosomal Jade-1 localization. ....	53
Figure 6. Jade-1 localizes to the ciliary base independently of the microtubule network. ....	54
Figure 7. Jade-1 co-localizes with NPHP1 at the transition zone of primary cilia. ....	55
Figure 8. Jade-1 interacts with the canonical Wnt negative regulating NPH protein complex. ....	56
Figure 9. Confirmation of the interaction between Jade-1 and NPHP4. ....	57
Figure 10. Endogenous Jade-1 co-localizes with endogenous NPHP4. ....	58
Figure 11. NPHP4 stabilizes Jade-1 by protecting the protein from degradation. ....	59
Figure 12. NPHP4 increases nuclear translocation of Jade-1 in a phosphorylation-dependent manner. ....	61
Figure 13. NPHP4 and Jade-1 additively reduce canonical Wnt activity in a mutually dependent fashion. ....	63
Figure 14. Genetic interaction of Jade-1 and NPHP4 in the developing zebrafish embryo. ....	65
Figure 15. F.CK1 $\alpha$ increases the expression size of V5.Jade-1 and abolishes repression of canonical Wnt reporter. ....	66
Figure 16. The Jade-1 N-terminus is regulated by both CK1 $\alpha$ and NPHP4. ....	68
Figure 17. Point mutation of V5.Jade-1 at S18 alters the influence of CK1 $\alpha$ but not NPHP4. ....	70
Figure 18. Increased expression of F. $\beta$ -catenin reduces protein levels of V5.Jade and F.CK1 $\alpha$ at different thresholds. ....	71
Figure 19. Jade-1 is phosphorylated in the presence of CK1 on a PLK1-like motif. ....	73

**LIST OF TABLES**

Table 1. List of Chemicals, Reagents and Solutions .....	23
Table 2. List of Assays/Kits .....	25
Table 3. List of primary antibodies and their providers .....	25
Table 4. List of secondary antibodies and their providers.....	26
Table 5. List of enzymes and their providers .....	26
Table 6. Genes and isoforms investigated.....	27
Table 7. List of plasmids used and their providers.....	27
Table 8. List of oligonucleotides used.....	28
Table 9. Composition of buffers & solutions .....	30
Table 10. List of materials and their providers.....	32
Table 11. List of equipment and their providers .....	34

**ABBREVIATIONS**

μl	Microliter
μM	Micromolar
5HT	5-hydroxytryptamine
ADPKD	Autosomal dominant polycystic kidney disease
AKT	Ak thymoma
AMP	Adenosine monophosphate
ANOVA	Analysis of variance
APC	Adenomatous polyposis coli
APS	Ammonium persulfate
ARPKD	Autosomal recessive polycystic kidney disease
ATP	Adenosine triphosphate
β-TrCP	beta-transducin repeat containing E3 ubiquitin protein ligase
BBS	Bardet-Biedl syndrome
BSA	Bovine serum albumin
Ca <sup>2+</sup>	Calcium ion
CaCl <sub>2</sub>	Calcium chloride
CamKII	Cam Kinase II
cAMP	Cyclic adenosine monophosphate
cDNA	Complementary DNA
CE	Convergent extension
CECAD	Cologne Cluster of Excellence in Cellular Stress Responses in Aging-associated Diseases
CEP	Centrosomal protein
CID	Collision-induced dissociation
CK1	Casein kinase 1
CLS	Ciliary localization sequence
CMV	Cytomegalovirus
Co	Control
COPI	Coat protein I
CPC	Ciliary pore complex
Cyt	Cytosolic fraction
DAG	Diacylglycerol
DAPI	4',6-diamidino-2-phenylindole
DIC	Differential interference contrast
DMEM	Dulbecco's modified Eagle's medium

---

DMSO	Dimethyl sulfoxide
DNA	Deoxyribonucleic acid
dNTP	Deoxyribonucleotide triphosphate
Dsh	Dishevelled
DTT	Dithiothreitol
ECL	Enhanced chemiluminescence
EDTA	Ethylenediaminetetraacetic acid
EPS	Epidermal growth factor receptor pathway substrate
ERK	Extracellular signal-regulated kinase
ESRD	End stage renal disease
F	Flag
FBS	Fetal bovine serum
Fz	Frizzled receptor
g	Standard gravity
G	Glomerulum
G0	Gap 0 phase
G1	Gap 1 phase
G2	Gap 2 phase
GFP	Green fluorescent protein
GSK3 $\beta$	Glycogen-synthase-kinase-3 $\beta$
GTP	Guanosine-5'-triphosphate
h	Human
HC	Heavy chain
HDAC	Histone deacetylase
HEBS	HEPES-buffered saline solution
HEK	Human embryonic kidney
HEPES	4-(2-hydroxyethyl)-1-piperazineethanesulfonic acid
HGF	Hepatocyte growth factor
Hh	Hedgehog
HIS	Histidine-tag
hpf	Hours post fertilization
HPRT1	Hypoxanthine phosphoribosyltransferase 1
hr	Hour
HRP	Horseradish peroxidase
hTERT	Human telomerase reverse transcriptase
IB	Immunoblot
IFT	Intraflagellar transport

---

IgG	Immunoglobulin G
INPP5E	Inositol polyphosphate-5-phosphatase E
INVS	Inversin
IP	Immunoprecipitation
Jade-1	Gene for apoptosis and differentiation in epithelia
Jbn	Joubertin
JBTS	Joubert syndrome
JNK	c-Jun N-terminal kinase
K <sup>+</sup>	Potassium ion
kb	Kilobase
KCl	Potassium chloride
kDa	Kilodalton
KIF	Kinesin Family
LB Medium	Lysogeny broth
LC-MS	Liquid chromatography–mass spectrometry
LEF-1	Lymphoid enhancer-binding factor-1
LRP	Low density lipoprotein receptor-related protein
M	Mitosis
MAPK	Mitogen-activated protein kinases
MDCK	Madin-Darby canine kidney
MEK	Mitogen-activated protein kinase kinase
MgSO <sub>4</sub>	Magnesium sulfate
MKS	Meckel-Gruber syndrome
ml	Milliliter
mM	Millimolar
MO	Morpholino
mRNA	Messenger RNA
MS	Mass spectrometry
mTOR	Mammalian target of rapamycin
Na <sup>+</sup>	Sodium ion
NaCl	Sodium chloride
NCBI	National Center for Biotechnology Information
Nde1	NudE nuclear distribution E homolog 1
NEB	New England BioLabs
Nek2	NIMA (never in mitosis gene a)-related kinase 2
NLS	Nuclear Localization Sequence
NPC	Nuclear Pore Complex

---

NPH	Nephronophthisis
NPHP	Nephrocystin
NPHPL1	NPHP-like 1
Nuc	Nuclear fraction
OA	Okadaic acid
OCD	Oriented cell division
Ofd1	Oral-facial-digital syndrome 1
PAGE	Polyacrylamide gel electrophoresis
PBD	Polobox-domain
PBS	Phosphate-buffered saline
PCMD	Periciliary membrane domain
PCP	Planar cell polarity
PCR	Polymerase chain reaction
PD	Pronephric duct
PDGF	Platelet-derived growth factor
PDGFR	Platelet-derived growth factor receptor
PFA	Paraformaldehyde
PHF17	Plant homeo domain finger protein 17
PI <sub>3</sub> K	Phosphatidylinositol 3-kinases
PKC	Protein Kinase C
PKD	Polycystic kidney disease
PLC	Phospholipase C
PLK1	Polo-like kinase 1
PMSF	Phenylmethylsulfonyl fluoride
PT	Pronephric tubule
Ptc	Patched
p Value	Probability
pVHL	Von-Hippel-Lindau protein
RLU	Relative luciferase units
RNA	Ribonucleic acid
RPE	Retinal pigment epithelium
RPGR	Retinitis pigmentosa GTPase regulator
SDS	Sodium dodecyl sulfate
SE	Standard error (of the mean)
SEM	Scanning electron microscopy
Shh	Sonic hedgehog
siRNA	Small interfering RNA

---

Smo	Smoothened
SOC	Super optimal broth medium
SV-40	Simian vacuolating virus 40
T2R	Taste Receptor
TAE	Tris-acetate-EDTA
TAZ	Transcriptional coactivator with PDZ-binding motif
Tcf	T cell factor
TEM	Transmission electron microscopy
TEMED	N,N,N',N'-tetramethylethylenediamine
T <sub>m</sub>	Melting temperature
Tris	Tris(hydroxymethyl)aminomethane
TZ	Transition Zone
U	Units
UTR	Untranslated region
UV	Ultraviolet
V	Volts
VHL	Von-Hippel-Lindau
WCL	Whole cell lysate
Wnt	Wingless/Int1
WT	Wild-type
% (v/v)	Volume concentration
% (w/v)	Mass concentration

## 1 ABSTRACT

**Background:** Nephronophthisis (NPH) is the leading genetic cause of end-stage renal disease in children, with patients requiring dialysis or kidney transplantation by an average age of 13. Major hallmarks of this disease include interstitial fibrosis, tubular basement membrane disruption, and cyst progression along the cortico-medullary boundary of the kidney. Currently it is not possible to slow or reverse disease progression, and together with other inherited cystic kidney diseases the lack of therapeutic options represents a significant burden for patients and on health care systems. The last decade of research has highlighted the importance of an antenna-like organelle called the primary cilium which is present on virtually all mammalian cells. In the kidney, primary cilia project from the apical surface of kidney epithelial cells into the tubule lumen and are thought to be important for inter-cellular communication required for tissue maintenance. Specifically, primary cilia are involved in the regulation of the Wnt signaling pathway, which is activated during normal injury repair. This work explores the relationship between the gene products mutated in NPH, which localize to the primary cilium, and the regulation of the canonical Wnt signaling pathway by Jade-1, a recently identified ubiquitin ligase for the main effector of canonical Wnt signaling,  $\beta$ -catenin.

**Main Findings and Conclusions:** This work demonstrates that Jade-1 localizes to the ciliary transition zone and interacts with members of the NPH protein complex. Nephrocystin-4 (NPHP4) specifically stabilizes protein levels of Jade-1 in a phosphatase-dependent manner, which increases Jade-1 nuclear translocation and enhances the ability of Jade-1 to negatively regulate canonical Wnt signaling. Jade-1 is phosphorylated by casein kinase-1  $\alpha$  (CK1 $\alpha$ ), a member of the  $\beta$ -catenin destruction complex, and this abrogates the ability of Jade-1 to negatively regulate Wnt signaling. Exogenous  $\beta$ -catenin decreases protein levels of CK1 $\alpha$  and Jade-1 but not NPHP4, which highlights a complex relationship between these proteins. The non-linear nature of Wnt signaling regulation underlines the importance of studying functional protein-protein relationships in context dependent manner. Within the context of published literature, the current data suggests that the cooperative action of NPHP4 and Jade-1 might be most crucial to re-establish noncanonical Wnt signaling immediately following injury repair. Failure of this pathway could contribute to cyst formation in NPH.

## 2 ZUSAMMENFASSUNG

Hintergrund: Die Nephronophthise (NPH) gilt als die häufigste genetische Ursache für eine terminale Niereninsuffizienz bei Kindern. Dabei kann bereits durchschnittlich im Alter von 13 Jahren eine Nierenersatztherapie, Dialyse oder Nierentransplantation, erforderlich werden. Histopathologisch ist die NPH durch eine interstitielle Fibrose, Veränderungen der tubulären Basalmembran und eine tubuläre Atrophie mit Zystenentwicklung entlang des kortiko-medullären Übergangs gekennzeichnet. Bisher ist es weder möglich, den Krankheitsverlauf zu verlangsamen, noch aufzuhalten. Das Fehlen therapeutischer Optionen zur Behandlung der NPH und weiterer erblicher zystischer Nierenerkrankungen führt zu einer signifikanten Herausforderung für das Gesundheitssystem. Zahlreiche Studien der letzten Jahre konnten zeigen, dass in der Pathogenese der NPH und anderer zystischer Nierenerkrankungen primäre Zilien eine zentrale Rolle spielen. Zilien sind antennenartige Organellen, die von der Zelloberfläche ausgehen und auf fast allen Säugerzellen zu finden sind. In der Niere ragen diese primären Zilien von der apikalen Oberfläche der Nierenepithelzellen in das tubuläre Lumen hinein und sind in als sensorische Organellen in wichtige Signalübertragungsprozesse involviert. Ein wichtiger Signalweg, der durch Zilien moduliert wird, ist die Wnt-Signalkaskade, die insbesondere während der Nierenentwicklung und bei Reparaturvorgängen nach Gewebeschädigung von großer Bedeutung ist. Wichtigster Effektor der Wnt-Signalkaskade dabei ist  $\beta$ -catenin, das wiederum von Jade-1, einer kürzlich identifizierten Ubiquitinligase, reguliert wird. Die hier vorliegende Arbeit untersucht das Zusammenspiel zwischen ziliären Proteinen und bekannten NPH-Genen bei der Regulation des kanonischen Wnt-Signalwegs durch die Ubiquitinligase Jade-1 und dessen Rolle in der Pathogenese der NPH.

Hauptaussagen und Zusammenfassung: Die vorliegende Arbeit konnte zeigen, dass Jade-1 an die ziliäre Transitionszone lokalisiert und dort mit Komponenten des NPH-Proteinkomplexes interagiert. NPHP4 stabilisiert in Abhängigkeit von Phosphatasen spezifisch die Expression von Jade-1. Dies wiederum führt dazu, dass Jade-1 verstärkt in den Nukleus transloziert und so die negative Regulation des Wnt-Signalwegs durch Jade-1 verstärkt wird. Die Phosphorylierung von Jade-1 erfolgt durch CK1 $\alpha$ , einer Hauptkomponente des  $\beta$ -catenin-Degradationskomplexes. Sie verhindert, dass Jade-1 negativ auf die Wnt-Signalkaskade einwirken kann. Die Tatsache, dass exogen zugeführtes  $\beta$ -catenin zu einer Verminderung der CK1 $\alpha$  und Jade-1 aber nicht der NPHP4-Proteinmenge führt, lässt auf ein komplexes Zusammenspiel dieser Proteine schließen, das möglicherweise während der epithelialen Zellteilung in Heilungsprozessen zeitlich präzise reguliert wird. Im Einklang mit der publizierten Literatur deuten die hier präsentierten Daten darauf hin, dass das kooperative Wirken von NPHP4 und Jade-1 womöglich eine entscheidende Rolle dabei spielt, nach einem Gewebe- oder Zellschaden nicht-kanonische Wnt-Signalkaskaden zu reaktivieren. Ein Ausfall dieser NPHP4-Jade1 Signaltransduktions-Achse könnte zur Zystenbildung beitragen.

### 3 INTRODUCTION

#### 3.1 Cystic Kidney Disease

More than 12.5 million people worldwide currently suffer from cystic kidney disease, which is characterized by fluid-filled cysts arising from tubular epithelial cells of the renal nephron that ultimately impair renal function (1; Fig 1). Currently, there are no approved drug treatments or preventive strategies available. As most patients ultimately reach end stage renal disease (ESRD) and require dialysis or kidney transplantation, these diseases continue to present a major challenge for the health care system. Cystic kidney diseases are most often hereditary although acquired forms may arise sporadically during development or aging, and can sometimes result as a consequence of dialysis or pharmacological treatments (2). Hereditary (poly-) cystic kidney diseases are caused by germline mutations in single genes and are inherited as Mendelian traits. Age of onset, symptom severity, disease progression, the renal phenotype and extra-renal involvement vary widely within this disease group (2). The most common form of inherited cystic kidney disease is Autosomal Dominant Polycystic Kidney Disease (ADPKD) which has an incidence of 1:500 to 1:1000 live births and is characterized by the progressive formation of multiple cysts leading to grossly enlarged kidneys, with patients becoming symptomatic from early adulthood on and ESRD occurring in 60% of patients by age 70 (3, 4; Fig 1B). Recessive disorders causing polycystic kidneys include Autosomal Recessive Polycystic Kidney Disease (ARPKD), Nephronophthisis (NPH) and other genetic syndromes that can be associated with a renal phenotype NPH such as Joubert syndrome (JBTS), Bardet-Biedl syndrome (BBS) and Meckel-Gruber syndrome (MKS). While less common, these recessive disorders generally develop at a much earlier age and involve more severe disease phenotypes (1).

##### 3.1.1 Nephronophthisis

Nephronophthisis (NPH) is the most common genetic cause of ESRD in children and adolescents with an estimated prevalence of 1 in 50,000 (5). NPH is characterized by the histological triad of interstitial fibrosis, tubular basement membrane disruption, and tubular atrophy with multiple cysts localized primarily to the corticomedullary border of the kidney. The majority of the cysts are derived from the distal convoluted and collecting tubules of the nephron (4; Fig 1B). Initial symptoms including polyuria and polydipsia begin at an average of 6 years of age, with renal failure occurring by an average age of 13 in the most common form of this disease (5, 6). Unlike other forms of cystic kidney diseases, kidneys are generally normal or reduced in size. Genetic research has identified sixteen causative genes (*NPH1-15* and *NPHPL1*) although these account for only 30% of cases of NPH, indicating that further causative genes will be identified in future (7–10). However,

heterozygous mutations in several related disease genes could increase total mutational load and account for NPH symptoms in patients without a homozygous mutation, as has been demonstrated for BBS proteins (11, 12). Extra-renal symptoms in NPH-related diseases such as Senior-Løken Syndrome and JBTS include retinal degeneration, liver fibrosis, or cerebellar vermis aplasia and occur in 10-20% of patients (5), the severity of which may depend on the type of mutation (7) or modifier genes involved (13). The overlapping extra-renal phenotypes caused by mutation of genes encoding different “cystoproteins” may be explained in part by a common localization or function of these protein products. Many cystoproteins form interaction complexes, including several of the nephrocystin proteins encoded by the NPH genes 1 to 11 (13, 14), therefore similar phenotypes arising from different genetic mutations may occur due to the disrupted function of the same interaction complex. Protein function overlap or co-dependency is further hinted at by relatively recent demonstrations that nephrocystin proteins co-localize to the same subcellular organelle: the primary cilium. Accumulating evidence that in fact all cystoproteins analyzed to date localize to the primary cilium or basal body generated the “ciliary hypothesis”, which stated that all proteins responsible for monitoring the need for renal epithelial cell division localize at least in part to primary cilia, and the formation of renal cysts could result from defective proliferation control by these organelles (15). The idea that one subcellular organelle could link a broad spectrum of disease phenotypes led to a new classification of human genetic diseases, the ciliopathies.

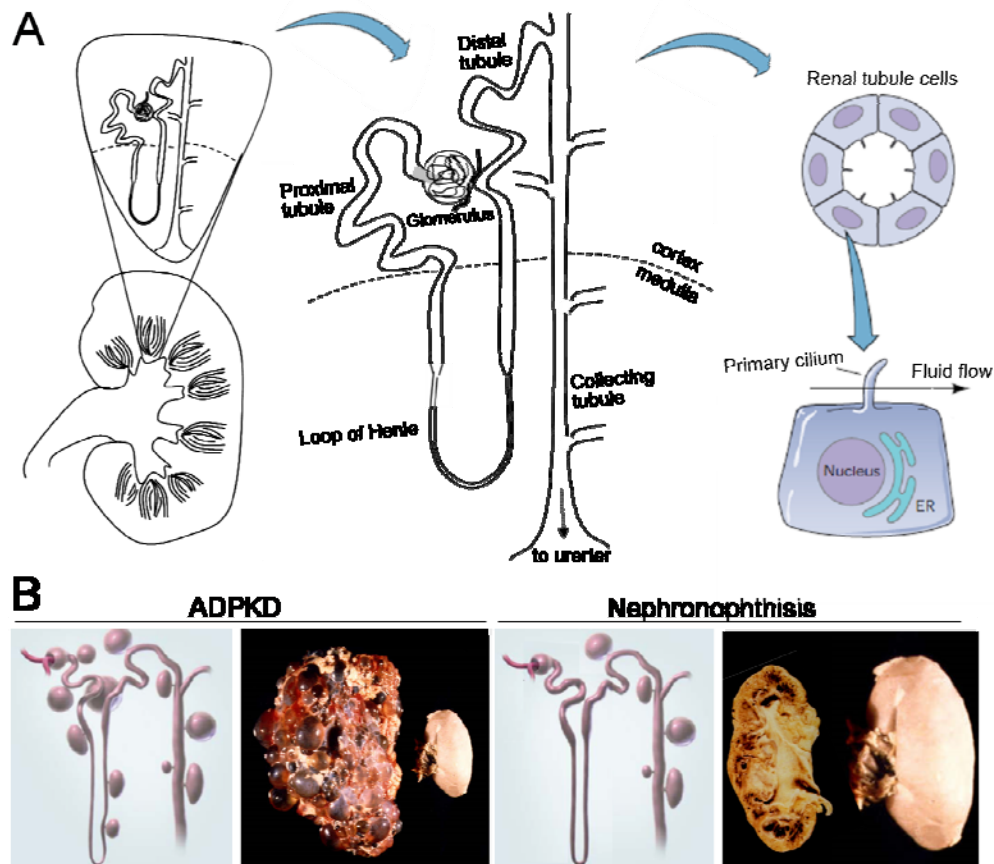


**Figure 1. Healthy and polycystic kidneys.**

**A.** One nephron segment in a healthy kidney, illustrating location of nephron tubules and the location of primary cilia on tubular epithelial cells. The kidneys contain approximately 600,000 to one million nephron segments which filter 180L litres of urine per day. Blood enters the glomerulus which retains proteins but expels fluid into the proximal tubule. Fluid continues through the loop of Henle to the distal tubule before joining the collecting duct en route to the ureter. The nephron tubule system regulates the osmolarity of the urine, re-absorbing salts and water as required. Epithelial cells lining the tubules of the nephron each possess a primary cilium projecting into the lumen, which bends in the direction of fluid flow. Adapted in part from (16). **B.** Schematic drawing of a nephron's segments and cystic kidney images from ADPKD (left panels) and NPH (right panels). The magnifications of the pictures are not equal: both diseased kidneys are shown in comparison to the size of a healthy kidney. Kidneys in ADPKD are grossly enlarged with multiple cysts in all nephron segments, while NPH kidneys are normal to small in size with cysts primarily derived from the collecting tubules and localized at the corticomedullary border. Adapted from (2)(Reproduced with permission from Wilson 2004 NEJM, Copyright Massachusetts Medical Society) and (17) (Reprinted from "Identification of a New Gene Locus for Adolescent Nephronophthisis, on Chromosome 3q22 in a Large Venezuelan Pedigree", Volume 66, Heymut Omran *et al*, Copyright (2000), with permission from Elsevier), and The PKD Foundation.

### 3.1.2 Ciliopathies

The classification of various distinct genetic diseases associated with renal cysts as ciliopathies occurred only recently in medical history. In 1994 mutation of the *Tg737* gene in mice was reported to cause a cystic kidney phenotype similar to ADPKD (18); however, the function of the *Tg737* gene was unclear at that time. In 1999, *C. elegans* protein *lov-1* was identified as a homolog to human PKD1, and shown to localize to sensory neuronal cilia (19). In 2000, sequencing of the *Chlamydomonas reinhardtii* flagellar protein IFT88 revealed homology to Polaris, the protein product of mouse and human *Tg737* (20). This work further demonstrated that IFT88 was required for cilia assembly and that kidney tubule cells in the *Tg737* mutant mouse lacked elongated luminal cilia. Two years later, the protein products encoded by two genes mutated in ADPKD, polycystin-1 and polycystin-2, were demonstrated to colocalize with Polaris/IFT88 at the mammalian primary cilium (21). This prompted intense investigation into the protein products of genes known to cause cystic kidney disease when mutated and it transpired that all cystoproteins localize to primary cilium, basal body or centrosomes (1, 7, 13, 22, 23). The subsequent association of multiple diverse human genetic disorders with ciliary dysfunction thus defined a collective group of “ciliopathies”, where distinct clinical entities manifest with a subset of overlapping clinical features, including polycystic kidneys (24).

The ciliopathy concept creates an explanation for the pleiotropic phenotypes associated with this group of diseases, because the cystoproteins included within the ciliary proteome are highly conserved throughout evolution and are expressed in many organ systems (13). For example, function of the pancreas and liver also depend upon tubular systems with luminal monocilia, which may explain the involvement of these organ systems in hereditary renal cystic diseases (25). Additionally, NPH-associated retinitis pigmentosa could be due to an interrupted interaction of several NPH proteins with key proteins in the connecting cilium of photoreceptor cells in the retina, which is the structural equivalent to the transition zone of renal epithelial cells (26–29). Primary cilia or ciliary motor proteins are also involved in olfactory function, axonal elongation, and left-right asymmetry, which may explain ciliopathy-associated phenotypes such as anosmia, brain malformations, and *situs inversus* (13, 30). Mutations in genes encoding known centrosomal or ciliary proteins have also been demonstrated as causative in BBS-associated obesity and NPH-associated skeletal defects (30).

Although the ciliopathy concept nicely links symptoms in separate organ systems to the same subcellular organelle, the converse challenge for this model will be to explain how the dysfunction of a single organelle leads to disparate phenotypes: for example, the predominant total-kidney cyst formation seen in ADPKD vs. the more specifically localized cysts of NPH; or the lack of retinitis pigmentosa in ADPKD but not NPH. It has been demonstrated that the same ciliary protein can have different roles in different tissue types (31), therefore extra-renal phenotypes might depend on which protein is affected. Within the kidney, it has been suggested that ciliary dysfunction initiates cyst formation but extraciliary cystoprotein functions determine the final phenotypic fate (32). Indeed,

many cystoproteins localize to multiple subcellular regions and interact with members of cell-cell or cell-matrix adhesion complexes (1, 13). Examples include the adherens junction localization of nephrocystin-1 (33) and polycystin-1 (34) which are the respective protein products of the most frequent gene mutations causing NPH and ADPKD, or the nuclear localization of NPHP2 (35) or NPHP7 (36). Such multiplicity of potential functional roles call for caution to avoid a simple “guilt by association” description of the ciliary proteins in cyst formation (13). That the relationship between cysts and cilia is not as straightforward as promised was demonstrated by the Polaris transgene rescue in the *Tg737* null mouse, where mice developed renal cysts despite a rescued ciliary phenotype (37). Additionally, the latest NPH gene identified, *NPHP1L/XPNPEP3* isoform 1, is the first gene not consistent with the ciliary hypothesis, with the XPNPEP3 protein localizing to mitochondria rather than primary cilia (38). However, mice with a Polaris transgene expression displayed unusually elongated renal primary cilia, and the zebrafish *xpnpep3* morphant phenocopies other known ciliary morphants and can be rescued by a human version of *XPNPEP3* lacking a mitochondrial localization sequence; the implied ciliary involvement is supported by the role of XPNPEP3 in cleavage of known ciliary cystoproteins during development. These observations suggest that any disruption in the homeostatic function of primary cilia, including cross-talk between the primary cilium and the rest of the cell, may be enough to initiate renal cyst formation. In order to tease apart which cellular functions are disrupted during cyst formation and whether these require functional primary cilia, it will be important to closely study this organelle and elucidate the precise ciliary and extraciliary functional roles of cystoproteins involved in ciliopathies.

### 3.2 The Primary Cilium

A cilium is an antennae-like structure protruding from the surface of virtually every mammalian cell, and protruding from the apical surface of differentiated renal epithelial cells. Much of the current knowledge has been gained from studies of the structurally similar flagellae of the green algae *Chlamydomonas reinhardtii*. After cell division, both the mother and the daughter centriole migrate together to the plasma membrane to become the basal body. Both centrioles are barrel-like structures but only the mother centriole, which was inherited rather than duplicated during cell division, extends subdistal appendages which are required for microtubule enucleation as well as distal appendages which anchor to the plasma membrane and delineate a boundary from which the ciliary membrane will extend (22, 39). The ciliary membrane extends to surround a central axoneme consisting of nine peripheral doublet microtubules assembled on top of the mother centriole template (Fig 2A). This “9 + 0” axoneme organization is characteristic of non-motile primary cilia. Motile cilia are often expressed in multiple copies on the cell surface, and contain dynein arms as well as an additional central microtubule pair allowing for bi-directional movement characteristic of their long-recognized roles in cell or fluid propulsion. Although first reported in 1898 and studied

structurally for the past 45 years (40) a lack of more than circumstantial evidence regarding function led to primary cilia being largely overlooked by the biomedical community as vestigial organelles or at best, a mechanism to sequester centrioles during interphase (41, 42). However, advances in microscopy and biochemical technology during the past 15 years have allowed for a recent explosion of research, establishing the primary cilium's place as a critical functional element in an increasing list of human tissues.

Early evidence connecting primary cilia to cell function described a link between the presence of the cilium and the cell cycle, whereby serum stimulation induced cell cycling coupled with biphasic ciliary disassembly, with the second wave occurring at the initiation time of DNA synthesis and centriole duplication (43). Ciliation was noted to occur in the late G1 phase of dividing cells, and it was proposed that at this point the cell could exit mitosis, and the retained cilium in G0 could remove the centriole from the mitotic cycle. That primary cilia are disassembled prior to mitosis and reassembled after cytokinesis has since been well established, although the direction of causality continues to be unclear (44, 45). The ciliary control of cell-cycle regulation is ambiguous; for example, a reduction of the intraflagellar transport protein IFT27 elongates the cell cycle (46), but a reduction of IFT88 promotes cell-cycle progression (47). In general, kinase activity within the ciliary region seems important in regulating ciliary disassembly and cell-cycle re-entry. For example, Aurora A kinase-dependant activation of the tubulin deacetylase HDAC is required for disassembly (48), as is the recruitment of phosphorylated Tctex-1 to the transition zone, which accelerates ciliary disassembly and cell-cycle reentry (49). Conversely, dysfunction of the *JBTS1* gene product, ciliary-localizing phosphatase INPP5E, results in cilia destabilization (50, 51). However, examples also exist describing protein kinase requirement for ciliary assembly (52) as well as for cell-cycle control over primary cilia dynamics. For example, ciliary assembly depends on the cell-cycle dependent removal of the disassembly-linked phosphoprotein Nde1 from the centrosome (53), while disassembly depends on cell-cycle dependent accumulation of Nek2 to the mother centriole at G2 (54). In any case, though the hierarchy of command remains uncertain, the importance of this reciprocal relationship between cell cycle and the primary cilium is clear, with recent *in vivo* evidence demonstrating that interrupting the ciliary regulation of cell cycle reentry influences whether the cell divides or differentiates in the developing brain (49). Teasing apart the roles of the cilium, centrosome, and the cell cycle in differentiation and tissue homeostasis will require a deeper understanding of the molecular mechanisms governing communication between the primary cilium, the external environment, and the cell.

### 3.2.1 Ciliary Communication with the Cell – the “Ciliary Pore Complex”

Communication between the cilium and the cell requires the cilium to act as a separate functional unit, and the cilium is considered an independent subcellular organelle despite a lack of membrane boundary between the ciliary lumen and the cytoplasm. However, even though the ciliary membrane is continuous with the apical cell membrane, numerous examples describe localization of both membrane and axonemal proteins restricted to or specifically concentrated at the primary cilium (55–59). Thus, both membrane and cytoplasmic proteins cannot freely diffuse into the ciliary compartment. Nearly 200 proteins have been identified within the primary cilium by proteomic and computational analysis (59), and including the basal body the complete ciliary proteome could include over 1000 different polypeptides, although whether all would be required for function in every cell type remains unclear (60, 61). Protein synthesis has not been shown to occur in the ciliary lumen, so to maintain this distinct ciliary protein composition the cell must regulate either the entry or retention of proteins within the cilium by a functional barrier. The absence of protein synthesis also requires a highly efficient mechanism in place to shuttle proteins within the cilium, which is achieved by the intraflagellar transport (IFT) system described below. Understanding this composition and action of this barrier as well as the molecular mechanisms driving IFT will allow a better understanding of how the communication between the cilium and the cell is regulated.

Positioned in the cytosol at the base of the cilium, the centrosome is a prime candidate to regulate protein transport to and from the cilium. The centrosome consists of the mother and daughter centrioles whose migration toward the apical membrane after mitosis initiates ciliogenesis, as well as a variety of peri-centriolar proteins of as yet unknown functions. Early studies using electron microscopy noted satellite arms projecting uniquely from the mother but not daughter centriole during early ciliogenesis (62), which have since been further characterized as distal and subdistal appendages. Subdistal appendages are thought to play a role in anchoring microtubules (63), whereas distal appendages are involved in the recruitment and tethering of the basal body to the plasma membrane (64, 65). The ciliary axoneme consists of doublet (A & B) microtubules which are assembled on top of the triplet (A, B & C) microtubules of the mother centriole. The distal appendages attach to the mother centriole immediately proximal to the doublet axoneme, attaching to the C tubule just prior to its termination and in this context are called “transition fibers” (Fig 2 B-D). In contrast, immediately after the transition of A & B tubules from the centriole to the axoneme exists the “ciliary necklace”, consisting of Y-shaped bridges that connect the outer doublet microtubules of the axoneme to the ciliary membrane (64, 66; Fig 2 E-G). Together these structures are termed the “transition zone”, and both are independently important for cilia integrity. For example CEP 164, which localizes specifically to distal fibers, and CEP290/NPHP6, which localizes to the Y-links of the ciliary necklace, are both required for assembly of primary cilia (67, 68).

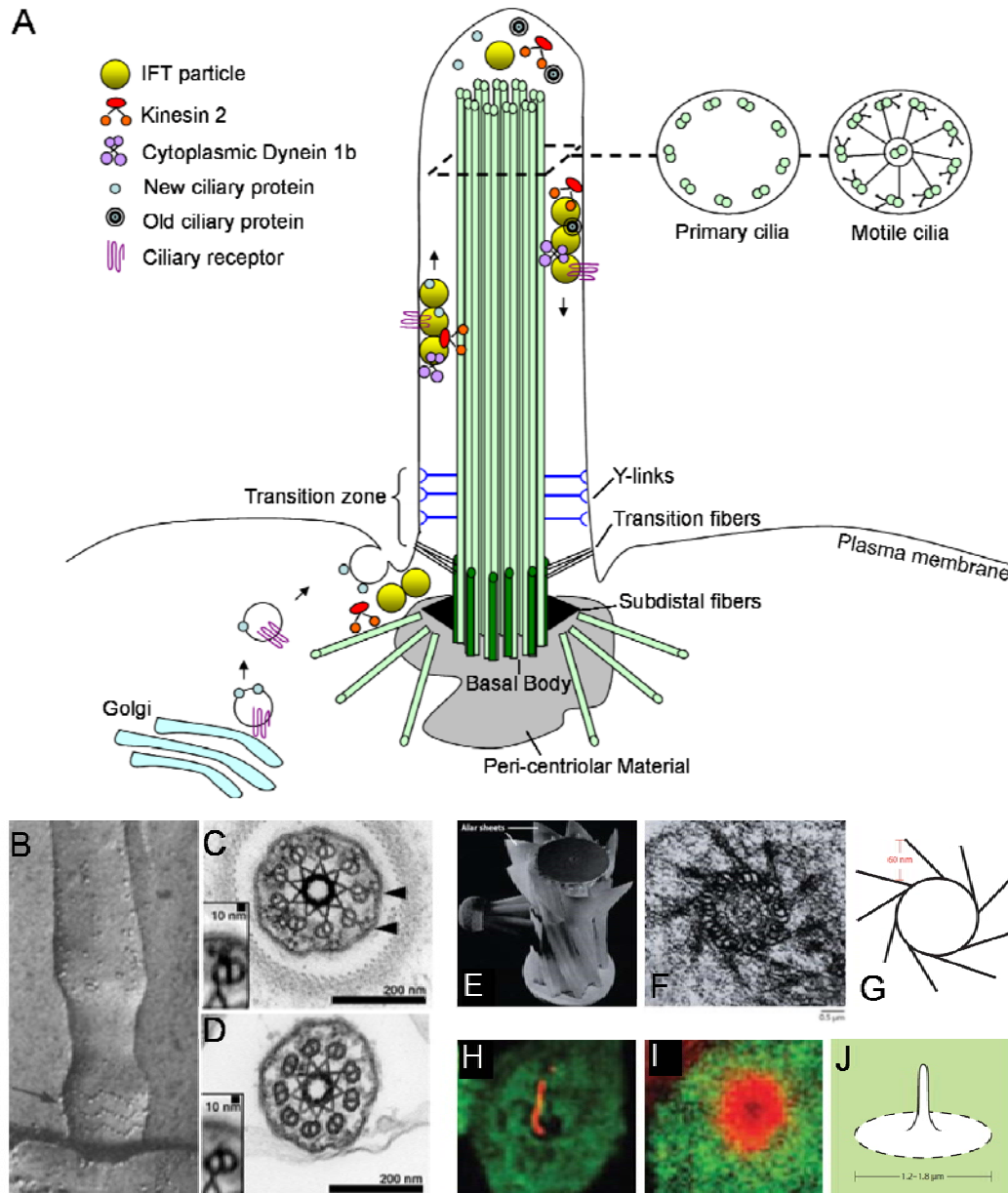


**Figure 2. The primary cilium.**

**A.** Schematic illustrating ciliary structure and protein transport. The basal body is surrounded by peri-centriolar material and is comprised of the mother centriole which projects distal/transition fibers that adhere to the plasma membrane at the base of the cilium, as well as subdistal fibers which are involved in microtubule enucleation. The ciliary axoneme is composed of 9 doublet microtubules assembled on top of the mother centriole template. Motile cilia contain a central microtubule pair and dynein arms required for movement, whereas primary cilia do not. Newly synthesized proteins are transported in vesicles from the Golgi apparatus to the apical membrane at the base of the cilium where the vesicle is exocytosed, leaving the proteins to interact with IFT particles and unidirectional motors. The entire IFT train must cross the transition fibres and Y-links of the transition zone to gain access to the ciliary lumen. Anterograde transport requires hetero-trimeric Kinesin-2 motor complex while retrograde transport uses cytoplasmic dynein1b. Transition zone proteins strictly regulate entry of new proteins and exit of old proteins from the cilium as described in the main text. **B.** Scanning electron microscopy (SEM) image of the ciliary neck component of the transition zone as visualized by freeze-fracture (arrow) (66; © Gilula and Satir, 1972. Originally published in *Journal of Cell Biology*. doi:10.1083/jcb.53.2.494.). **C-D.** Transmission electron microscopy (TEM) image of ciliary

necklace Y-links (arrowheads, C), which disappear if NPHP6 expression is interrupted (D) (68; © Craige et al., 2010. Originally published in *Journal of Cell Biology*. doi: 10.1083/jcb.201006105). **E.** Model of distal fibers (alar sheets) and microtubule-nucleating subdistal fibers attached to mother centriole (69; © Anderson 1972. Originally published in *Journal of Cell Biology*. doi:10.1083/jcb.54.2.246). **F.** TEM image cross-section of the distal/transition fibers (69; © Anderson 1972. Originally published in *Journal of Cell Biology*. doi:10.1083/jcb.54.2.246). **G.** Schematic of the transition fibers, highlighting 60nm distance between each (70; Nachury et al., 2010, with permission from Annual Reviews). **H-I.** Immunofluorescence image of glycosylphosphatidylinositol-fluorescent protein (green) is excluded from a specialized periciliary membrane domain surrounding the cilium (red, J), while Galectin-3 (red, K) concentrates in this region (reproduced from (71), copyright © by the National Academy of Sciences, U.S.A.). **J.** Schematic of the periciliary membrane domain highlighting size of specialized apical membrane region (70; Nachury et al., 2010, with permission from Annual Reviews).

The idea that the transition zone could act as an impermeable ciliary barrier was initially suggested by two studies in 1972: the first, using freeze-etching combined with electron microscopy, identified the ciliary necklace and proposed it to be involved in the “control of localized membrane permeability”(66); whereas the second, using 3D reconstruction techniques to model transition fibers, described these structurally as trapezoidal sheets, possibly capable of limiting the size of particles entering the cilium (69). Both of these ideas have since found support, and several authors have now likened the selective regulation of protein entry to the cilium to that of the nuclear pore, proposing that the transition zone acts as a “ciliary pore complex” (CPC; 70, 72–75). Structurally, the sheets formed by the transition fibers form a “nine-bladed propeller-like structure jammed at the entrance of the ciliary lumen”, with the space between consecutive sheets theoretically large enough to allow free diffusion of particles smaller than 60 nm in diameter (70). Diffusion studies in photoreceptor cells have provided evidence that small molecules such as the 27 kDa green fluorescent protein (GFP) move freely between the ciliary lumen and cytoplasm (76) suggesting that the lumen likely has a similar composition to the cytoplasm in terms of ions and small proteins. However, there is a reduction of diffusion rate across the connecting cilium for even small particles compared to aqueous solution which is not explained by the size obstruction of the axoneme, and suggests that even the ciliary entry of smaller sized proteins could be regulated (77). This regulation is reminiscent of that occurring at the nuclear pore complex (NPC), which excludes nuclear entry of proteins larger than 60 kDa, slows proteins 30-60 kDa, and allows free diffusion of anything under 30 kDa. At the cilium, it was recently shown that proteins larger than 40 kDa require the presence of specific nucleoporins at the CPC (78). The same group had previously demonstrated that the 170 kDa ciliary motor protein KIF17 required importin-β2 as well as a ciliary concentration of the GTP-bound form of the small G-protein Ran (75), both of which are similarly required at the NPC to translocate and release nuclear cargo. The ciliary protein polycystin-1 also requires Rab and Arf GTPase activity for ciliary localization (79). Such parallels between ciliary and nuclear import lead to an important question regarding how ciliary versus nuclear cargoes are trafficked to the correct location. One possibility is the recognition of distinct

targeting sequences within the cargo proteins. Importins are known to recognize a nuclear localization sequence (NLS) on their cargo, and it was shown that a specific lysine-rich C-terminal sequence on KIF17 acted as a ciliary localization sequence (CLS; 75). When this target sequence was replaced with the NLS from the SV-40 large T antigen, KIF17 was targeted to the nucleus. Ciliary-targeting sequences have been identified on a number of ciliary proteins, and some common motifs are surfacing (70). For example, the CLS of the photoreceptor rhodopsin contains the amino acid sequence Q-V-(S/A)-P-A, while the *PKD* gene products associated with ADPKD, polycystin-1 and polycystin-2, contain a conserved motif (K/R)-V-x-P, suggesting V-x-P as a common sequence important for ciliary targeting (70, 79–82). Other CTS sequences include an A-x-(S/A)-x-Q motif identified in several G protein-coupled receptors (83), and critical C-C-C and K-T-R-K residues in the cytoplasmic tail of fibrocystin, the product of the human ARPKD gene *PKHD1* (84).

Proteins that are destined for the cilium are thought to be contained within post-Golgi vesicles and exocytosed at the apical plasma membrane at point of transition fiber contact (72, 73). Once there, proteins must be transported across the transition zone and throughout the cilium. Although it is not clear exactly how crossing the transition zone is regulated, the mechanism of protein transport through the cilium is well established. IFT was first observed in 1993 using DIC microscopy to visualize the flagella of *Chlamydomonas reinhardtii* where the IFT protein trains were shown to move at a rate of ~2  $\mu\text{m}$  per second from the ciliary base to tip, and ~3.5  $\mu\text{m}$  per second in the reverse direction (85). The suggestion that these IFT trains were the same as the electron dense “rafts” bound periodically to both the flagellar membrane and the B tubule of the ciliary axoneme seen by electron microscopy was subsequently verified (86). All axonemal microtubules are oriented with their plus end towards the distal tip of the cilium (87), so transport of cargo such as membrane receptors or axoneme components requires microtubule motors operating in a plus-end direction to reach the distal end of the cilium as well as minus-end direction to recycle components back to the ciliary base. These motors are now well established as the anterograde heterotrimeric kinesin-II and the retrograde cytoplasmic dynein1b (72, 88–90), both of which are carried in an inactive state by the other motor when not in use (91–93). More recently, a second anterograde motor, homodimeric OSM-3/KIF17, was shown to act cooperatively with kinesin-II in the proximal cilium as well as independently along the singlet microtubules of the distal cilium (94, 95). Since KIF17 has been shown to be important for correct ciliary localization of the olfactory channel subunit CNGB1b (96) as well as for cone opsin in the photoreceptor outer segment (97), it has been suggested that multiple anterograde motors might be important in specific cilia types for correct protein localization and function (98, 99).

*Chlamydomonas reinhardtii* mutants have demonstrated that the function of both anterograde and retrograde IFT are required to maintain flagellar length (86, 88). This suggests a constant turnover of ciliary proteins must be maintained by transport and entry of proteins to the cilium. In addition to motor proteins, the IFT complex consists of at least 15 different polypeptides which sediment in density gradients as two complexes, termed A and B (89). Several of these IFT particles have been

implicated not only in ciliary protein transport but also for protein entry across the transition zone. Despite their most well known function within the cilium proper, most IFT particles including motor proteins localize predominantly to the basal body region, outside of the cilium (89, 90, 100). Intriguingly, electron microscopy has demonstrated that IFT52 localizes to the transition fibers at the point of membrane contact where golgi vesicles are thought to exocytose, leaving their cargo to be associated with IFT particles for ciliary transport (72, 101, 102). IFT particles could also be directly involved with ciliary targeting of golgi vesicles, as IFT20 localizes to these golgi vesicles as well as IFT rafts and is required for the ciliary localization polycystin-2 (102, 103). It is well known that IFT particles are recycled as they can continue to maintain the cilium without new protein synthesis for several hours (93, 104). Retrograde IFT is required for protein exit from the cilium (88, 105), and it is thought that IFT particles are dissociated at the point of ciliary exit, subsequently reforming to carry new cargo (93). Distinct apical staining patterns suggest the existence of a diffusion barrier which might function as a specialized periciliary membrane domain (PCMD) of condensed lipids which maintains a rich concentration of proteins intended as ciliary cargo close to the basal body region (70, 71, 106; Fig 2H-J). IFT particles share evolutionarily conserved sequence domains with the prototypical coat protein I (COPI) and clathrin transport proteins (107), and it has been proposed that the IFT particles may polymerize into a flat coat which serves as a focal point for motor proteins to propel the unit through this diffusion barrier (70). The location of IFT particles to the transition fibres supports this possibility; however, both the IFT proteins and cargo would still need to translocate through the Y-links at the ciliary necklace. Evidence exists to suggest that regulating protein transport across this region of the transition zone may involve known ciliopathy proteins, including the nephrocystins.

### 3.2.2 Nephrocystin proteins at the ciliary pore complex.

Many ciliopathy related proteins form complexes at the base of the primary cilium, and several MKS, JBTS, and NPH proteins have been shown by immunofluorescence to localize specifically to the transition zone (14, 23). Using tandem affinity purification followed by mass spectrometry, reciprocal interaction studies identified two nephrocystin complexes: NPHP1-4-8 and NPHP 5-6 (14). All three proteins in the first complex localize to the transition zone, while NPHP6 localizes to both the basal body and transition zone and NPHP5 to the basal body (14, 68). Although not required for ciliary assembly, studies in *C. elegans* have reported a mild stunted or misshaped ciliary phenotype following *nphp-1* or *nphp-4* knockdown, the penetrance and severity of which is exacerbated significantly by combined knockdown with transition zone mks proteins (108, 109), highlighting the functional overlap of TZ proteins which may account for the variety of disease phenotypes associated with disruption individual protein function in this structure (31). Interestingly, combined *mks/nphp-1* or *mks/nphp-4* mutant strains lacked the Y-links which form the ciliary necklace (109). Independently,

NPHP6 has been shown by electron microscopy to localize specifically to the Y-links within the transition zone and to be required for the formation of these structures (68). When these Y-links are disrupted, the ciliary membrane at the transition zone is located further away from the axoneme (68, 109), suggesting that NPH proteins play a role in the structural integrity of this region. Furthermore, disrupted Y-links due to NPHP6 knockdown have led to altered flagellar protein composition and reduced retrograde transport velocity (68), and *nphp-4* knockdown in *C. elegans* leads to decreased ciliary access or motility of motor proteins such as OSM3/KIF17 and OSM6/IFT52 (108). Together these results suggest that NPH proteins at the transition zone are not only important for keeping proteins from entering cilia, but also for facilitating entry and exit of required proteins, supporting the notion that NPH proteins located at the ciliary neck Y-links contribute to a functional ciliary gate (23, 109, 110). The mechanism of action of NPH proteins at this gate is not clear; however, due to the known role of IFT particles in trafficking ciliary proteins it has been suggested that TZ nephrocystins may modulate the packaging of ciliary cargo to IFT trains (99), which is supported by observations that a murine *Nphp1* mutant develops retinal degeneration due to inefficient IFT transport to outer segments of photoreceptor cells rather than impaired connecting cilium formation (111). Indeed, the recently reported novel NPH genes *NPHP12* and *NPHP13* were identified to respectively encode IFT proteins IFT139 and IFT144 (8, 10), further establishing an intimate link between NPH proteins and IFT. Other reports that several nephrocystin proteins interact with the TZ guanine exchange factor RPGR (26, 27, 112, 113), which in analogy to its function at the nuclear pore may be important for GTP-dependent release of G-protein bound cargo, have prompted speculations that the nephrocystin proteins may be involved specifically in the release of cargo after transport into the ciliary lumen (73). As the importance of the cilium in the cell's reception of environmental signals is increasingly recognized, it becomes apparent that regulating ciliary protein entry or IFT competence would influence the availability of signaling components such as transmembrane receptors or downstream effector proteins and have a profound effect on the capacity for communicating signals to the rest of the cell.

### **3.3 The role of primary cilia as signaling pathway platforms.**

The importance of primary cilia to act as a mechanism for the cell to receive environmental signals was initially obvious only in specialized sensory cells involved in vision and olfaction. The high-turnover light-sensitive rhodopsin molecules of retinal photoreceptor cells are produced in the cell body and their translocation to the outer segment depends upon IFT-mediated transport through a primary “connecting” cilium. The presence of multiple primary cilia projecting from the dendrites of olfactory neurons into the mucus membrane of the nasal epithelium was shown long ago to be required for odorant perception (114, 115), and many odorant receptors have since been shown to localize to these organelles (116, 117). The sensory role for apparently “non-specialized” primary cilia was less

obvious, but in recent years they have also been shown to be important for signal reception in a number of different tissues, prompting their likening to a “cellular antenna”(114, 118, 119) . For example, the inhibitory hormone somatostatin receptor 3 has been shown to exclusively localize to neuronal primary cilia in all brain regions except the cerebellum (120), and the serotonin receptor 5HT<sub>6</sub> localizes to primary cilia in the striatum, nucleus accumbens, olfactory tubercle and islands of Calleja (121). More recently, the melanin-concentrating hormone receptor1 has also been shown to localize to neuronal cilia (83), while the somatostatin receptor 3 has additionally been localized to primary cilia of pancreatic islets and the pituitary gland (56). Motile cilia also have been shown to have chemo- and mechano-sensory functions. For example, four members of the sensory bitter taste receptor (T2R) family are specifically expressed on motile airway epithelial cilia (122), and accumulating data suggests that sensory-motor-response circuit controlling beat frequency in multiciliated epithelia of the respiratory tract, oviduct and ependymal lining of the ventricles of the brain is mediated by the cilia themselves (123).

As cilia-specific receptors continue to be identified, the role of these organelles in communicating the signal to the rest of the cell is also being elucidated. One of the better understood ciliary signaling pathways is the hedgehog (Hh) signaling pathway, which is important for dorsal-ventral patterning during embryonic development. In 2003 it was reported that two different mouse mutants which disrupted mouse homologues of *IFT172* and *IFT88* had defective Hh signaling, suggesting ciliary involvement in the function of this signaling pathway (124). It has since been demonstrated that primary cilia are a key component of both the activation and repression of Hh signaling: under basal conditions the Hh effector proteins Gli2 and Gli3 are processed to their repressor form at the ciliary tip (125), whereas when a Hh ligand binds to its receptor Patched (Ptc), the activator Smoothed (Smo) translocates into the cilium (126) where it inhibits the processing of Gli2 & Gli3, allowing their nuclear translocation and target gene activation (127). Of interest, depletion of the small GTPase Septin 2 at the TZ increased diffusion of several ciliary membrane proteins but decreased retention of Smo, reducing the Hh signaling response (128) and supporting an argument whereby specificity of ciliary protein entry and exit is critical for signaling pathways. In addition to Hh signaling, primary cilia are also required for platelet-derived growth factor-AA (PDGF-AA) signaling. The PDGF receptor alpha (PDGFR $\alpha$ ) localizes to fibroblast primary cilia which are required for downstream MEK1/2-ERK1/2 pathway activation (129). The primary cilium has also been shown to regulate second messenger cyclic AMP (cAMP) formation. Adenylyl cyclase III, which converts ATP to cAMP, is located in olfactory cilia where it is required to transform chemosensory information to electrical signals (130). More recently it has also been shown to localize to neuronal and astrocyte cilia where it might play a similar role, altering membrane potential through calcium influx and possibly regulating neuronal firing rate (131).

Interestingly, renal cilia have also been shown to regulate calcium signaling. The bending of cilia in response to fluid flow increases calcium influx followed by intracellular calcium release (132,

133). This effect is a specific response to laminar fluid flow rather than mechanical pressure (134) and is abolished in previously responsive confluent cell monolayers lacking cilia due to chemical removal (135), as well as in collecting tubule cell preparations or intact segments lacking cilia due to *Tg737* genetic mutation (136–138). The mechanically sensitive ion channel mediating this effect is thought primarily to be the ciliary cystoprotein polycystin-2 (139, 140), which requires co-expression of polycystin-1 for correct apical localization and ion channel function (141). Indeed, flow-induced calcium response is completely abrogated in human primary cultures of PKD cyst-lining cells lacking polycystin-1, despite cells retaining otherwise normal calcium signaling (142). In non-ciliated *Tg737* mutant cells which also do not respond to flow, basal calcium levels are increased, which suggests de-regulated calcium entry in stimulated and non-stimulated conditions (136, 137). Indeed, *Tg737* mutant cells show altered polycystin-2 localization throughout the apical membrane rather than concentration in the cilium (136), which again highlights the important role of the transition zone in maintaining restricted localization of signaling molecules within the cell *versus* the cilium.

Calcium signaling has a number of downstream effects which may contribute to cyst formation if de-regulated. For example, cAMP activity in normal cells inhibits MAPK signaling and cell proliferation, but stimulates this pathway in cystic cells (143). This switch in cAMP activity is mimicked in normal cells by blocking calcium influx, which causes cAMP to activate B-Raf instead of Raf-1 and leads to aberrant activity of the MEK/ERK pathway (144). The switch in cAMP activity involves a calcium-restriction-dependent decrease in PI3K/AKT activity (144), which is an upstream regulator of mTOR. Of interest, AKT/mTOR signaling is upregulated in ARPKD and ADPKD (145, 146); however, clinical use of an mTOR inhibitor reduced cyst size but did not improve renal function (147, 148), indicating that other causal triggers must exist contributing to cyst expansion. One possibility involves abnormal secretion in cyst lining cells. In ADPKD, altered cell polarity in cystic epithelia results in an apicobasal reversal of the Na<sup>+</sup>/K<sup>+</sup>-ATPase sodium pump localization and aberrant apical secretion of sodium ions into the cystic lumen, providing a gradient that causes further fluid secretion and cyst expansion (4). That this might be a major causal trigger is supported by results of a recent 3 year double blind clinical trial demonstrating that Tolvaptan, a vasopressin V2-receptor antagonist which suppresses proliferation and luminal fluid secretion, slowed kidney growth (149). Of interest, the apicobasal reversal of the Na<sup>+</sup>/K<sup>+</sup>-ATPase sodium pump localization mirrors the normal developmental status of the kidney, where apical location of sodium pumps is thought to be required for dilation of the newly formed lumen of kidney tubules (4). Unlike in ADPKD, kidneys in nephronophthisis are generally reduced in size, with an increase in apoptosis rather than hyperproliferation allowing for cyst expansion at the expense of native tissue (1, 13). The “developmental state” of cyst-lining epithelia may also reflect causal triggers more applicable to NPH such as defects in cell polarity, cell-matrix or cell-cell interactions, which have also been identified in cyst lining epithelia (4). These defects could result from de-regulated TZ control of ciliary-mediated signaling pathways. In particular, de-regulated calcium signaling in response to flow may lead to

changes in the polarity of the cell due to interrupted balance of the three major Wnt signaling pathways as further described in the following section: Wnt/Ca<sup>2+</sup>, Wnt/PCP, and canonical Wnt (150). The canonical Wnt signaling pathway is known to play a crucial role in kidney development, while Wnt/PCP signaling is important in cell polarity, and both of these Wnt pathways could be mediated via the Wnt/Ca<sup>2+</sup> pathway (150). A failure for Wnt signaling to progress from canonical Wnt in early development to polarity-directed pathway activation could result in aberrant protein localization and be influenced by incorrect interpretation of calcium influx by the cilium. Thus, Wnt signaling represents a prime candidate for investigation as a de-regulated signaling pathway in the formation of kidney cysts.

### 3.3.1 The Wnt signaling pathway and kidney cyst formation

Inter-cellular communication by secreted Wnt ligands is required to establish signaling gradients needed for dorsoventral and anteroposterior axes specification during vertebrate development (151, 152), but Wnt signaling also plays key roles in regulating cell fate decisions and migration (153), cell cycle progression and stem cell maintenance (154). In adults, Wnt signaling drives tissue renewal in rapidly self-renewing organs such as the intestine and skin, where Wnt pathway activation is required not only to maintain stem cell populations but also to drive expansion of new epithelial cell precursors (153, 155, 156). Deregulation of Wnt signaling can therefore lead to disastrous consequences both for the developing embryo and for the adult organism, where de-regulated Wnt signaling is a major contributor to cancer (156, 157). De-regulated canonical Wnt signaling in mouse models also leads to kidney cyst formation, possibly due to aberrant proliferation, although discerning the sequence of events is complicated by findings that renal cysts develop in both gain- and loss-of-function mutants (158–161). As with ciliary dysfunction, it appears that any deviation from normal Wnt function is sufficient to induce renal cyst formation. Maintaining a delicate balance of canonical Wnt activation may also be critical for appropriate regulation of other intimately linked noncanonical Wnt signaling pathways, such as the Wnt/Planar Cell Polarity (PCP) pathway. Wnt/PCP signaling regulates developmental processes including convergent extension (CE) and oriented cell division (OCD). CE is a process required for the intercalation of tubule cells and resultant tubule extension rather than expansion, while OCD ensures that the mitotic spindle axis is oriented so the cell divides along the length of the tubule. Both of these events are required for normal kidney tubule development and are abnormal in cells lining kidney cysts, perhaps contributing to tubule expansion rather than elongation (162, 163). Wnt ligands have been shown to compete for receptor binding and use several of the same downstream mediators, suggesting that activation of one Wnt pathway may be at the expense of another (164, 165). This crosstalk between Wnt pathways also means that dysfunction in one pathway could disrupt the regulation of another. As an example, transgenic mice overexpressing the canonical Wnt ligand Wnt9b develop renal cysts (166), whereas

mice lacking Wnt9b expression have defects in PCP-regulated convergent extension and oriented cell division, but this also leads to the development of renal cysts (167), rendering it difficult to determine the causative event leading to cyst formation in either scenario. Evidence that defects in orientation of dividing cells does not precede cyst initiation suggests that PCP defects may be a secondary effect in renal cystic pathogenesis (163); however, it has also been pointed out that the low incidence of cancer in ciliopathy patients suggests that PCP defects rather than aberrant  $\beta$ -catenin signaling features more predominantly (168).

Canonical Wnts are classified as those that mimic the  $\beta$ -catenin overexpression effects of neural tube malformation or secondary body axis induction, although many of these act in a context dependent manner (169). Put in simplistic terms, activation of canonical Wnt target genes occurs when the major effector of this pathway, cytosolic  $\beta$ -catenin, escapes degradation by the constitutively active “destruction complex” and is allowed to enter the nucleus where it interacts with T cell factor (TCF) or lymphoid enhancer-binding factor (LEF) transcription factors (Fig 3A). When the canonical Wnt pathway is inactive, kinase members of the destruction complex, glycogen synthase kinase-3 $\beta$  (GSK3 $\beta$ ) and casein kinase 1 (CK1), sequentially phosphorylate  $\beta$ -catenin, targeting it for  $\beta$ -transducin repeat containing E3 ubiquitin protein ligase ( $\beta$ -TrCP) mediated ubiquitylation and subsequent degradation by the proteasome. Binding of a Wnt ligand to a Frizzled (Fz) receptor in the presence of low-density lipo-protein receptor-related protein-5 or -6 (LRP-5/6) coreceptors recruits the entire destruction complex to the membrane where it can no longer interact with  $\beta$ -TrCP and instead binds and phosphorylates LRP-5 or -6, enhancing the Wnt response (156, 170, 171). The switch in destruction complex function is mediated by the Wnt-induced activation of the protein Dishevelled (Dsh or Dvl), which aids in the clustering of Fz and LRP receptors and relocation of the destruction complex to the plasma membrane (172–174). In contrast to its cytosolic/nuclear role in enhancing canonical Wnt response, membrane-bound Dsh is important in mediating the non-canonical Wnt/PCP signaling, which functions independently of  $\beta$ -catenin. Although Wnt/PCP signaling is not as well defined, it requires Dsh to localize asymmetrically at the cell membrane where it is involved in downstream activation of small GTPases Rho and Rac, as well as activation of c-Jun N-terminal kinase (JNK) and inhibition of GSK3 $\beta$ , both of which influence microtubule dynamics (172; Fig 3B). The mechanisms controlling the switch in Dsh activation are also not yet clear; however, evidence exists to suggest that calcium signaling may play a key role in antagonizing the canonical Wnt pathway (150, 165, 175). As noted above, calcium influx due to ciliary bending releases a pool of intracellular calcium leading to various downstream effects that could contribute to cyst formation if de-regulated. Expression of a Dsh mutant able to activate Wnt/PCP but not canonical Wnt signaling also leads to an increase of intracellular calcium release (176). The switch to Dsh-dependent Wnt/PCP activation may depend on the expression of ciliary proteins including the nephrocystins, and may require ciliary-dependent restraint of Dsh-dependent canonical Wnt signaling.

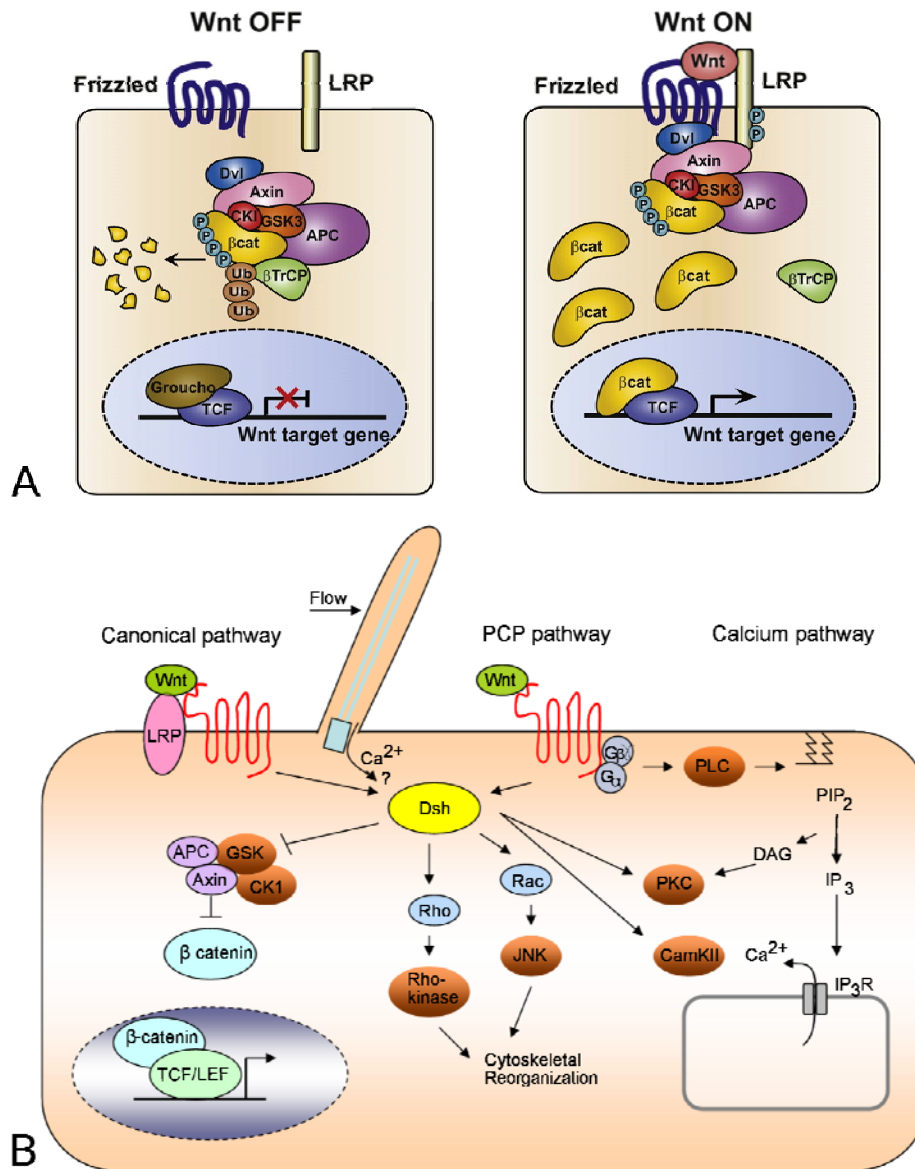


**Figure 3. Wnt signaling pathways.**

**A.** Canonical Wnt signaling in an inactive “off” state (left), where  $\beta$ -catenin is constitutively degraded by the destruction complex, and its active “on” state (right), where the destruction complex binds LRP at the plasma membrane and can no longer ubiquitinate  $\beta$ -catenin, leading to its accumulation and nuclear translocation (171; Reprinted from *Cell*, Vol 149, Vivian Li *et al.*, Wnt signaling through inhibition of  $\beta$ -catenin degradation in an intact Axin1 complex, 1245-1256, Copyright 2012, with permission from Elsevier). **B.** Simplified schematic illustrating the relationship between three major Wnt signaling pathways. A Wnt ligand binds to a Fz receptor and activates either the Wnt/ $\beta$ -catenin (left), Wnt/PCP (middle), or Wnt/calcium signaling pathways depending on context (see main text). Dsh activates  $\beta$ -catenin signaling by inhibiting destruction complex member GSK3 $\beta$ , which promotes signaling cascades involved in cell proliferation. Dsh can also activate PCP signaling via downstream GTPases Rac and RhoA, leading to activation of JNK and Rho-kinase, which play an important role in cytoskeletal reorganization. Activation of Wnt/calcium signaling involves G protein-coupled receptors and Phospholipase C (PLC) mediated PIP<sub>2</sub> cleavage into Diacylglycerol (DAG) and IP<sub>3</sub>, promoting intracellular calcium release leading to Protein Kinase C (PKC) and Cam Kinase II (CamKII) activation. In addition to its role in PCP signaling, Dsh can directly activate of PKC and CamKII. Calcium influx due to ciliary bending may have a role in the degradation or membrane sequestration of Dsh. Figure based on (176–178), see main text for more detail.

### 3.3.2 The Wnt signaling pathway and the role of cilia & NPH proteins

The involvement of primary cilia in Wnt regulation is a highly debated topic, but several lines of evidence support a functional link. One of the first examples describing primary cilia as important in Wnt regulation was demonstrated in 2005 where the inversin (*INVS*) gene product NPHP2 interacted with Dsh and abrogated the ability of Dsh to stimulate canonical Wnt signaling (178). Furthermore, NPHP2 over-expression reduced cytosolic but not membrane-bound Dsh protein levels, and was required for convergent-extension movements in *Xenopus laevis* embryos. Morpholino knockdown of inversin caused renal cysts in developing zebrafish embryos that could be rescued by expression of diversin, a protein known to be important in Wnt/PCP signaling. As application of flow on cultured cells increased the protein levels of NPHP2, it was speculated that the initiation of urine flow in the developing kidney leads to an NPHP2-mediated switch from canonical Wnt signaling that is required in early development to  $\beta$ -catenin-independent Wnt signaling pathways that might be necessary to further develop or maintain tubular geometry, reflecting the developmental decrease in canonical Wnt activity post-nephrogenesis (179). It has since been reported that *Invs* mutant mice do not show abnormalities in canonical Wnt reporter activity or  $\beta$ -catenin localization during late kidney development (180), although human nephronophthisis patients with *INVS* nonsense mutations do display intensely upregulated diffuse  $\beta$ -catenin in non-dilated, dilated and cystic tubules, as well as nuclear  $\beta$ -catenin and Dsh in a subset of patient tubular cells (181).

The discrepancy of *in vivo* data pertaining to the requirement of NPHP2 in canonical Wnt regulation extends to the requirement of the cilium itself. Homozygous deletion of the axonemal kinesin subunit KIF3a, which is required for ciliogenesis, leads to upregulated canonical Wnt reporter activity in the developing mouse and increased nuclear  $\beta$ -catenin response to Wnt3a stimulation in *Kifa*<sup>-/-</sup> embryonic fibroblasts (182). The same study replicated these results using cells derived from two other knockouts that blocked ciliogenesis, *Odf1* and *Ift88*. These findings however, have since been contradicted *in vivo* and *in vitro* in embryonic mice lacking primary cilia due to the loss of *Ift88*, *Ift172*, *Kif3a*, or the retrograde motor protein *Dync2h1* (183) although a kidney-specific knockout of *Kif3a* led both to renal cysts and to upregulated  $\beta$ -catenin and canonical Wnt target gene *c-myc* (184). In the developing zebrafish embryo, *ift88* morpholino knockdown also led to loss of primary cilia and interrupted Hh signaling but did not display any of the common phenotypic readouts for canonical or non-canonical Wnt signaling, prompting the authors to suggest that cilia were required for Hh signaling but the basal body may be more important in Wnt regulation (185). Indeed, knockdown of any one of the centrosomal proteins *bbs1*, *bbs4*, or *bbs6* leads to upregulated canonical Wnt response as well as convergent extension defects in zebrafish (186); furthermore, the accompanying loss of basal body function interrupted the antagonism of canonical Wnt3a signaling by non-canonical Wnt5, which supports a role for the basal body in altering the behaviour of downstream Wnt effector molecules such as Dsh. However, the cilium itself is likely not completely irrelevant to canonical Wnt regulation, as loss of either of the ADPKD gene products polycystin-1 and polycystin-2, which

localize to primary cilia, leads to upregulated canonical Wnt target gene expression in cystic kidney epithelia (187, 188), and many of the canonical Wnt proteins localize to the cilium as well as the basal body (182, 189, 190). Although the relationship between cilia, the centrosome, and the Wnt signaling pathways leaves much to be discovered, it is largely believed that the ciliary/centrosome complex may influence the cellular response to canonical and non-canonical Wnt signaling in a reciprocal, if not proportionate, manner (60, 191).

In line with this, many of the nephrocystin proteins have also been shown to negatively regulate canonical Wnt signaling or to promote PCP, although whether this is due to their function at the centrosome or cilium is unclear. In addition to NPHP2/INVS, both NPHP3 and NPHP4 have independently been shown to negatively regulate Dsh-stimulated canonical Wnt reporter activity and to result in PCP defects if protein expression is reduced (192, 193). NPHP2 and NPHP4 have both been linked to degradation of cytosolic Dsh (178, 193), whereas NPHP8 homolog *rpgrlp11*, which is required for several PCP processes in zebrafish development, protects Dsh from degradation (194). Meanwhile, NPHP7 was shown to negatively regulate  $\beta$ -catenin-stimulated reporter activity, despite increasing nuclear  $\beta$ -catenin accumulation (195). Many of the nephrocystin proteins interact with each other, but the mechanisms by which these nephrocystin complexes are regulated or contribute to Wnt regulation are largely unknown. Recently, a novel mechanism linking canonical Wnt regulation with primary cilia was introduced. The ciliary Von-Hippel-Lindau protein (pVHL) was shown to stabilize protein levels of the short isoform of the gene for apoptosis and differentiation in epithelia (Jade-1; alias plant homeo-domain finger protein (PHF)17 isoform 1S), which can act as a transcription factor and regulator of apoptosis (196, 197). Jade-1 was recently also identified as a novel E3-ubiquitin ligase targeting cytosolic as well as nuclear  $\beta$ -catenin for proteasomal degradation (198) and may therefore be able to “fine-tune”  $\beta$ -catenin levels, contributing to the ciliary regulation of the Wnt response. Indeed, loss of pVHL disrupts ciliogenesis and leads to cystic kidneys in patients with VHL disease (199–201), which fits into a model where cyst formation involves derepressed canonical Wnt signaling due to decreased Jade-1 stabilization. It was previously reported that pVHL localizes to the primary cilium (200), although whether Jade-1 also localizes to the primary cilium is unknown. If the primary cilium is a connection point between Jade-1 and pVHL, it stands to reason that other ciliary Wnt regulators may likewise interact with Jade-1. In particular, Jade-1 could be a means by which nephrocystin proteins are able to influence Wnt regulation, thus contributing to the critical balance required for this signaling pathway in the kidney.

#### 4 THESIS AIMS

The biological factors leading to kidney cyst formation are largely unknown; however, progress toward understanding cystic kidney pathology has recently been propelled by the recognition that all proteins mutated in genetic forms of cystic kidney disease localize to primary cilia or the centrosomal region. In the past decade the primary cilium has been shown to be involved in several cellular signaling pathways, including canonical Wnt signaling. Specifically, the centrosome appears to be involved in targeting beta-catenin, the main effector of canonical Wnt signaling, for proteasomal destruction. De-regulated Wnt signaling in mice causes kidney cysts, and therefore may be a critical pathway regulated by the ciliary cystoproteins. In particular, several nephrocystin proteins have been reported to negatively regulate canonical Wnt signaling although mechanisms remain unclear. Recently, Jade-1 was identified to be an E3 ubiquitin ligase for  $\beta$ -catenin. Jade-1 was shown to be stabilized by the cystoprotein pVHL although it is unknown how this stabilization occurs, or whether ability to influence canonical Wnt signaling via the stabilization of Jade-1 might extend to other ciliary cystoproteins, such as the nephrocystins.

The specific hypothesis of this PhD project is that NPH proteins will stabilize Jade-1, leading to decreased canonical Wnt signaling. Loss of Jade-1 stabilization may therefore be a critical factor in the pathogenesis of the cystic kidney phenotype in Nephronopthisis.

The major aims of this PhD work are to:

1. Identify whether Jade-1 is a ciliary protein.
2. Characterize a potential connection between Jade-1 and the NPH proteins and their role in modulating Wnt signaling.
3. Determine the mechanisms underlying regulation of Jade-1 by the cilium and by nephrocystin proteins.

## 5 MATERIALS AND METHODS

### 5.1 Materials

#### 5.1.1 Chemical Reagents

**Table 1. List of Chemicals, Reagents and Solutions**

Chemical/Reagent/Solution	Product Number	Provider
Acetic Acid	7332.1	Carl Roth
Acrylamide	7906.2	Carl Roth
Agarose	A9539-500G	Sigma
Ammonium persulfate (APS)	A0834	Applichem
Ampicillin Sodium Salt	K029.2	Carl Roth
Aqua dest. Injectabile (PCR grade water)	PZN-1087335	Berlin-Chemie AG
Bovine Serum Albumin (BSA)	1066	Gerbu
Bromphenol Blue	A512	Carl Roth
Calcium chloride dihydrate	HN04.2	Carl Roth
Collagen A	L7220	Biochrom
Complete Protease Inhibitor Tablets (EDTA-free)	11873580001	Roche
Coumeric Acid	C-9008	Sigma
Dimethyl sulfoxide (DMSO) Hybri-Max	D2650	Sigma
Dithiothreitol (DTT)	6908.1	Carl Roth
Dulbecco's Modified Eagle Medium (DMEM)	D6429	Sigma
DMEM-F12	D6421	Sigma
Deoxyribonucleotide triphosphate (dNTP)-mix	200415	Stratagene
Ethidiumbromide solution (1%)	2218.2	Carl Roth
Ethylenediaminetetraacetic acid (EDTA)	E-5134	Sigma
Ethanol 96% + 1% Methyl ethyl ketone	WAL641.5000	Geyer
Ethanol 99.8%	9065.3	Carl Roth
Fetal Bovine Serum (FBS)	S 0115	Biochrom AG
Fetal kidney cDNA library (human)	780608	Stratagene
GeneRuler 1kb DNA Ladder	SM0311	Fermentas
Glucose (D+)-Monohydrate	1.04074.1000	Merck
Glycerol	3783	Carl Roth
Glycine	3908.2	Carl Roth
HEPES Buffer 1M	H0887	Sigma

Chemical/Reagent/Solution	Product Number	Provider
Hydrogen Peroxide 30%	107209	Merck
Incidin Plus	3011520	Ecolab
Isopropanol	5752.3	Carl Roth
LB-Agar	X965.1	Carl Roth
LB-Medium	X964.2	Carl Roth
L-Glutamine 200mM Conc.	25030-024	Invitrogen
Lipofectamine-2000	11668-027	Invitrogen
Loading Dye Solution (6X)	R0611	Thermo Scientific
Luminol	9253	Fluka
Magnesium acetate tetrahydrate	275.1	Carl Roth
Magnesium chloride heptahydrate	1.05833.0250	Merck
Methanol	4627.5	Carl Roth
MG132 Insolution	474791	Merck/Calbiochem
Normal Donkey Serum	017-000-121	Dianova
Okadaic Acid Sodium Salt	459620-20	Merck/Calbiochem
Oligofectamine	12252011	Invitrogen
Opti-MEM	31985-047	Invitrogen
PageRuler Plus Prestained Protein Ladder	26620	Fermentas
Passive Lysis Buffer 5x	E1941	Promega
Paraformaldehyde (PFA)	P6148	Sigma
Phenylmethylsulfonyl fluoride (PMSF)	P7626-25G	Sigma
Polyacrylamide	T802.1	Carl Roth
Potassium acetate	4820.1000	Merck
Potassium chloride	6781	Carl Roth
Potassium dihydrogen phosphate	P-018.2	Carl Roth
Power SYBR Green	4367669	Applied Biosystems
ProLong Gold antifade reagent with DAPI	P-36931	Invitrogen
Protein G Sepharose	GEHE17-0618-01	VWR
Qiazol	79306	Qiagen
RNase-free water Ultra Pure	10977-035	Invitrogen
Sepharose CL-4B	CL4B200	Sigma
Sodium-Bicarbonate Solution 7,5%	S8761	Sigma
Sodium chloride	3957.1	Carl Roth
Sodium dodecyl sulfate (SDS) pellets	CN30.3	Carl Roth
Sodium fluoride	S-1504	Sigma
Sodium(di-) hydrogen phosphate heptahydrate	1.06574.1000	Merck

Chemical/Reagent/Solution	Product Number	Provider
Sodium(tetra-) diphosphate decahydrate	1.06591.0500	Merck
Sodium orthovanadate	S6508-50G	Sigma
N,N,N',N'-tetramethylethylenediamine (TEMED)	2367.3	Carl Roth
Tris Hydrochlorid (HCl)	9090.3	Carl Roth
Trizma Base	T1503	Sigma
Triton X-100	1.08603.1000	Merck
Trypsin-EDTA Solution (1x)	T3924	Sigma
Tween20	3472	Caesar&Lorentz

### 5.1.2 Assays/Kits

**Table 2. List of Assays/Kits**

Assay/Kit	Product Number	Provider
Big Dye Terminator version 3.1 Sequencing kit	4337455	Applied Biosystems
Turbo DNA- <i>free</i> <sup>TM</sup>	AM1907	Ambion
Dual Luciferase Assay System	E1910	Promega
GeneJet PCR Purification Kit	K0702	Fermentas
GeneJet Gel Extraction Kit	K0692	Fermentas
GeneJet Plasmid Miniprep Kit	K0503	Fermentas
High Capacity cDNA Reverse Transcription	4368814	Applied Biosystems
KOD Hot Start DNA polymerase kit	71086	Merck/Novagen
NucleoBond® Xtra Midi prep kit	740410	Machury-Nagel
T4 DNA Ligase	EL0011	Fermentas
Venor® GeM Mycoplasma Detection Kit	11-1050	Minerva Biolabs
Zenon® Tricolor Mouse IgG2b Labeling Kit	Z25260	Molecular Probes
Zenon® Tricolor Rabbit IgG Labeling Kit	Z25360	Molecular Probes

### 5.1.3 Antibodies

All antibodies react specifically against human.

**Table 3. List of primary antibodies and their providers**

Antigen (epitope)	Clone	Source	IF	WB	Provider
14-3-3 $\beta$ (N-term)	(polyclonal)	Rabbit	-	1:1000	Santa Cruz
cMYC (N-term)	(polyclonal)	Rabbit	-	1:500	Cell Signaling
Fibrillarin (aa. 1-100)	(polyclonal)	Rabbit	-	1:500	Abcam
Flag (DYKDDDDK)	M2 (monoclonal)	Mouse	1:1000	1:10000	Sigma

Antigen (epitope)	Clone	Source	IF	WB	Provider
Flag (DYKDDDDK)	(polyclonal)	Rabbit	1:1000	1:1000	Sigma
Jade-1 (a.a. 5.201)	(polyclonal)	Rabbit	1:100	-	Genetex
Jade-1 (a.a. 1-301)	(polyclonal)	Rabbit	1:100	-	Proteintech
Jade-1 (Ab1: a.a. 450-509)	(polyclonal)	Rabbit	1:100	-	Sigma
NPHP1	62 (monoclonal)	Mouse	1:100	-	Zentgraf Lab
NPHP4 (a.a. 673–1032)	12H6-2B12 (monoclonal)	Mouse	1:100	-	Saunier Lab
Tubulin, acetylated- (acetylated Lys40 ± 4)	6-11B-1 (monoclonal)	Mouse	1:1000	-	Sigma
Tubulin, β-	E7 (monoclonal)	Mouse	-	1:5000	DSHB
Tubulin, gamma- (a.a. 437-451+ Nterm CG)	(polyclonal)	Rabbit	1:250	-	Sigma
V5 (GKPIPPELLGLDST)	SV5-Pk1 (monoclonal)	Mouse	1:1000	1:5000	Serotec
V5 (GKPIPPELLGLDST)	(polyclonal)	Rabbit	1:1000	1:1000	Millipore

**Table 4. List of secondary antibodies and their providers**

Antibody	Product Number	Provider
Cy3-AffiniPure Donkey α-Rabbit IgG (H+L)	711-165-152	Jackson ImmunoResearch
DyLight-488 AffiniPure Donkey α-Mouse IgG(H+L)	715-485-150	Jackson ImmunoResearch
DyLight-488 AffiniPure Donkey α-Rabbit IgG(H+L)	711-485-152	Jackson ImmunoResearch
DyLight-549 AffiniPure Donkey α-Mouse IgG(H+L)	715-505-150	Jackson ImmunoResearch
Polyclonal goat anti-rabbit immunoglobulins/HRP	P0448	Dako
Polyclonal goat anti-mouse immunoglobulins/HRP	P0447	Dako

#### 5.1.4 Enzymes

**Table 5. List of enzymes and their providers**

Enzyme	Product Number	Provider
DpnI 5000U	R0176L	New England Biolabs
Hind III restriction enzyme	R0104L	New England Biolabs
KpnI restriction enzyme	R0142L	New England Biolabs
MluI restriction enzyme	R0198L	New England Biolabs
NarI restriction enzyme	R0191L	New England Biolabs
NotI restriction enzyme	R0189L	New England Biolabs

### 5.1.5 Genes of Interest

**Table 6. Genes and isoforms investigated**

Gene (Human)	Gene ID (NCBI)	Isoform
$\beta$ -catenin	1499	NM_001904
CK1 $\alpha$ 2	1452	NM_001892.4
EPS	58513	NM_021235.2
GSK3 $\beta$	2932	NM_002093.3
Jade-1 short isoform	79960	NM_024900.3
NPHP1	AF023674	NM_001128178.1
NPHP2/INVS	BC111761	GenBank: BC006370.2
NPHP3	27031	NM_153240
NPHP4	261734	NM_015102
NPHP5	9657	NM_001023570.2
NPHP7	84662	NM_032575
NPHP8	23322	NM_015272
NPHP9	284086	NM_178170
PLK1	5347	NM_005030.3

### 5.1.6 Plasmids and their providers

**Table 7. List of plasmids used and their providers**

Vectors used	Provider
pcDNA <sup>TM</sup> 6/V5-His B	Invitrogen (V220-20)
M50 Super 8x TOPFlash	Addgene plasmid 12456 (Moon Lab)
M51 Super 8x FOPFlash	Addgene plasmid 12457 (Moon Lab)
<i>Renilla</i> luciferase pGL4.74	Promega (E6921)
F.EPS <sup>1-225</sup> pcDNA6	Nephrolab Cologne
V5.EPS <sup>1-225</sup> pcDNA6	Nephrolab Cologne
F.NPHP1 WT FL pcDNA6	Nephrolab Cologne
F.NPHP2/INVS WT FL pcDNA6	Open Biosystems clone ID 40012263
F.NPHP3 WT FL pcDNA6	Nephrolab Cologne
F.NPHP4 WT FL pcDNA6	Nephrolab Cologne
V5.NPHP4 WT FL pcDNA6	Nephrolab Cologne
F.NPHP5 WT FL pcDNA6	Nephrolab Cologne
F.NPHP7 WT FL pcDNA6	Nephrolab Cologne
F.NPHP8 WT FL pcDNA6	AG Walz, ZKF, University Hospital Freiburg

Vectors used	Provider
F:NPHP9 WT FL pcDNA6	Nephrolab Cologne
F:PLK1	Nephrolab Cologne

### 5.1.7 Oligonucleotides

All oligonucleotides were purchased from Biomers (Konstanz, Germany).

All inserts were designed for human genes.

**Table 8. List of oligonucleotides used**

CLONING PRIMERS	
Insert Name/Primer Name	Sequence (5' → 3')
<b>β-catenin FL WT</b>	
FP: hbcata 1 mlu	CGCGGGACGCGTATGGCTACTCAAGCTGATTTG
RP: h.beta catenin 782 not	CGCGGGGCGGCCCGCCTTACAGGTCAGTATCAAACCA
<b>CK1α1 WT FL</b>	
FP: hCK1alpha 1 mlu	CGCGGGACGCGTATGGCGAGTAGCAGCGGCTCC
RP: hCK1 alpha 305 not	CGCGGGGCGGCCCGCCTTATGCTTTCTGCTTTAACATTGT
<b>GSK3β WT FL</b>	
FP: hGSK3β 1 mlu	CGCGGGACGCGTATGTCAGGGCGGCCCAAGAAC
RP: hGSK3β 433 not	CGCGGGGCGGCCCGCCTCAGGTGGAGTTGGAAGCTGA
<b>Jade1 WT FL</b>	
FP: hJade-1 1 mlu	CGCGGGACGCGTATGAAACGAGGTCGCCTTCCC
RP: hJade-1 509 not	CGCGGGGCGGCCCGCCCTATAAGGTGTCAGTGTCAAT
<b>Jade1 1-149</b>	
FP: hJade-1 1 mlu	CGCGGGACGCGTATGAAACGAGGTCGCCTTCCC
RP: hJade-1 149 not	CGCGGGGCGGCCCGCCCTATGCAGCATCCATGTC
<b>Jade1 150-299</b>	
FP: hJade-1 150 mlu	CGCGGGACGCGTTGGCTGGAAGTACCAATGAA
RP: hJade-1 299 not	CGCGGGGCGGCCCGCCCTAGGGCTCCATCTTCTCTGG
<b>Jade1 300-509</b>	
FP: hJade-1 300 mlu	CGCGGGACGCGTATCACCAGGTGTCACACATT
RP: hJade-1 509 not	CGCGGGGCGGCCCGCCCTATAAGGTGTCAGTGTCAAT

## MUTAGENESIS PRIMERS

Insert Name/Primer Name	Sequence (5' → 3')
<b>Jade1 S13A</b>	
FP: hJade1 S13A fp	AGCAGCAGTGAGGATGCTGACGACAATGGCAGCCTGTCA
RP: hJade1 S13A rp	GCTGCCATTGTGTCGTCAGCATCCTCACTGCTGCTGGGAAG
<b>Jade1 S18A</b>	
FP: hJade1 S18A fp NarI	TCTGACGACAATGGCGCCCTGTCAACTACTTGGTCCCAG
RP: hJade1 S18A rp NarI	CCAAGTAGTTGACAGGGCGCCATTGTGTCGTCAGAATCCTC
<b>Jade1 S20A</b>	
FP: hJade1 S20A fp HindIII	GATTCTGACGACAATGGAAGCTTGGCAACTACTTGGTCCCA GAATTCC
RP: hJade1 S20A rp HindIII	CTGGGACCAAGTAGTTGCCAAGCTTCCATTGTCGTCAGAAT CCTC
<b>Jade1 S89A</b>	
FP: hJade1 S89A fp KpnI	GTCCAGGTGCCTGTGGCCCCGGGTACCATCCCTCAGCCT
RP: hJade1 S89A rp KpnI	CTGAGGGATGGTACCCGGGGCCACAGGCACCTGGACCCC
<b>Jade1 T92A</b>	
FP: hJade1 T92A fp NarI	CCTGTGAGCCCCGGGCGCCATCCCTCAGCCTGTGGCCAGG
RP: hJade1 T92A rp NarI	CACAGGCTGAGGGATGGCGCCCCGGGCTCACAGGCACCTG
<b>Jade1 S121A</b>	
FP: hJade1 S121A fp NarI	CAACTCGGGAGGCTCGGCGCCTGATGACACGATGTACTT
RP: hJade1 S121A rp NarI	CAACTCGGGAGGCTCGGCGCCTGATGACACGATGTACTT
<b>Jade1 S377A</b>	
FP: hJade1 S377A fp NarI	AGGAAACCCGAGGAGGCTCTTGGCAAGGGCGCCGCACAGG AGAATGGGGCC
RP: hJade1 S377A rp NarI	GGCCCCATTCTCCTGTGCGGCGCCCTTGCCAAGAGCCTCCTC GGTTTTCT

## qPCR Primer Pairs

Gene Name/Primer Pair	Sequence (5' → 3')
<b>Jade1 (human)</b>	
FP: qPCR Jade1 exon 7 fp	TGAAGCCCACCCGTAGCGGA
RP: qPCR Jade1 exon 9 rp	CTCCTGTGCAGCCCCCTTGC
<b>HPRT (human)</b>	
FP: hHPRT1 fp	TGACACTGGCAAAAACAATGCA
RP: hHPRT1 rp	GGTCCTTTTCACCAGCAAGCT

Sequencing Primers	
Gene /Primer Name	Sequence (5' → 3')
<b>pcDNA6 (-mlu) fsp1</b>	CGTGTACGGTGGGAGGTCTA
<b>pcDNA6 (-mlu) rsp 1</b>	AGGAAAGGACAGTGGGAGTG
<b>hJade1 bp.426-446 fsp</b>	CCTCAATGACATGGATGCTGC
<b>h. Jade1 bp.516-537 fsp</b>	GAGGGTCCTAGAGGAATTTGA
<b>h.beta catenin bp.1213-1232 fsp</b>	CTTGTTTCAGCTTCTGGGTTC
<b>h.beta catenin bp.1425-1405 rsp</b>	GTGTCGGCTGGTCAGATGACG
siRNA Oligonucleotides	
Gene Name/Oligo Name	Sequence (5' → 3')
<b>Jade1/HsPHF17_7</b> (Qiagen catalog no. SIO3077718)	GAAGACCATCTTAGCAGAGAA
<b>Jade1/HsPHF17_1</b> (Qiagen catalog no. SIO0137627)	AAGCGGGAGCAGGATGTCTTA
<b>Jade1/HsPHF17_5</b> (Qiagen catalog no. SIO3042669)	AGCAGCGATGCTACGACAATA
<b>NPHP4</b>	AAGCAACGAGATGGTGCTACA
<b>Scrambled (control)</b>	AAATGTACTGCGCGTGGAGAC

### 5.1.8 Buffers & Solutions

**Table 9. Composition of buffers & solutions**

Buffer / Solution	Composition
Annealing buffer (2x)	60 mM HEPES pH 7.4 4 mM Mg(CH <sub>3</sub> COO) <sub>2</sub> 200 mM CH <sub>3</sub> CO <sub>2</sub> K
Cell Culture Medium (293 T)	10% (v/v) FBS in DMEM
Cell Culture Medium (RPE-1)	10% FBS (v/v) 2 mM L-Glutamine 1.2 g/L Sodium bicarbonate in DMEM-F12
Cell Fraction Buffer A	10mM HEPES 1.5mM MgCl <sub>2</sub> 10 mM KCl pH 7.9
Cell Freezing Solution	70 % (v/v) FBS 20 % (v/v) DMEM 10 % (v/v) DMSO

---

Buffer / Solution	Composition
Dulbecco's PBS (DPBS)	1 mM CaCl <sub>2</sub> 0,5 mM MgCl <sub>2</sub> in 1xPBS
ECL Detection Solution	100 mM Tris 1,25 mM Luminol 0,2 mM Coumaric acid 0,75% (v/v) H <sub>2</sub> O <sub>2</sub> pH 8.5
HEBS (2X)	50 mM HEPES 280 mM NaCl 10 mM KCl 1.5 mM Na <sub>2</sub> HPO <sub>4</sub> pH 7.08
IP Lysis Buffer	20 mM Tris 1% (v/v) TritonX-100 50mM NaCl 15 mM Na <sub>4</sub> P <sub>2</sub> O <sub>7</sub> 50 mM NaF pH 7.5
Laemmli Sample Buffer (1X)	50 mM Tris 2% (w/v) SDS 10% (v/v) Glycerol Bromphenol Blue 50 mM DTT pH 6.8
Laemmli Sample Buffer (2X)	100 mM Tris 4% (w/v) SDS 20% (v/v) Glycerol Bromphenol Blue 100 mM DTT pH 6.8
Laemmli Sample Buffer (3X)	150 mM Tris 6% (w/v) SDS 30% (v/v) Glycerol Bromphenol Blue 150 mM DTT pH 6.8
Ligation Buffer (10X)	400 mM Tris 100 mM MgCl <sub>2</sub> 100 mM DTT 5 mM ATP pH 7.8

---

Buffer / Solution	Composition
Phosphate Buffered Saline (PBS)	137 mM NaCl 2.7 mM KCl 10 mM Na <sub>2</sub> HPO <sub>4</sub> 2 mM KH <sub>2</sub> PO <sub>4</sub>
Resolving Gel	750 mM Tris 10% (v/v) PAA 0.2% (w/v) SDS pH 8.8
Running Buffer	25 mM Tris 192 mM Glycine 0.1% (w/v) SDS
Stacking Gel	250 mM Tris 5% (v/v) PAA 0.2% (w/v) SDS pH 6.8
SOC Medium	2% (w/v) Tryptone 0.5% (w/v) Yeast Extract 8.6 mM NaCl 2.5 mM KCl 20 mM MgSO <sub>4</sub> 20 mM Glucose
TAE (1X)	40 mM Tris 20 mM Acetic Acid 1mM EDTA pH 8.5
Transfer Buffer	25 mM Tris 188 mM Glycine 0.1% (w/v) SDS
Wash Buffer	30 mM Tris 300 mM NaCl 0.3% Tween20 pH 7.5

### 5.1.9 Materials

**Table 10. List of materials and their providers**

Material	Product Number	Provider
10 cm dish for Agar Plates	82.1473	Sarstedt
Blotting paper (Type BF4, 580 x 580)	FT-2-521-580580G	VWR
Cell culture dishes (12-well)	3513	Corning

Material	Product Number	Provider
Cell culture dishes (6-well)	3516	Corning
Cell culture dishes (10-cm)	430167	Corning
Cell culture dish (96-well F-Form)	655180	Greiner BioOne
Cell culture dish (96-well U-Form)	650180	Greiner BioOne
Combs (10 well, 1 mm) for acrylamide gels	NC3010	Invitrogen
Coverslips (round 18 mm Nr. 1.5)	631-0153	VWR
Eppendorf tubes (1.5 ml)	72.690.001	Sarstedt
Fast Optical 96-well plates	4346907	Applied Biosystems
Gel cassette (1 mm)	NC2010	Invitrogen
Hemocytometer (Neubauer Improved)	-	BlauBrand
Polypropylene conical tube (15 ml)	188271	Greiner BioOne
Polypropylene conical tube (50 ml)	227261	Greiner BioOne
MicroAmp Optical Adhesive Film	4311971	Applied Biosystem
Millipore Immobilon-P Transfer Membranes	T831.1	Carl Roth
Needle (20G) Microlance™3 (1½")	301300	BD
Nunc Cryotube™	368632	Thermo Scientific
PCR Soft-tubes 0.2 ml assorted colours	711088	Biozym
PCR Soft-tubes 0.2 ml clear	710920	Biozym
PCR Soft-tubes 0.2 ml 8 Tubes/Flat Caps, clear	710970	Biozym
Pipette tips (200 µl yellow)	70.762	Sarstedt
Pipette tips (1000 µl blue)	70.760.002	Sarstedt
Safe Lock 1,5 ml Eppendorf tubes	211-2130	VWR
Stripettes (5 ml)	4051	Corning
Stripettes (10 ml)	4101	Corning
Stripettes (25 ml)	4251	Corning
SuperFrost®/Plus microscope slides	7695002	Th.Geyer Group
Syringe (Plastipak™ 1 ml)	7392/2007	BD
TipOne (0.1-10 µl XL), sterile	S1110-3810-c	Starlab
TipOne (1-200 µl beveled), sterile	S1111-1816-c	Starlab
TipOne (101-1000 µl graduated), sterile	S1111-2831-c	Starlab
Ultra-Clear Tubes (UZ Tubes)	344062	Beckman Coulter
Weighing tray 140 x 140 mm	2159.1	Carl Roth
Weighing tray 89 x 89 mm	2150.1	Carl Roth

### 5.1.10 Equipment

**Table 11. List of equipment and their providers**

Equipment	Model	Provider
Analogue tube rolloer	SRT6	Stuart
Autoclave	V-150	Systec
Avanti centrifuge	J-301	Beckman
Axiovert microscope and apotome system	200M	Carl Zeiss MicroImaging
Centrifuge (refrigerated)	5810 R	Eppendorf
Eppendorf Research® Multipipette (10-100 µl)	3122000043	Eppendorf
Fast Real-Time PCR System	7900HT	ABI
Fusion Solo chemiluminometer	60-FU-SOLO	PeqLab
Hamilton syringe (50 µl Type 705)	549-1155	VWR
HERAcell Incubator	240	Heraeus
HERAcell Incubator	150	Heraeus
Heraeus B12 Function Line incubator	50042307	Kendro Laboratory Products
Horizontal electrophoresis system	1582 - 030305	Dan-Kar
Incubator (Agarose)	T 6030	Heraeus
Innova Incubator Shaker	4400	New Brunswick Scientific
Inverted microscope	CK2	Olympus
JuLi™ Smart Fluorescence Cell Imager	DBJ01B	Bulldog Bio
Laminar Flow Cabinet	HS12	Heraeus
MacsMix Tube Rotator	MX100	Miltenyi Biotech
Microcentrifuge	5424	Eppendorf
Microcentrifuge (refrigerated)	5415 R	Eppendorf
Microcentrifuge (refrigerated)	5417R	Eppendorf
Mithras multimode microplate reader	LB 940	Berthold Technologies
Multifuge	4KR	Heraeus
Nanodrop Spectrophotometer	1000	PeqLab
Pipetboy acu	155 015	Integra Biosciences AG
Pipetman Pipette set (P2, P10, P100)	F167500	Gilson
Pipetman Pipette set (P20, P200, P1000)	F167300	Gilson
Power supply (for Dan-Kar system)	EPS200	Pharmacia Biotech
Powerpac 200 Power supply	1655052	Bio-Rad
Powerpac 3000 Power supply	1655057	Bio-Rad
Shaker	KS 260	IKA
Suction Pump	MD 4C	Vacuubrand

Thermal cycler (MJ mini)	PTC-1148	Bio-Rad
Thermomixer Comfort 1.5 ml Thermoblock	5360 000.011	Eppendorf
Thermomixer Comfort shaker & heating plate	5355 000.011	Eppendorf
Ultra-centrifuge (Optima)	TLX-120	Beckman
Ultra-centrifuge rotor	TLA-55	Beckman
UV Transilluminator system	MW312	Intas
Vortex Mixer	MS525-20	Heidolph (Reax)
Water bath	WNB 22	Memmert
Water bath (digital heating bath)	HBR4	IKA
XCell SureLock™ Mini-Cell electrophoresis system	100601-1408	Invitrogen

### 5.1.11 Software

Table 12. List of software used and their providers

Software	Version	Provider
Axiovision	4.8	Carl Zeiss MicroImaging
Edit-Seq	5.06	DNASTAR
FinchTV	1.4.0	Geospiza Inc.
Fusion-CAPT	15.16	Vilber Lourmat
GDS	3.10	Intas Science Imaging Instruments GmbH
Graphpad Prism 5 for Windows	5.2	GraphPad Software Inc.
Macromedia Freehand MX	2003	Adobe
Microsoft Office Suite	2003	Microsoft
MikroWin	2000	Berthold Technologies
Nanodrop 1000	3.7	Thermo Scientific
SeqManII	5.06	DNASTAR
SDS Software	2.4	Applied Biosystems

Software (online)	Website
Ensemble.org	<a href="http://www.ensembl.org/">http://www.ensembl.org/</a>
NCBI Primerblast software	<a href="http://www.ncbi.nlm.nih.gov/tools/primer-blast/">http://www.ncbi.nlm.nih.gov/tools/primer-blast/</a>
NCBI Pubmed	<a href="http://www.ncbi.nlm.nih.gov/pubmed/">http://www.ncbi.nlm.nih.gov/pubmed/</a>
NEB Double Digest Finder	<a href="http://www.neb.com/nebecomm/doubledigestcalculator.asp">http://www.neb.com/nebecomm/doubledigestcalculator.asp</a>

## 5.2 Methods

### 5.2.1 Plasmids & siRNA

#### 5.2.1.1 Cloning PCR

All Flag- and V5-tagged constructs were generated by PCR from a fetal human kidney cDNA library (Stratagene) using KOD Hot Start polymerase kit using a modified version of the manufacturer's instructions (per 50  $\mu$ l reaction: 30  $\mu$ l PCR grade water; 4.5  $\mu$ l  $\text{MgSO}_4$  (25 mM); 2.5  $\mu$ l DMSO; 5  $\mu$ l dNTPs (2 mM); 0.5  $\mu$ l forward primer (100  $\mu$ M); 0.5  $\mu$ l reverse primer (100  $\mu$ M); 1  $\mu$ l cDNA library (10 ng); 5  $\mu$ l KOD Buffer (10x); 1  $\mu$ l KOD Hot Start DNA polymerase (1 U/ $\mu$ l)). Cloning primers were used as indicated in Table 8. Reaction ingredients were assembled in 0.2 ml PCR soft-tubes on ice. The reaction was run using an MJ mini thermal cycler. The PCR Polymerase was activated at 95°C for 2 minutes, followed immediately by a 40 repetitions of a three-step cycle consisting of: 1) Denaturing for 20 seconds at 95°C; 2) Annealing for 20 seconds at [Primer  $T_m$  - (5-10) °C]; 3) Extension for 1 minute/kbp at 70°C. The PCR cycle was optimized by adding a final incubation step of 10 minutes at 70°C to allow for re-annealing of double stranded DNA. PCR products were purified using the GeneJet PCR Purification kit according to the manufacturer's instructions.

#### 5.2.1.2 siRNA Annealing

Annealing of siRNA was based on the published protocol (202). All siRNA oligonucleotides were resuspended in 10 mM Tris (pH 8.0) using an appropriate volume to produce a final concentration of 100 pmol/ $\mu$ l. Equal volumes of each strand were combined in a 1:1 ratio on ice, and diluted with RNase-free water to a concentration of 40  $\mu$ M. An equal volume of 2x Annealing buffer was added to yield a final concentration of 20  $\mu$ M. The mixture was heat-shocked for 1 minute at 95°C and subsequently incubated for 1 hour at 37°C. Annealing success was evaluated by running samples on a 3% agarose gel (section 3.2.1.5) and comparing product size to a single stranded oligonucleotide sample.

#### 5.2.1.3 Mutagenesis PCR

All mutagenesis reactions used the plasmid templates and primers as indicated in Table 8 and were based on the QuikChange protocol (203). Primers were designed to alter the amino acid of interest to alanine by changing the minimum number of bases required. A silent mutation was added to yield a novel restriction site for diagnostic digest as indicated in Table 8. Primers were designed to

have a  $T_m$  not less than 78°C and a GC content over 40%, with the mutation site flanked by 15 bases upstream and 21 bases downstream. The following components were assembled per 50 µl reaction in a 0.2 ml PCR soft-tube on ice: 32 µl PCR grade water, 5 µl DMSO, 4.5 µl MgSO<sub>4</sub> (25 mM), 0.5 µl dNTP-mix (25 mM each), 5 µl KOD Buffer (10x); 1 µl KOD Hot Start DNA polymerase (1 U/µl); 1 µl DNA plasmid template (10 ng/µl); 0.2 µl forward mutagenesis primer (50 µM); 0.2 µl reverse mutagenesis primer (50 µM). Using an MJ mini thermal cycler, the polymerase was activated at 95°C for 2 minutes, followed immediately by 16 repetitions of a three-step cycle consisting of: 1) Denaturing for 45 seconds at 95°C; 2) Annealing for 1 minute at 55°C; 3) Extension for 2 minute/kilobase-pair at 68°C. The PCR cycle was optimized by adding a final incubation step of 10 minutes at 68°C to allow for re-annealing of double stranded DNA. Reaction efficiency was assessed using a 1% agarose gel to check for amplification of the vector in comparison to a control run without enzyme. For successful reactions the remainder of the sample was incubated with 1 µl of Dpn1 for 2 hours at 37°C followed by heat inactivation at 70°C for 10 minutes, in order to digest methylated template DNA.

#### 5.2.1.4 Enzymatic Digest

Enzymatic digests were performed using enzymes and buffers from New England BioLabs (NEB) according to a modified version of the manufacturer's protocol. All cloning PCR products intended to be used for novel plasmid generation contained an N-terminal mlu1 restriction site and a C-terminal not1 restriction site. Cloning PCR products digested using these enzymes could therefore be ligated to the vector pcDNA6 backbone of an existing plasmid which had been digested in a similar fashion. A digest intended for subsequent gel extraction (section 3.2.1.6) was performed as a 30 µl reaction using PCR grade water plus the following components: 500ng DNA, 3 µl BSA (15 µM), 3 µl NEB buffer #3, 0.5 µl Mlu1 (5 U/µl), and 0.5 µl Not1 (5 U/µl). Reactions were incubated at 37°C for 2 hours and analysed using a 1% agarose gel (section 3.2.1.5).

After bacterial transformation (section 3.2.2) all clones were screened in a diagnostic digest. For newly cloned plasmids Mlu1 and Not1 enzymes were used, and for mutated plasmids either Mlu1 or Not1 was used together with the enzyme corresponding to the inserted novel restriction site (as indicated in Table 8). Diagnostic digests were performed in a 15 µl reaction using PCR grade water plus the following components: 400ng DNA, 1.5 µl BSA (15 µM), 1.5 µl NEB buffer (as appropriate for enzymes used and selected using NEB Double Digest Finder software), 0.4 µl each enzyme (at 5 U/µl). Reactions were incubated at 37°C for 30 minutes and analysed using a 1% agarose gel (section 3.2.1.5).

### 5.2.1.5 Agarose Gel Electrophoresis

DNA electrophoresis was performed according to standard protocols (204). Gels were made by pouring 11 ml of warm 1% Agarose in 1 x TAE buffer on a glass plate measuring 5 x 7.5 cm and fixing a Plexiglas comb (3 mm teeth) at one end. For general use, a stock of 1% Agarose solution was kept warm in a Heraeus T 6030 incubator. For siRNA, freshly prepared 3% Agarose in 1 x TAE buffer was used. After cooling, the comb was removed and the entire gel was placed in the Dan-Kar horizontal electrophoresis system filled with 1 x TAE buffer. DNA samples were mixed with an appropriate volume of 6X loading dye solution and 15  $\mu$ l of this solution was loaded per well using a 100  $\mu$ l pipette, with one well per gel reserved for 3  $\mu$ l of a 1kb DNA ladder to enable sample size estimation. Gels were run at 90V for 30 minutes using an EPS200 power supply. DNA was visualized using an Intas UV Transilluminator system and photographed using Intas GDS Windows software. DNA sample size was assessed in comparison to the 1kb DNA ladder.

### 5.2.1.6 Gel Extraction

Plasmid inserts and vectors (section 3.2.2) intended for ligation (section 3.2.1.7) were digested with Mlu1 and Not1 restriction enzymes (section 3.2.1.4) and separated using a 1% agarose gel (section 3.2.1.5). Required DNA bands were excised from the gel using a scalpel under UV-light. Protective clothing and face mask were worn at all times. The excised gel slice was melted at 60°C and DNA was extracted using the GeneJet Gel Extraction Kit as per the manufacturer's instructions, with a final elution volume of 30  $\mu$ l.

### 5.2.1.7 Ligation

Appropriate pairs of insert DNA and vector DNA were ligated after extraction from agarose gel (section 3.2.1.6). Ligations were performed using the T4 ligase kit with a modified protocol of the manufacturer's instructions: in a 20  $\mu$ l reaction in PCR grade water the following components were added: 2  $\mu$ l T4 ligase buffer (10x), 2  $\mu$ l vector DNA, 8  $\mu$ l insert DNA, and 0.4  $\mu$ l T4 ligase (5 U/ $\mu$ l). Reactions were incubated 1 hour at room temperature. A control reaction substituting water in place of insert DNA was included.

## 5.2.2 Clone Selection and Plasmid Amplification

Ligated plasmids were prepared as described in 3.2.1. In all cloning conditions a modified pcDNA<sup>TM</sup>6/V5-His B vector purchased from Invitrogen was used. To modify for standard cloning using an Mlu1/Not1 digest insert (section 3.2.1), an internal Mlu1 site was removed by standard

mutagensis PCR (section 3.2.1.3). A cloning cassette was then inserted using the HindIII and NotI sites after the CMV promoter. The cloning cassette contained the following sites: HindIII restriction site; Kozak sequence; Flag-tag sequence; 9 x HIS-tag sequence; BamHI restriction site; glycine spacer; *eco*R1 restriction site; MluI restriction site; NotI restriction site. The purchased pcDNA<sup>TM</sup>6/V5-His B vector included an ampicillin resistance gene.

### 5.2.2.1 Bacteria

ElectroMAX<sup>TM</sup> DH10B<sup>TM</sup> T1 Phage-Resistant electrocompetent *E. coli* cells were purchased from Invitrogen (Product number 12033-015) and stored in 50  $\mu$ l aliquots at -80°C until use.

### 5.2.2.2 Transformation

Bacterial transformation was performed using standard techniques (205). DH10 bacteria were thawed on ice. 5  $\mu$ l of ligation or control ligation (section 3.2.1.7) was added to 25  $\mu$ l bacteria and incubated on ice for 10 minutes. Bacteria were heat shocked for 45 seconds at 42°C using an IKA digital heating water bath. After heat-shock, bacteria were incubated on ice for 2 minutes prior to adding 175  $\mu$ l of warmed SOC medium. Bacteria were then incubated at 37°C for 1 hour using an Eppendorf Thermomixer shaker with 1.5 ml Thermoblock at 800-1200 rpm, and subsequently 50  $\mu$ l was pipetted onto a pre-warmed selective agar plate. Bacteria were streaked over the plate using a glass spatula sterilized by ethanol and fire. After drying, plates were incubated in a Heraeus B12 Function Line incubator at 37°C overnight. Selective agar plates were made by dissolving 4g of LB-Agar in water and adding 100  $\mu$ g/ml of ampicillin antibiotic. The solution was autoclaved and poured into 92 x 16 cm Sarstedt petri dishes under laminar flow. After cooling plates were stored at 4°C until use.

### 5.2.2.3 Bacterial culture

Bacteria grown on agar plates were incubated overnight at 37°C. Surviving colonies that had been transformed with the experimental ligation product were compared to surviving colonies that had been transformed with the control ligation product and an appropriate number of colonies were picked using a 200  $\mu$ l pipette tip and dropped into a 15 ml conical tube containing 3 ml of LB Medium (206). This bacterial mini culture was incubated at 37°C in the Thermoshake incubator for at least 8 hours or until cloudy at which time 1 ml was used for amini-prep (section 3.2.2.4). After diagnostic digest (section 3.2.1.4) and analysis following agarose gel separation (section 3.2.1.5), the remaining 2 ml from a positive clone was used to start a midi culture consisting of 200 ml LB medium. Midi preps

were incubated overnight at 37°C in the Innova 4400 shaker incubator. LB medium was freshly prepared using 20g/L of LB-Medium in water and adding 100 µg/ml ampicillin antibiotic.

#### **5.2.2.4 Plasmid preparation**

Plasmids were purified from 1 ml mini cultures by SDS/alkaline lysis and silica membrane purification using the GeneJet Plasmid Miniprep Kit according to the manufacturer's instructions and using an Eppendorf 5424 microcentrifuge. Plasmids were purified from a 200 ml midi culture by modified alkaline/SDS lysis and charged silica bead column purification using the NucleoBond Xtra midi prep kit according to the manufacturer's instructions. Bacterial pellets were acquired using the Heraeus multifuge and DNA pellets were acquired using the Beckman Avanti centrifuge. Pellets were washed twice with 75% (v/v) Ethanol and left to dry in an open 50 ml conical tube. When clear, 200-400 µl of 10 mM Tris buffer (pH 7.5) was added on top of the pellet and incubated overnight. The resultant DNA solution was vortexed, briefly centrifuged using the Eppendorf 5810R centrifuge, and transferred to a 1.5 ml Eppendorf tube. The solution was then centrifuged at 20,000 x g using the Eppendorf 5424 microcentrifuge and transferred to a sterile 1.5 ml safe-lock Eppendorf tube. Plasmid concentration was determined using the Nanodrop 1000 spectrophotometer according to manufacturer's instructions.

#### **5.2.2.5 Sequence verification**

Insert DNA sequences of newly cloned or mutated plasmids were verified by purchasing automated DNA sequencing service from the Cologne Centre for Genomics. Samples were prepared for sequencing using the Big Dye Terminator version 3.1 sequencing kit according to the manufacturer's instructions with a modified reaction protocol. Samples were prepared as a 10 µl reaction in PCR grade water plus the following components: 2.25 µl Big Dye Terminator sequencing buffer, 0.25 µl Big Dye Terminator version 3.1, and 0.25 µl sequencing primer (100µM). Using an MJ mini thermal cycler, the following cycle was repeated 32 times: 1) Denaturing for 10 seconds at 96°C; 2) Annealing for 5 seconds minute at 55°C; 3) Extension for 4 minutes at 60°C. In every case, the forward and reverse pcDNA6 sequencing primers were used (Table 3.1.7). Longer inserts required additional sequencing reactions using the primers indicated in Table 3.1.7. Sequence readings were assessed using EditSeq and SeqManII (DNASTAR) software as well as FinchTV software.

### 5.2.3 Cell Culture

#### 5.2.3.1 Cell lines: HEK 293T and RPE-1

Immortalized Human Embryonic Kidney (HEK) 293T cells were provided by Dr. Brian Seed (Harvard Medical School, Boston). Retinal pigmented epithelial (RPE)-1 cells were purchased from ATCC (human telomerase reverse transcriptase (hTERT) immortalised cell RPE-1 cell line; Product number CRL-4000™). Although this is a telomerase-immortalized cell line it was important not to exceed 35 passages or 80% confluency as doing so interfered with the uniformity of cell profile. HEK 293T cells were incubated in 293T medium and stored in the HERAcell 240 incubator which maintained 37°C with 5% carbon dioxide. RPE-1 cells were incubated in RPE-1 medium and stored in the HERAcell 150 incubator which maintained 37°C with 5% carbon dioxide. When experimentally required, cilia growth was stimulated in RPE-1 cells by growing cells to 70-80% confluency and then serum-starving for 24-48 hours in RPE-1 medium lacking FBS supplement.

All cell culture techniques were performed according to standard protocols (207). All cells were maintained in 10 cm culture dishes and handled until harvesting exclusively under laminar flow. Cells were passaged upon reaching 80% confluency. To passage the cells, the cell media was aspirated using the Vacuubrand suction pump and cells were washed with sterile PBS. After PBS aspiration, 1 ml trypsin was added prior to incubation at 37°C until cells were no longer adherent. A single cell suspension was achieved after addition of 9 ml warm medium by gentle trituration using a 10 ml stripette, avoiding air bubbles. The resultant 10 ml cell suspension was divided into 2 ml portions and added to new cell culture dishes each containing 8 ml of warm medium. Dishes were gently rocked from side to side to evenly disperse cells and centripetal force was avoided when returning dishes to the incubator. When experiments required use of a 6-well or 12-well culture dish, 2 ml of the re-suspended cells was added to 10 ml of medium and mixed using a 10 ml stripette. The resultant 12 ml solution was then evenly distributed over the 6-well or 12-well culture dish. When experiments required the use of a 96-well cell culture plate, re-suspended cells were counted using a Neubauer Improved hemacytometer and appropriate amount of medium was added to achieve 400,000 cells per ml. The cell suspension was transferred to a V-bottom dish and 100 µl of the cell suspension was added per well using an Eppendorf Research® Multipipette multipipette.

When necessary, cells were frozen to maintain a stock at a lower passage number. To freeze, a confluent 10 cm dish of cells was trypsinized and resuspended in appropriate cell culture medium. Cells were gently pelleted at room temperature using the Eppendorf 5810R centrifuge at 86 x g and the supernatant was removed. The cell pellet was resuspended in 1 ml of Cell Freezing Medium and transferred to a 1.8 ml Nunc Cryotube, which was placed in a thick Styrofoam box and frozen at -20°C for 2 hours before transferring to -80°C. To thaw, cell vials were hand-warmed and resuspended in 9 ml of warm medium in a 15 ml conical tube. Cells were gently centrifuged at room temperature using

the Eppendorf 5810R centrifuge at 86 x g and the supernatant was removed. Cells were again resuspended in 9 ml of warm medium and transferred to a 10 cm culture dish and incubated at 37°C overnight in a quarantined incubator. The following day cells were washed with warm medium or split 1:1 depending on growth, and afterward were split as described above upon reaching 80% confluency. One dish was reserved for two days without changing the medium in order to complete a mycoplasma test using the Venor® Mycoplasma Detection kit according to the manufacturer's instructions.

### 5.2.3.2 Transfection: CaCl<sub>2</sub> Method

HEK 293T cells were transfected using the CaCl<sub>2</sub> method for all standard plasmid transfections (208, 209). For experiments requiring a larger amount of protein, 10 cm dishes were used. Appropriate amounts of plasmids were added to a 1.5 ml Eppendorf tube containing 400 µl CaCl<sub>2</sub> for each experimental data point. When required, DNA amounts between experimental data points were balanced by adding an appropriate amount of pcDNA6 vector not containing a coding insert (empty vector). Under laminar flow, 400 µl of 2 x HEBS solution was added to the CaCl<sub>2</sub> solution dropwise while vortexing. The complete solution was then added drop-wise to a 10 cm dish of HEK 293T cells at 60% confluency. For experiments requiring transfection of a 6-well culture dish, DNA was pipetted into 100 µl of CaCl<sub>2</sub>, and 100 µl of 2 x HEBS was added drop-wise while vortexing under laminar flow. For experiments requiring transfection of a 12-well culture dish, DNA was pipette into 50 µl of CaCl<sub>2</sub>, and 50 µl of 2 x HEBS was added drop-wise while vortexing under laminar flow. In all cases, the medium was replaced 6-8 hours after transfection and cells were harvested the following day.

### 5.2.3.3 Transfection: Lipofectamine Method

For experiments in a 96-well format and for experiments require siRNA knockdown, cells were grown to 80% confluency and transfected using Lipofectamine 2000 according to a modified version of the manufacturers instructions. Under laminar flow, the required amount of DNA with or without siRNA was added to 90 µl of Opti-MEM in a 1.5 ml Eppendorf tube or a V-bottom 96-well cell culture dish. In a separate 1.5 ml Eppendorf tube, 2.5 µl of Lipofectamine per µg of DNA transfected was incubated in 90 µl of Opti-MEM at room temperature for 5 minutes. After 5 minutes, the lipofectamine solution was added to the DNA solution and incubated for 20 minutes at room temperature. After this time, the mixed solution was added to an appropriate amount of warm cell culture medium and the cell media was exchanged. In the case of a 96-well transfection, 50 µl of the mixed solution was added directly to each of 3 separate wells using a multipipette.

#### 5.2.3.4 Reagent incubation

When required, cells were incubated with 1  $\mu$ M okadaic acid in DMEM for 45 minutes, or with 1  $\mu$ M MG132 in DMEM for 4 hours. Control cells were incubated with an equal concentration of the appropriate solvent in DMEM. In all cases, solutions were prepared using pre-warmed medium in a conical tube under laminar flow, and the cell media was exchanged.

#### 5.2.4 Biochemistry/ Molecular Biology

All basic biochemistry and molecular biology was performed according to standard techniques (210) with modifications as indicated. All experiments were validated by a minimum of three biological replicates.

##### 5.2.4.1 Whole cell lysate

To prepare whole cell lysates (WCL), cells were harvested on ice 24 hours after transfection in 1 ml cold PBS and transferred to a 1.5 ml Eppendorf tube. Cells were pelleted at 20,000  $\times g$  using the Eppendorf 5415 R microcentrifuge for 30 seconds at 4°C. The supernatant was aspirated and cells were resuspended in 80  $\mu$ l Laemmli sample buffer (1X). During resuspension it was ensured that the entire pellet was lifted and suspended in the sample buffer. Samples were boiled for 10 minutes using an Eppendorf Thermomixer shaker with 1.5 ml Thermoblock set to 0 rpm and 95°C, and then re-pelleted for 5 minutes at 20,000  $\times g$  using the Eppendorf 5424 microcentrifuge. 30  $\mu$ l of the supernatant was analyzed by Western Blot (section 3.2.4.4).

##### 5.2.4.2 Immunoprecipitation

Immunoprecipitation (IP) experiments were performed as described previously. HEK 293T cells were harvested on ice 24 hours after transfection in 6 ml cold PBS and transferred to a 15 ml conical tube. When required, 1 ml of the resultant cell suspension was removed to a 1.5 ml Eppendorf tube for processing as a whole cell lysate (section 3.2.4.1). The remaining cell suspension was pelleted using the Eppendorf 5810 R centrifuge for 5 minutes at 4°C and 86  $\times g$ . The supernatant was discarded, and the pellet was resuspended in 1 ml IP Lysis Buffer plus 2 mM  $\text{Na}_3\text{VO}_4$  and 250  $\mu$ M PMSF. Cells suspensions were incubated on ice for 15 minutes, and then centrifuged at 20,000  $\times g$  for 15 minutes at 4°C using the Eppendorf 5415 R microcentrifuge. The supernatant was transferred to an Ultra-Clear ultracentrifuge tube and ultracentrifuged at 100,000  $\times g$  for 30 minutes at 4°C using the

Optima ultracentrifuge and TLA-55 rotor. 50  $\mu$ l of the post-ultracentrifugation supernatant was kept as the “IP lysate” and boiled for 5 minutes at 95°C after adding 50  $\mu$ l of Laemmli sample buffer (2X). The remaining post-ultracentrifugation supernatant was transferred to a 1.5 ml Eppendorf tube and incubated using the MacsMix tube rotator for 1 hour at 4°C with 30  $\mu$ l of prepared anti-Flag-agarose beads (M2). When required, supernatants were instead incubated for 1 hour at 4°C with 1  $\mu$ g anti-V5-antibody (monoclonal) followed by a second 1 hour incubation at 4°C with 30  $\mu$ l Protein G sepharose. After incubation, the sepharose or agarose was pelleted using the Eppendorf 5415 R microcentrifuge at 800 x *g* for 3 minutes at 4°C, and the supernatant was discarded. Pellets were washed 3 times by resuspending in 1 ml IP lysis buffer and centrifuging at 800 x *g* for 3 minutes at 4°C using the Eppendorf 5415 R microcentrifuge. After the last wash and supernatant removal, 30  $\mu$ l of Laemmli sample buffer (2X) was added to the pellet and gently mixed by flicking. Samples were boiled at 95°C for 5 minutes, and then re-pelleted for 5 minutes at 20,000 x *g* using the Eppendorf 5424 microcentrifuge. 30  $\mu$ l of the supernatant was analyzed by Western Blot (section 3.2.4.4).

#### 5.2.4.3 Subcellular Fractionation

HEK 293T cells were harvested on ice 24 hours after transfection in 6 ml cold PBS and transferred to a 15 ml conical tube. When required, 1 ml of the resultant cell suspension was removed to a 1.5 ml Eppendorf tube for processing as a whole cell lysate (section 3.2.4.1). The remaining cell suspension was pelleted using the Eppendorf 5810 R centrifuge for 5 minutes at 4°C and 48 x *g*. The supernatant was discarded and the cell pellet was resuspended in 100  $\mu$ l of the hypotonic Cell Fraction Buffer A plus 4.0  $\mu$ l Complete Protease Inhibitor Cocktail (25X stock solution as per the manufacturer’s instructions). Cells were incubated on ice for 10 minutes, and then disrupted 14 times using a 21-gauge needle and 1 ml syringe. The mixture was gently centrifuged at 100 x *g* for 30 minutes at 4°C using the Eppendorf 5415 R microcentrifuge in order to pellet the nuclear fraction. The supernatant was transferred to an Ultra-clear ultracentrifuge tube and ultracentrifuged at 100,000 x *g* for 60 minutes at 4°C using the Optima ultracentrifuge and TLA-55 rotor. 40  $\mu$ l of the resultant supernatant was transferred to a new 1.5 Eppendorf tube and mixed with 20  $\mu$ l of Laemmli sample buffer (3X), boiled for 5 minutes at 95°C, and centrifuged for 1 minute at 20,000 x *g* using the Eppendorf 5424 microcentrifuge to yield the cytosolic fraction. Meanwhile, the nuclear pellet was resuspended in 1 ml cold PBS and centrifuged at 9200 x *g* for 10 minutes at 4°C using the Eppendorf 5415 R microcentrifuge. The supernatant was discarded, and the remaining pellet was resuspended in 140  $\mu$ l of Laemmli sample buffer (1X), boiled for 10 minutes at 95°C and centrifuged for 5 minutes at 20,000 x *g* using the Eppendorf 5424 microcentrifuge to yield the nuclear fraction. 30  $\mu$ l of the supernatant was analyzed by Western Blot (section 3.2.4.4).

#### 5.2.4.4 Western Blot and Protein Detection

Proteins were separated by SDS-PAGE electrophoresis and visualized by HRP chemiluminescence. Each gel cassette was prepared by mixing 6 ml of Resolving Buffer with 0.15% TEMED and 0.1% APS and adding a top layer of Isopropanol. After hardening, all isopropanol was removed and replaced with 1.7 ml Stacking Buffer was mixed with 0.15% TEMED and 0.1% APS. A 10-well comb was inserted and the stacking gel was allowed to dry. Gels were assembled into the XCell SureLock™ Mini-Cell electrophoresis system as per manufacturer's instructions and the chamber was filled with Running Buffer so that the interior space between the gels was completely full and the exterior part was filled to a depth of 2 cm. Samples were loaded using a 50 µl Hamilton syringe which was cleaned 5 times with running buffer between each sample. One well was reserved to load 3 µl of Page-ruler Plus protein ladder. After all samples were loaded, gels were run using a Powerpac 3000 using the following program: 70 V for 30 minutes, then 25 milliamps per gel for approximately 2 hours, or until the ladder used had extended the entire length of the gel.

Separated proteins were transferred from the gel to a Millipore Immobilon-P polyvinylidene difluoride membrane using a Powerpac 200 power supply set to 12 V for one hour. To prepare the membrane for transfer, it was soaked first in methanol and then in Transfer Buffer, and placed onto a square of blotting paper which had been cut to size and also soaked in Transfer Buffer. The resolving gel was cut to the length of the ladder, soaked in Transfer Buffer, and placed on top of the membrane. A second square of blotting paper soaked in Transfer Buffer was placed on top, and air bubbles were rolled out using the length of a stripette. After transfer was complete, the protein ladder was traced in pen and the membrane was incubated in Washing Buffer plus 5% BSA for a minimum of 30 minutes at room temperature. Membranes were then washed 3 x 5 minutes with Washing Buffer, and incubated with the appropriate primary antibody as indicated in figure legends at a concentration indicated in Table 3.1.3. Primary antibodies were diluted in Washing Buffer and re-used. After primary antibody incubation, membranes were washed 3 x 5 minutes in Washing Buffer, and then incubated for 30 minutes with the appropriate HRP-conjugated secondary antibody (Table 3.1.4) diluted 1:15000 in Washing Buffer. After this time, membranes were once more washed 3 x 5 minutes in Washing Buffer. Excess buffer was then shaken off and membranes were transferred to a plastic tray. 1 ml of ECL Detection Solution was then applied per membrane and proteins were visualized using a PeqLab Fusion Solo chemiluminometer and Fusion-CAPT software.

#### 5.2.4.5 Immunofluorescence

Immunofluorescence experiments were performed according to standard techniques (211). Cells were grown in 12-well culture dishes on glass coverslips placed into wells using tweezers sterilized by fire under laminar flow. For experiments using HEK 293T cells, coverslips were coated

with Collagen A by incubating for 1 hour at 37°C. Excess Collagen A was removed and cover-slips were allowed to dry before passaging cells into the dish (section 3.2.3.2). After required experimental treatment, cells were fixed with 4% PFA or ice-cold methanol as indicated in figure legends. Cells were then washed once with Dulbecco's PBS, permeabilized for 8 minutes with 0.05% Triton X-100 in Dulbecco's PBS, and then blocked for 1 hour with 5% normal donkey serum in Dulbecco's PBS. Primary antibodies were incubated sequentially with for 1 hour using concentrations indicated in Table 3. For all endogenous staining, anti-Jade-1 was incubated first, except when combined with endogenous NPHP4 staining, in which case anti-NPHP4 was used first. Secondary antibodies (Table 4) were diluted 1:500 and used according to figure legends. Cover-slips were washed for a minimum of 4 x 5 minutes with Dulbecco's PBS between all antibody steps. When required as indicated by figure legends, Zenon® Tricolor Labeling Kits were used according to the manufacturer's instructions. Cover-slips were washed extensively with Dulbecco's PBS prior to mounting onto glass slides using Prolong Gold antifade reagent with DAPI as a mounting medium. Cells were visualized using an Axiovert 200 microscope (objective EC Plan Neofluar x 40/1.3 Oil) equipped with an AxioCam MRm and apotome system. Images were captured using Axiovision 4.8 software.

#### 5.2.4.6 Luciferase Assay

Luciferase reporter assays were performed according to standard procedure (212) using a 96-well transfection format. HEK 293T cells were passaged as described in section 3.2.3.2 and the resultant cell suspension was counted using a Neubauer Improved cell counting chamber. Cells were diluted to 400,000 cells /ml, and plated using an Eppendorf Research® Multipipette multipipette. When cells had reached 80% confluency a total amount of 140 ng of DNA per well was transfected using Lipofectamine 2000 (section 3.2.3.4) as follows and according to figure legends: 50 ng TOPFlash or FOPFlash firefly luciferase; 25 ng constitutively active *Renilla* luciferase pGL4.74; 5 ng Flag.β-catenin WT/mutant; 50 ng V5.Jade1 WT/mutant or empty vector; 10 ng V5.NPH protein/F.NPH protein/F.CK1α or empty vector. In all cases, experimental plasmids were added to a prepared master mix containing Flag-tagged β-catenin (F.β-catenin) and the reporter plasmids. Non-stimulated cells received only the reporter plasmids balanced with empty vector. For knockdown experiments, 20 nM of siRNA was incubated in Lipofectamine together with plasmids, as indicated in figure legends. Each transfection was performed in triplicate, and each experiment was repeated at least three times. After 24 hours, cells were lysed for 15 minutes at room temperature using the Promega passive lysis 5X buffer and analysis according to the manufacturer's instructions. Firefly and *Renilla* luciferase activities were analyzed using the Promega dual-luciferase reporter assay system and the Mithras LB940 luminometer according to the manufacturer's instructions. Wnt reporter activity was quantified as relative luciferase units (RLU) by scoring the Firefly reporter activation as measured per transfection efficiency as quantified by the *Renilla* luciferase activity. Data were

normalized by setting the “ $\beta$ -catenin plus empty vector” treatment group to 100%, and significance was assessed for all  $\beta$ -catenin stimulated treatment groups using a one-way analysis of variance (ANOVA) with Tukey's post-hoc test (section 3.2.7). To assess the effect of Jade-1 siRNA, data were normalized to set  $\beta$ -catenin stimulation to 100% separately for each Jade-1 siRNA condition. The amount that NPHP4 reduced the signal was then analyzed by normalizing so that the reduction by NPHP4 in the negative siRNA condition was set to 100%.

#### **5.2.4.7 RNA Extraction**

HEK 293T cells were seeded in a 6-well format (section 3.2.3.2) and transiently transfected for 24 hours using the CaCl<sub>2</sub> method (section 3.2.3.3) according to the figure legend. RNA was extracted based on a modified version of the guanidinium thiocyanate-phenol-chloroform extraction method (213). After transfection, cells were washed with PBS, harvested in 700  $\mu$ l of Qiazol and transferred to a 1.5 ml RNase-free Eppendorf tube. Cells were incubated for 5 minutes at room temperature prior to the addition of 120  $\mu$ l of Chloroform. The mixture was shaken vigorously and incubated for 2 minutes at room temperature, then centrifuged at 12000 x g for 15 minutes at 4°C using the Eppendorf 5417R microcentrifuge. 300  $\mu$ l of the aqueous phase was then transferred to a new 1.5 ml RNase-free Eppendorf tube and an equal volume of isopropanol was added. The mixture was again vigorously shaken and incubated for 15 minutes at room temperature. The RNA was pelleted by centrifugation at 12000 x g for 15 minutes at 4°C using the Eppendorf 5417R microcentrifuge. The supernatant was discarded using a 1 ml pipette tip, then briefly re-spun and any remaining supernatant was removed using a 10  $\mu$ l pipette tip. The RNA pellet was then washed by adding 1 ml of 75% (v/v) Ethanol and vortexing, and re-pelleted by centrifugation at 7000 x g for 5 minutes at 4°C using the Eppendorf 5417R microcentrifuge. The supernatant was again discarded using a 1 ml pipette tip, briefly re-spun, and any remaining supernatant was removed using a 10  $\mu$ l pipette tip. The RNA pellet was then dried by leaving the open Eppendorf tube on a clean surface for 2-5 minutes until the pellet was clear. The pellet was resuspended in 30  $\mu$ l of RNase-free water and the yield was measured using the Nanodrop 1000 spectrophotometer according to manufacturer's instructions.

#### **5.2.4.8 Real-Time quantitative qPCR**

Extracted RNA (section 3.2.4.7) was brought to a concentration of 0.2  $\mu$ g / $\mu$ l in RNase-free water and treated with the Turbo DNase kit according to the manufacturers instructions. Reverse transcription was performed using the High Capacity cDNA Reverse Transcription kit according to the manufacturers instructions. Jade-1 mRNA was assessed by SYBR Green qPCR and normalized by

using human HPRT1 mRNA as an endogenous control. Primers used are described in Table 3.1.7. Primers were designed using NCBI Primerblast software to produce an amplicon size of 50-150 base pairs with a CG content of 40-70%, and were checked for intron inclusion using Ensemble.org. Primers were resuspended in RNase-free water and appropriate pairs were combined in a 1:1 ratio to yield a concentration of 50  $\mu$ M each. Primer pairs were validated in a separate experiment by running a standard curve PCR with 4 cDNA dilutions (50 ng; 5 ng; 0.5 ng; 0.05 ng) and a genomic DNA control. Only primer pairs with a demonstrated efficiency between 90 and 110% and  $R^2$  value close to 0.99 were used. For all experiments, Power SYBR Green was diluted to 54.7% (v/v) in RNase-free water and added to 50 ng of cDNA plus 300 nM primer mix. Experiments were run using Fast Optical 96-well plates covered with adhesive film. Experimental data points were assessed in triplicate reaction volumes of 25  $\mu$ l each, and internal controls consisted of an RNA sample from each experimental triplicate as well as non-template control run with each primer mixture. All qPCR experiments were performed on a real-time PCR system (7900HT, Applied Biosystems) according to the following protocol: 95°C for 10 minutes followed by 40 repeats of 95°C for 15 seconds plus 60°C for 1 minute. A dissociation curve was run after every experiment. Experiments were run as Absolute Quantification and data was converted to Relative Quantification prior to analysis using SDS software. At least three biological repetitions were performed and data were analyzed by Student's *t* test (section 3.2.7).

### 5.2.5 Zebrafish

All zebrafish work was performed in collaboration with Dr. Sandra Habbig and Dr. Julia Hatzold in the lab of Prof. Dr. Matthias Hammerschmidt. Morpholinos were obtained from Gene Tools (Philomath, OR) with sequences as follows:

ATG-targeting *nphp4*:            5' - GCGCTTCTCCACTCAGACATCAGAG - 3'  
ATG-targeting *jade-1*:            5' - TCGGGACACGGCTTCGCTTCATCCT - 3'  
5'UTR-targeting *jade-1*:        5' - CGTGGCCTTCAAGTGATGCGGAAAT - 3'

Morpholinos were diluted in Danieau's buffer (58 mM NaCl; 0.7 mM KCl; 0.4 mM MgSO<sub>4</sub>; 0.6 mM Ca(NO<sub>3</sub>)<sub>2</sub>; 5 mM HEPES; pH 7.6) and injected into wild-type zebrafish embryos at the 1- to 2-cell stage (214) using a PV 820 Pneumatic PicoPump (World Precision Instruments). Injection doses consisted of 1.5 nl of the morpholino solution at 20  $\mu$ M (low dose) or 100  $\mu$ M (high dose). Embryos were kept in E3 buffer (5 mM NaCl, 0.17 mM KCl, 0.33 mM CaCl<sub>2</sub>, 0.33 mM MgSO<sub>4</sub>, 0.00001% methylene blue) at 28 °C and were analyzed after 72 h for body curvature using a Leica stereomicroscope (M165FC) equipped with Leica camera (DFC425C). Over 150 fish were counted for each data point and only embryos displaying a distinct curvature of the tail angled more than 45° from the head-neck axis were scored as positive. Data for low-dose comparisons were collected from three

independent experiments per condition, and average phenotype frequencies were calculated a percentage of wild-type fish using a one-way ANOVA with Tukey's post-hoc test (section 3.2.7). Cystic morphants used for sectioning were PFA-fixed and embedded in paraffin. Samples were sectioned using a Leica microtome (RM2235) and stained using standard Hemotoxylin and Eosin staining protocol (215) and visualized using a Zeiss Axiophot with Zeiss Axiocam.

### 5.2.6 Mass Spectrometry

All experiments involving mass spectrometry were performed in collaboration with Dr. Markus Rinschen in the CECAD Proteomics Facility run by Dr. Tobias Lamkemeyer. Experiments were performed as previously described with slight modifications (216). HEK 293T cells were passaged into 10 cm cell culture dishes (section 3.2.3.2) and transfected using the  $\text{CaCl}_2$  method (section 3.2.3.3). After 24 hours, cells were lysed in a buffer containing 8M Urea and 50mM ammonium bicarbonate with added Pierce protease and phosphatase inhibitor cocktail (Thermo Scientific). Protein concentration was determined using by bicinchoninic acid (BCA) Protein Assay (Thermo Scientific). 400 $\mu\text{g}$  of proteins were reduced using DTT and alkylated using Iodoacetamide as previously described (216). Peptides were digested using trypsin at a w:w ratio of 1:50 at 37°C for 16 hours. After desalting procedure, phosphopeptides were enriched using Fe-NTA immobilized metal affinity chromatography columns (Thermo Scientific). After final clean-up (ZipTip columns, Milipore), samples were analyzed using an LTQ Orbitrap Discovery mass spectrometer (Thermo Scientific) coupled to a Proxeon EASY-nLC II nano-LC system (Proxeon/Thermo Scientific). Intact peptides were detected at a resolution of 30,000 in the mass-to-charge (m/z) range 200–2000 (MS). Internal calibration was performed using the ion signal of  $(\text{Si}(\text{CH}_3)_2\text{O})_6\text{H}$  at m/z 445.120025 as a lock mass. For LC-MS/MS analysis, up to five CID spectra (MS2) were acquired following each full MS scan. Sample aliquots were separated on a 15 cm, 75  $\mu\text{m}$  reverse phase column (Proxeon/Thermo Scientific). Gradient elution was performed from 10 to 40% acetonitrile within 90 minutes at a flow rate of 250 nl/min. Generated raw data were searched using the SEQUEST algorithm against the most recent version of the Uniprot human database (released 2012-06-01). The false discovery rate was adjusted to be lower than 0.01. This analysis and visualization of spectra was performed using the ProteomeDiscoverer software (Thermo Scientific). Identified phosphorylation sites were compared with previously discovered phosphorylation sites in the latest version of the database PhosphoSitePlus (2012-06-01; [www.phosphosite.org](http://www.phosphosite.org)).

### 5.2.7 Statistics

All data are presented as mean average plus standard error of the mean (SE), calculated using Microsoft Excel software. Data was normalized as indicated by figure legends and in the respective

---

methods sections. Statistical analysis was performed using Prism software and differences between means were assessed by one-way ANOVA or Student's *t* test as appropriate. Tukey's post-hoc test was used with or without Bonferroni correction as required.

## 6 RESULTS

### 6.1 Jade-1 is a dynamic protein that co-localizes with nephrocystins at the transition zone.

In order to investigate whether Jade-1 could be a candidate protein for a mediator of ciliary signaling regulation by nephrocystin proteins, it was necessary to determine whether these proteins localize together at the cilium, centrosome, or pericentrosomal region. Immunofluorescence staining using a ciliated Retinal Pigmented Epithelial (RPE-1hTERT) cell line demonstrated Jade-1 to be a highly dynamic protein. Nuclear and cytoplasmic staining patterns confirmed earlier reports (197, 198), but it was apparent that cells in close proximity to one another did not share uniform nuclear vs. cytoplasmic fluorescence intensities (Fig 4A). Furthermore, a distinct perinuclear staining pattern was observed in some cells, as was intense ciliary staining as confirmed by co-localization with the ciliary marker acetylated-tubulin. The variation of ciliary and nuclear fluorescence intensities between cells was confirmed using a second anti-Jade-1 antibody (Fig 4B), and this variation did not appear to correlate with any apparent state of cell division or confluency. Centrosomal localization of Jade-1 appeared consistent between cells as did mitotic spindle labeling in dividing cells. The centrosomal localization of Jade-1 was confirmed using a third commercial antibody to demonstrate colocalization with centriole-marker gamma-tubulin in Human Embryonic Kidney (HEK) 293T cells (Fig 5A), and localization at the base of the cilium as labeled by acetylated-tubulin in RPE-1 cells (Fig 5B). The localization of Jade-1 at the base of the cilium in RPE-1 cells despite dissociation of the microtubule network (Fig 6) confirmed Jade-1 to be a bona fide centriole-associated protein (217). In addition, Jade-1 was demonstrated to co-localize with NPHP1 at the transition zone (Fig 7), supporting the possibility of an interaction between Jade-1 and the nephrocystin complex at this location.

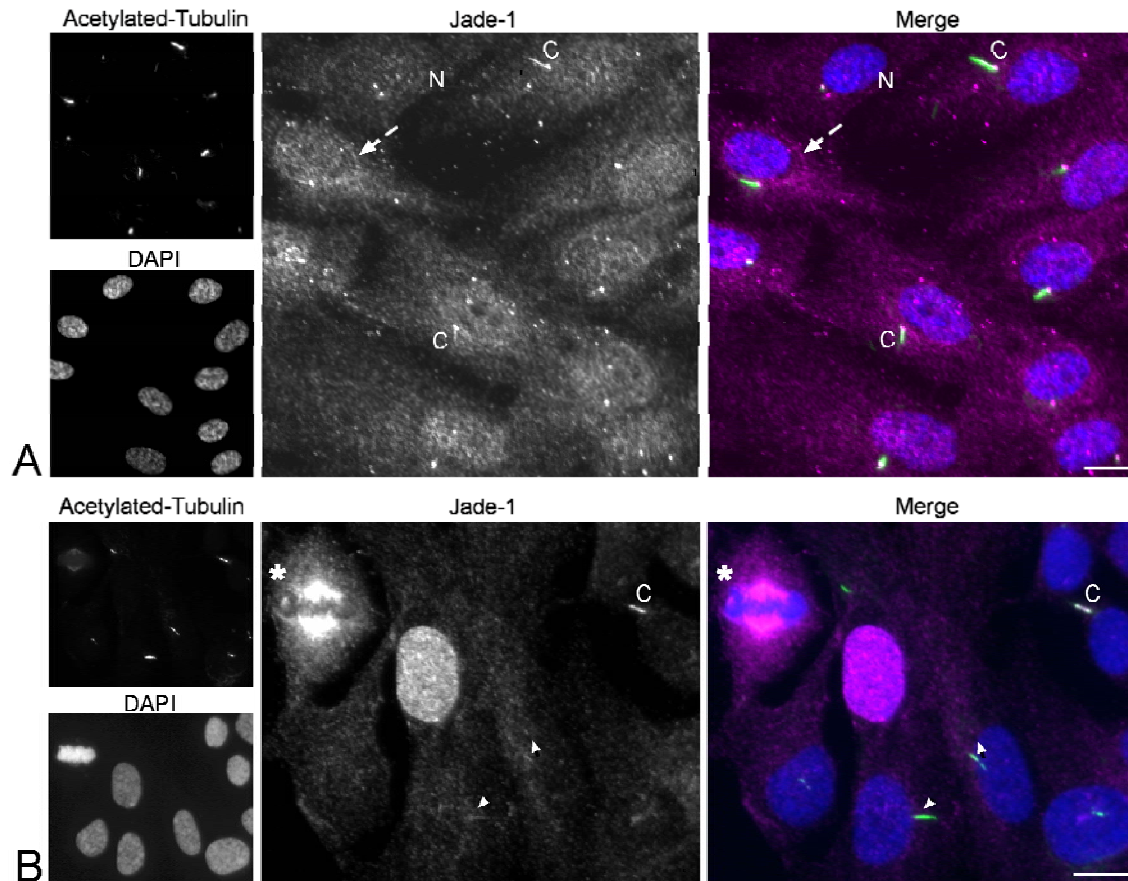


**Figure 4. Jade-1 is a dynamic protein that localizes to the nucleus, cytoplasm, and centrosome in ciliated RPE-1 cells.**

RPE-1 cells were grown to 60% confluency on glass coverslips prior to serum starvation for 24 hours to induce cilia formation. Cells were then fixed using PFA and immunostained using two separate anti-Jade-1 antibodies (magenta; Genetex, A; Proteintech, B) in combination with anti-acetylated-tubulin used to identify primary cilia (green) **A**. Within the same field of view, most cells demonstrated a nuclear accumulation of Jade-1, but some cells demonstrated an additional perinuclear staining pattern (dashed arrow), while others lacked nuclear Jade-1 accumulation (N). Furthermore, in only some cells Jade-1 showed an intense ciliary staining pattern (C), but regardless of ciliary status in all cells an accumulation of Jade-1 was seen at the ciliary base. **B**. Despite weaker overall labeling, weak ciliary and centrosomal labeling could still be identified in all cells (e.g. arrowheads), and sporadically cells were labeled with an intense signal in the nucleus or primary cilium. Jade-1 also intensely labeled the mitotic spindle in dividing cells (\*). Merged images include DAPI. Scale bar = 10  $\mu\text{m}$ . Data from figure A has been previously published in Borgal *et al.*, 2012 (218).

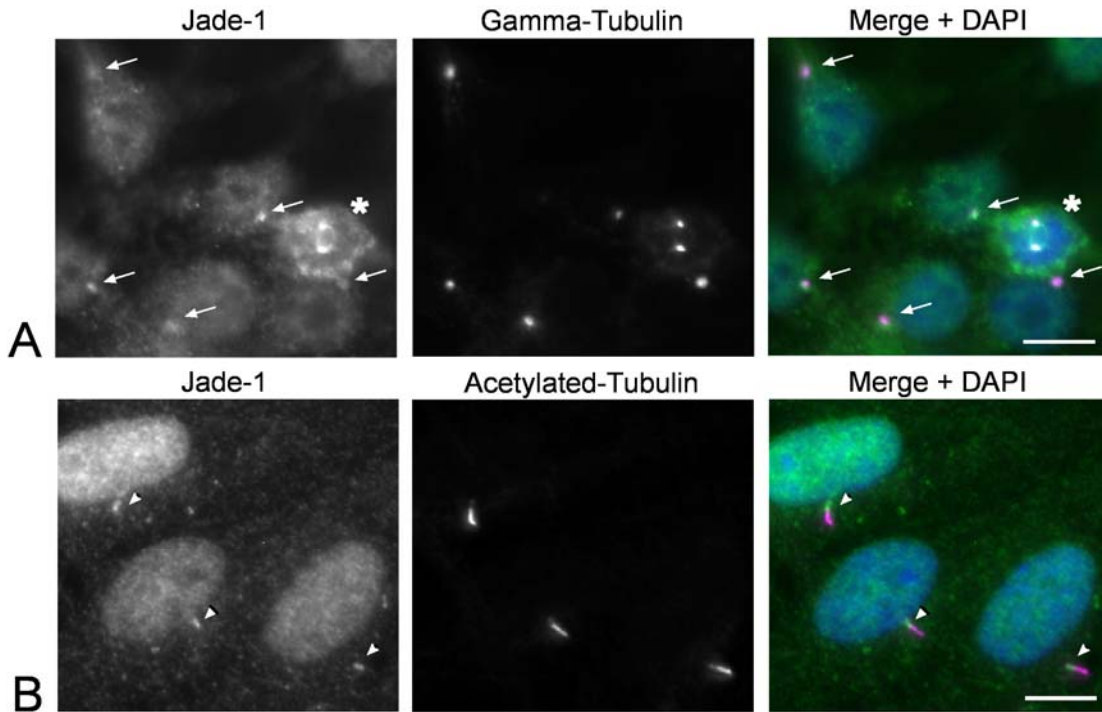


**Figure 5. Confirmation of centrosomal Jade-1 localization**

**A.** HEK 293T cells grown on collagen A-coated coverslips were PFA-fixed and immunostained using an anti-Jade-1 antibody (green) as well as anti-gamma-tubulin antibody (magenta) as a marker of the centrosome. Jade-1 localized to the cytosol and nucleus and an accumulation at the centrosome colocalized with gamma-tubulin (arrows). Jade-1 was also visualized at mitotic spindle and centrosome dividing cells (\*). **B.** RPE-1 cells grown on glass coverslips to 60% confluency and serum starved for 24 hours were immunostained using an anti-Jade-1 antibody (green) and anti-acetylated-tubulin antibody (magenta) to identify primary cilia. The Jade-1 immunofluorescence signal was concentrated in the nucleus and at the base of the cilium (arrow-heads). All stainings were done sequentially with anti-Jade-1 used prior to centrosomal or ciliary markers. Specificity of the antibody was confirmed by immunofluorescence staining of over-expressed V5.Jade-1 protein and by immunostainings using secondary antibody only (not shown). Merged images with DAPI. Scale bar = 10  $\mu$ m. Data has been previously published in Borgal *et al.*, 2012 (218).

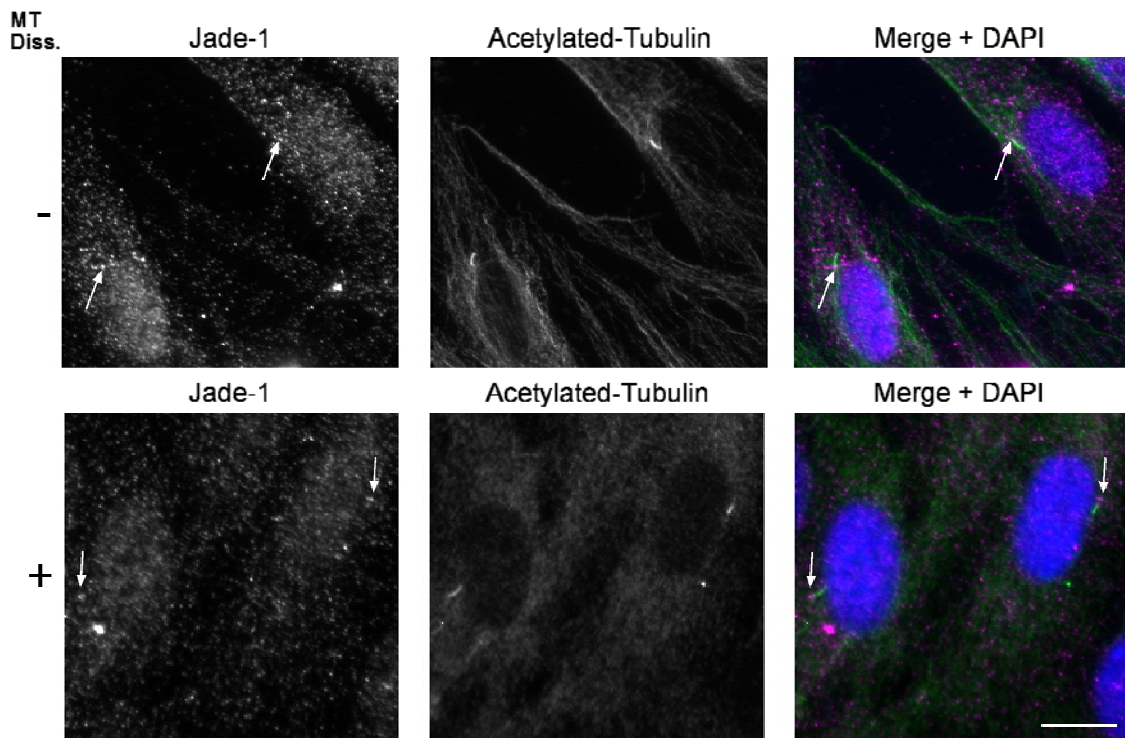


**Figure 6. Jade-1 localizes to the ciliary base independently of the microtubule network.**

Immunofluorescence images of RPE-1 cells which were serum starved for 48 hours and then PFA-fixed immediately (-) or after 30 minutes on ice (+), which is sufficient to dissociate the microtubule network. Cells were immunostained with anti-alpha tubulin (green) or anti-Jade-1 (magenta) antibodies. In both cases, endogenous Jade-1 localizes to the ciliary base (arrows). Merge with DAPI; Scale bar = 10  $\mu\text{m}$ . *Dissociation of the microtubuli network was performed by Claudia Dafinger. Data has been previously published in Borgal et al., 2012 (218).*

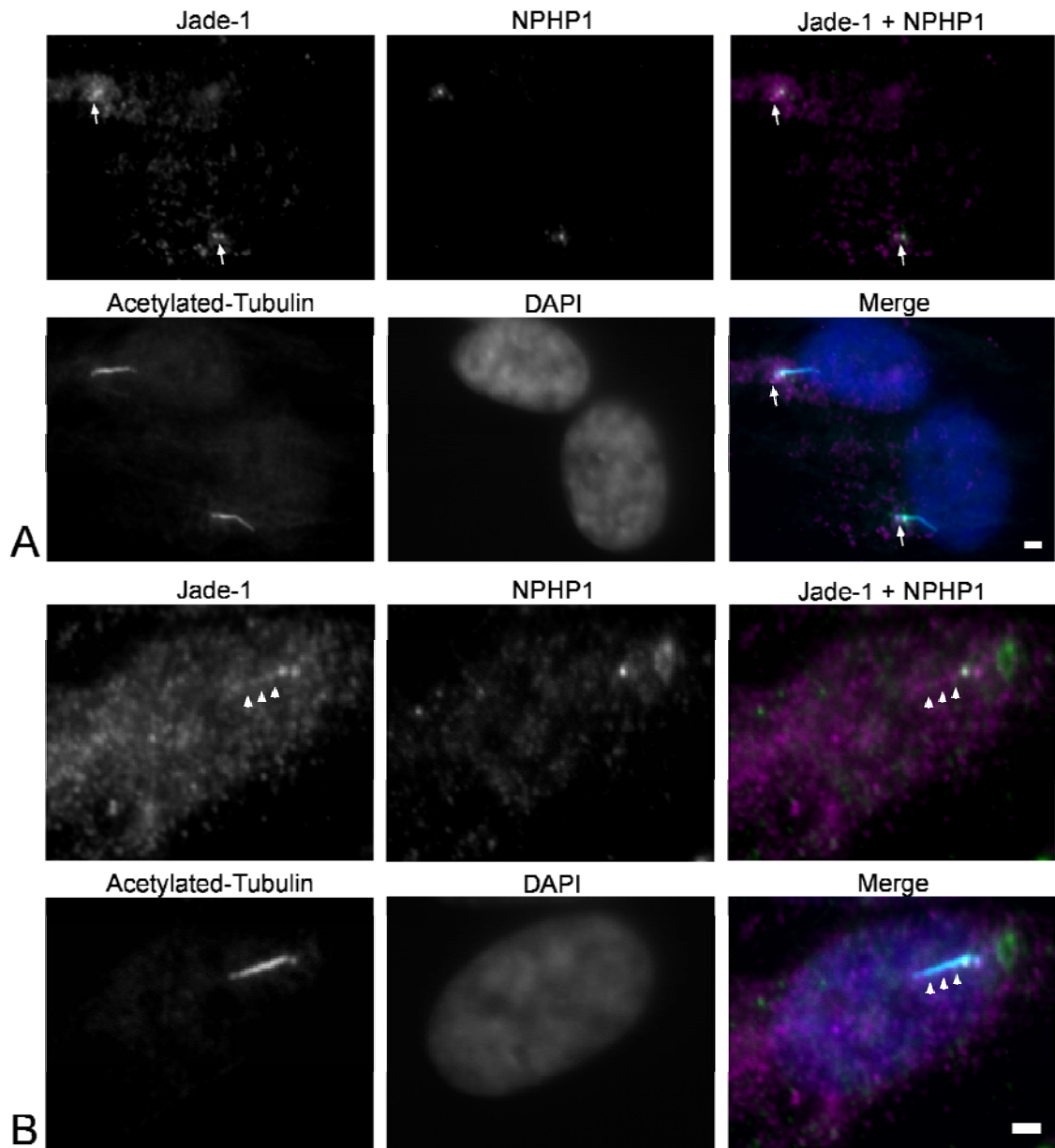


**Figure 7. Jade-1 co-localizes with NPHP1 at the transition zone of primary cilia**

RPE-1 cells were grown on glass coverslips and serum starved for 24 hours prior to PFA fixation and immunostaining with anti-NPHP1 (green), anti-Jade-1 (magenta), and anti-acetylated-tubulin (cyan) antibodies. **A.** Jade-1 was visualized at the basal body and co-localized with NPHP1 at the transition zone (arrows). **B.** At times, Jade-1 could also be visualized within the cilium (arrowheads). Merge with DAPI; Scale bar = 2  $\mu$ m. Data has been previously published in Borgal *et al.*, 2012 (218).

## 6.2 Jade-1 interacts with the nephrocystin protein complex.

The co-localization of Jade-1 and NPHP1 at the transition zone indicated that Jade-1 might interact with members of the nephrocystin complex. Immunoprecipitation experiments demonstrated that V5-tagged Jade-1 (V5.Jade-1) co-precipitated with Flag-tagged NPHP1 (F.NPHP1), as well as

with all of the other members of the nephrocystin protein complex tested: F.NPHP2, F.NPHP3, F.NPHP4, F.NPHP5, F.NPHP7, F.NPHP8, and NPHP9 (Fig 8A). In order to determine an optimal candidate to study in terms of influencing Wnt regulation by Jade-1, a TOPflash TCF/LEF reporter assay was used to screen for negative Wnt reporter activation by NPH proteins. All NPHP proteins tested restrained canonical Wnt reporter activity at high expression levels. When protein expression was decreased, only F.NPHP4 and F.NPHP9 retained a robust ability to negatively regulate reporter activity (Fig 8B). F.NPHP4 consistently interacted with V5.Jade-1. The contribution of this interaction to the negative Wnt regulator role for NPHP4 was therefore further investigated.

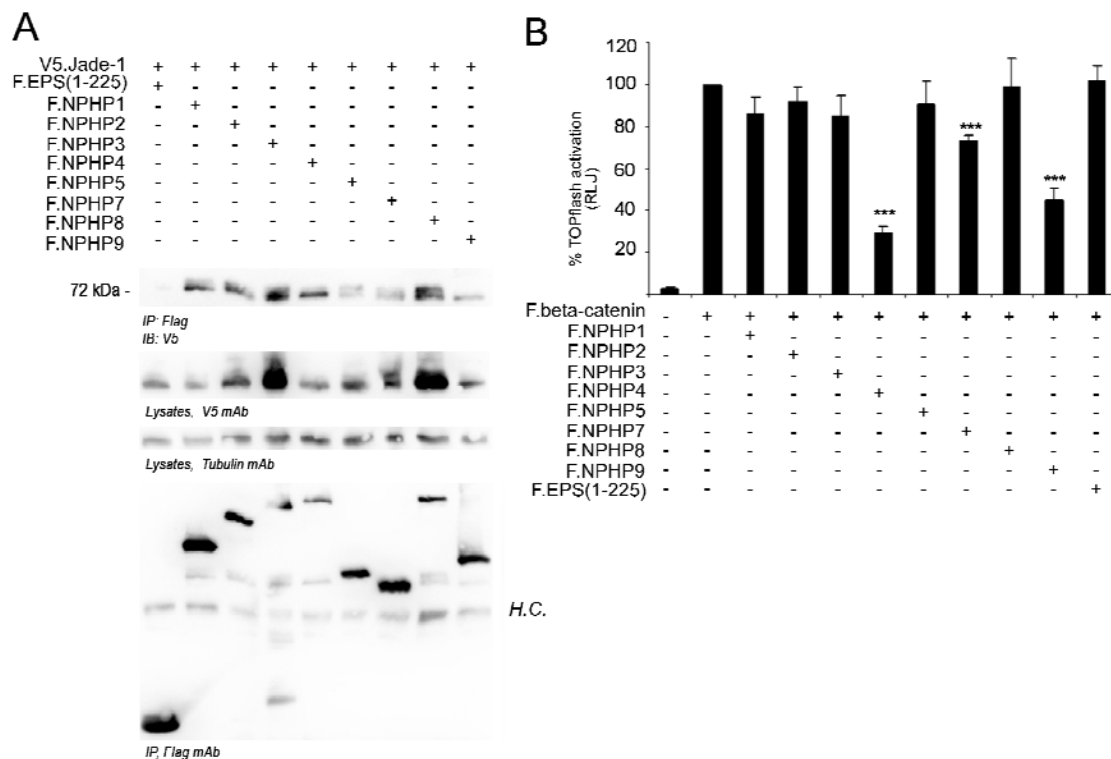


**Figure 8. Jade-1 interacts with the canonical Wnt negative regulating NPH protein complex.**

**A.** HEK 293T cells were transiently transfected with V5.Jade-1 and one of eight Flag-tagged NPH proteins or a control protein (F.EPS<sup>1-225</sup>). After 24 hours, immunoprecipitation was performed using an anti-Flag antibody. V5.Jade-1 co-precipitated with all nephrocystin proteins but not the control protein. **B.** HEK 293T cells were transiently transfected for 24 hours with TOPflash TCF/LEF reporter plasmid plus a constitutively active *Renilla* luciferase reporter plasmid used as a transfection control. Flag-tagged beta-catenin and NPH plasmids or F.EPS<sup>1-225</sup> were transfected as indicated; where required DNA amount was balanced with empty vector. Very low transfected plasmid amounts of F.NPHP4, F.NPHP7 and F.NPHP9 were still able to significantly reduce TOPflash reporter activity. Reporter activation in the presence of each F.NPH protein was evaluated in comparison to  $\beta$ -catenin alone, using paired t-test with Bonferroni correction (F. $\beta$ -catenin alone in comparison to: F.NPHP4 (t(4) = 24.14, p < 0.0001); F.NPHP7 (t(4) = 8.835, p = 0.0009); F.NPHP9 (t(4) = 9.174, p < 0.0008); error bars indicate mean  $\pm$  SE).

### 6.3 Overexpressed NPHP4 facilitates nuclear translocation of Jade-1 in a phosphorylation-dependent manner

The interaction between NPHP4 and Jade-1 was confirmed by immuno-precipitation experiments. V5.Jade-1 co-precipitated with F.NPHP4 but not a control protein (F.EPS<sup>1-225</sup>), while in the reverse experiment, V5.NPHP4 co-precipitated with F.Jade-1 but not a control protein (Fig 9A-B). Furthermore, endogenous Jade-1 co-precipitated with F.NPHP4 but not a control protein (Fig 9C). Endogenous Jade-1 was also demonstrated to co-localize with endogenous NPHP4 by immunofluorescence. NPHP4 and Jade-1 could both be visualized at the centrosome of ciliated RPE-1 cells (Fig 10A). NPHP4 was also visualized in a distinct peri-nuclear staining pattern, and in cells where endogenous Jade-1 was also localized to the peri-nuclear region there was a striking overlap between these two proteins (Fig 10B).

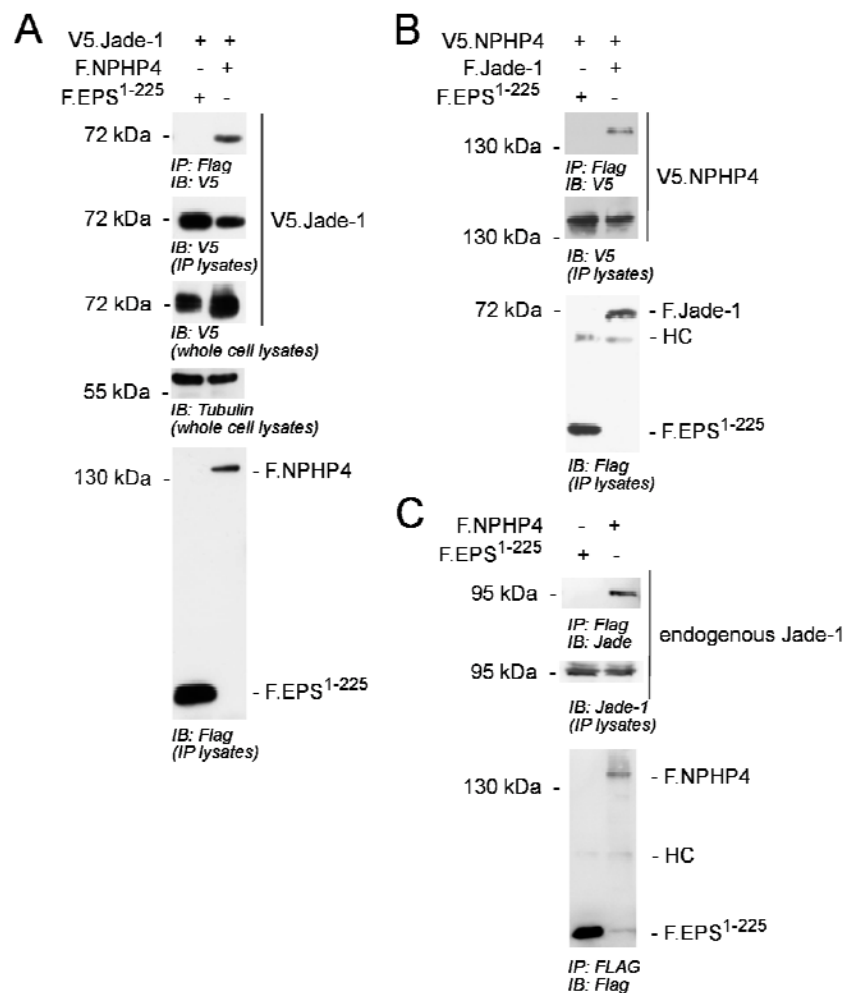


**Figure 9. Confirmation of the interaction between Jade-1 and NPHP4.**

**A.** HEK 293T cells were transiently transfected with V5.Jade-1 and F.NPHP4 or a control protein (F.EPS<sup>1-225</sup>) and after 24 hours immunoprecipitation was performed using an anti-Flag antibody. V5.Jade-1 co-precipitated with F.NPHP4 but not the control protein. Interestingly, overexpression of F.NPHP4 led to a decrease of V5.Jade-1 protein expression in the cytosolic IP lysate but an increase of V5.Jade-1 in the whole cell lysate, which was taken from the same culture dish prior to the IP

procedure. Endogenous tubulin staining from the whole cell lysates showed equal protein amounts. **B.** In the reverse experiment, HEK 293T cells were transiently transfected with V5.NPHP4 and either F.Jade-1 or F.EPS<sup>1-225</sup> and immunoprecipitation was performed 24 hours later using an anti-FLAG antibody. V5.NPHP4 was co-immunoprecipitated by F.Jade-1 but not F.EPS<sup>1-225</sup>. **C.** HEK 293T cells were transiently transfected with F.NPHP4 or a control protein, and 24 hours later immunoprecipitation was performed using an anti-Flag antibody. Endogenous Jade-1 was present in both cell lysates, but was detected only in the precipitates of F.NPHP4 and not the control protein. *IB*, immunoblot; *HC*, heavy chain. Blots are representative of three independent experiments. Data has been previously published in Borgal *et al.*, 2012 (218).

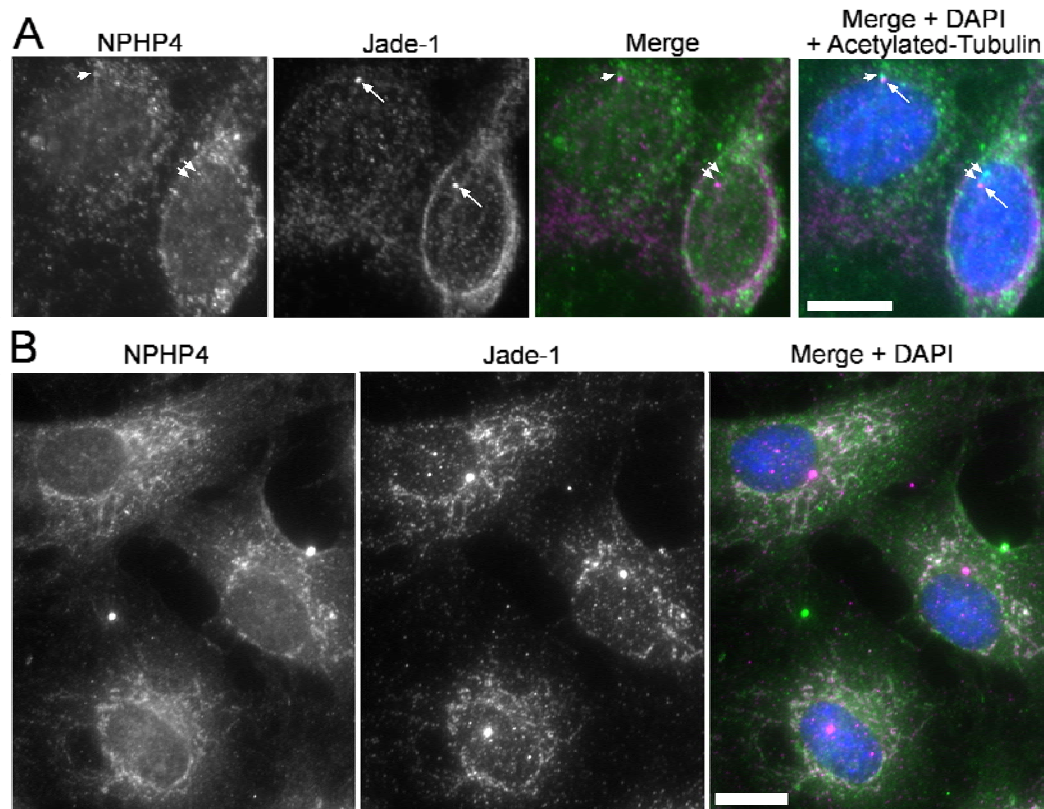


**Figure 10. Endogenous Jade-1 co-localizes with endogenous NPHP4.**

RPE-1 cells were serum starved for 24 hours then fixed with methanol (A) or PFA (B) and immunostained using anti-NPHP4 (green) and anti-Jade-1 (magenta) antibodies. **A.** NPHP4 (arrowheads) could be observed at the cilium together with Jade-1 (arrow). **B.** In all cells, endogenous NPHP4 was concentrated in the peri-nuclear region (green). In cells in which Jade-1 (magenta) was also localized to the peri-nuclear region, there was a striking co-localization between these two proteins. Scale bar = 10  $\mu$ m. Data has been previously published in Borgal *et al.*, 2012 (218).

Upon closer examination of the immunoprecipitation experiments, it was observed that while overexpression of F.NPHP4 decreased the amount of V5.Jade-1 protein in the mostly cytosolic IP lysate, overexpression of F.NPHP4 led to a consistent increase of V5.Jade-1 protein in the nuclei-containing whole cell lysate taken from the same experiment at the time of cell harvesting (Fig 9A). Together with the observed perinuclear localization of endogenous NPHP4 (Fig 10B, left panel) and

striking co-localization with endogenous Jade-1 in this region (Fig 10B, right panel), it was proposed that over-expression of NPHP4 might stabilize the overall protein level of Jade-1, and lead to its translocation from the cytosol to the nucleus. To confirm this stabilization, V5.NPHP4 was expressed together with V5.Jade-1 or V5.EPS, using V5.GFP as a transfection control. The overexpression of V5.NPHP4 led to the stabilization of V5.Jade-1 but did not alter the protein level of V5.GFP (Fig 11A). Overexpression of NPHP4 did not alter translation of Jade-1 as determined by qPCR experiments (Fig 11B); instead, results indicated that NPHP4 protected Jade-1 from proteasomal degradation, since the stabilization of V5.Jade-1 by the proteasome inhibitor MG132 provided no further effect compared to the stabilization of V5.Jade-1 by V5.NPHP4 (Fig 11C).

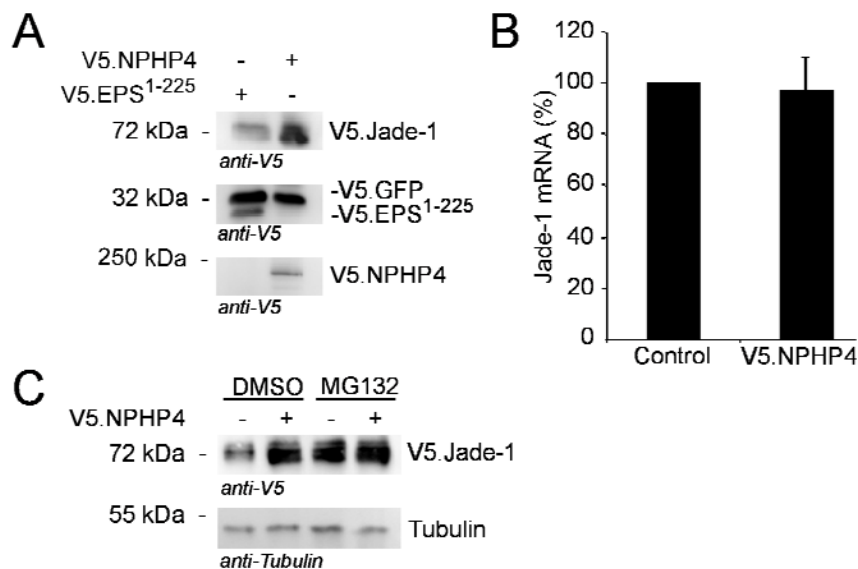


### Figure 11. NPHP4 stabilizes Jade-1 by protecting the protein from degradation

**A.** HEK 293T cells were transiently transfected with a plasmid master mix of V5.Jade-1 plus V5.GFP together with either V5.NPHP4 or a control protein (V5.EPS<sup>1-225</sup>) and harvested 24 hours later as a whole cell lysate. Overexpression of V5.NPHP4 but not expression of a control protein (V5.EPS<sup>1-225</sup>) led to increased protein expression of V5.Jade-1 but did not alter expression of V5.GFP, confirming a specific effect of NPHP4 on Jade-1. **B.** Overexpression of V5.NPHP4 did not alter mRNA levels of V5.Jade-1 as determined by qPCR. HEK 293T cells were transiently transfected with V5.NPHP4 or a control protein (V5.EPS<sup>1-225</sup>) and harvested after 24 hours (n=3; error bars indicate mean  $\pm$  SE). **C.** The proteasome inhibitor MG132 (1 $\mu$ M in DMEM, 4 hours) led to the stabilization of V5.Jade-1, but did not enhance the protein stabilization of V5.Jade-1 by V5.NPHP4. HEK 293T cells were transiently transfected with V5.Jade-1 plus V5.NPHP4 or empty vector for 24 hours prior to 4 hour incubation with fresh medium containing 1 $\mu$ M MG132 or DMSO. Cells were processed as a whole cell lysate. All blots are representative of at least three independent experiments. Data has been previously published in Borgal *et al.*, 2012 (218).

Cell fractionation was then used to determine whether the overexpressing NPHP4 led to a nuclear translocation of Jade-1 (Fig 12A). Overexpression of V5.NPHP4 but not a control protein (V5.EPS<sup>1-225</sup>) led to a reduction of cytoplasmic protein expression of V5.Jade-1 but an increase in nuclear V5.Jade-1 protein expression. Interestingly, V5.NPHP4 associated with the nuclear fraction in

contrast to V5.EPS<sup>1-225</sup>. Immunofluorescence analyses confirmed that nuclear V5.Jade-1 was increased in cells which co-expressed F.NPHP4 (Fig 12B), and in agreement with the observed endogenous NPHP4 staining pattern (Fig 10) further demonstrated that over-expressed NPHP4 did not localize within the nucleus, despite the close association indicated by cell fraction. Upon closer inspection of cell fraction experiments it was observed that when overexpressed together with a control protein, V5.Jade-1 fractionated as a smaller cytosolic band plus a larger nuclear band. When expressed together with V5.NPHP4, both the smaller and larger bands of V5.Jade-1 were associated with the nuclear fraction (Fig 12A). In all overexpression experiments, V5.Jade-1 was visualized as a double band, and it was noted that the addition of NPHP4 almost always led to an increase in the smaller of these two bands (Fig 11A; Fig 9A *WCL*). The question was therefore raised as to whether NPHP4 altered the phosphorylation status of Jade-1, and whether this contributed to nuclear translocation.

To answer this, two experiments using the phosphatase inhibitor okadaic acid were performed. In the first, V5.Jade-1 was co-expressed with V5.NPHP4 or empty vector in the presence or absence of okadaic acid (Fig 12C). Under standard conditions, V5.NPHP4 stabilized the smaller band of V5.Jade-1; however, in the presence of okadaic acid V5.NPHP4 was unable to do so. Cell fractionation was also performed in the presence or absence of okadaic acid (Fig 12D). Under standard conditions, over-expressed V5.Jade-1 predominantly associated with the nuclear fraction, in agreement with over-expression data visualized by immunofluorescence (Fig 12B). However, in the presence of okadaic acid over-expressed V5.Jade-1 associated predominantly with the cytosolic fraction, suggesting a reduced ability to translocate to the nucleus when phosphatase activity was disrupted.

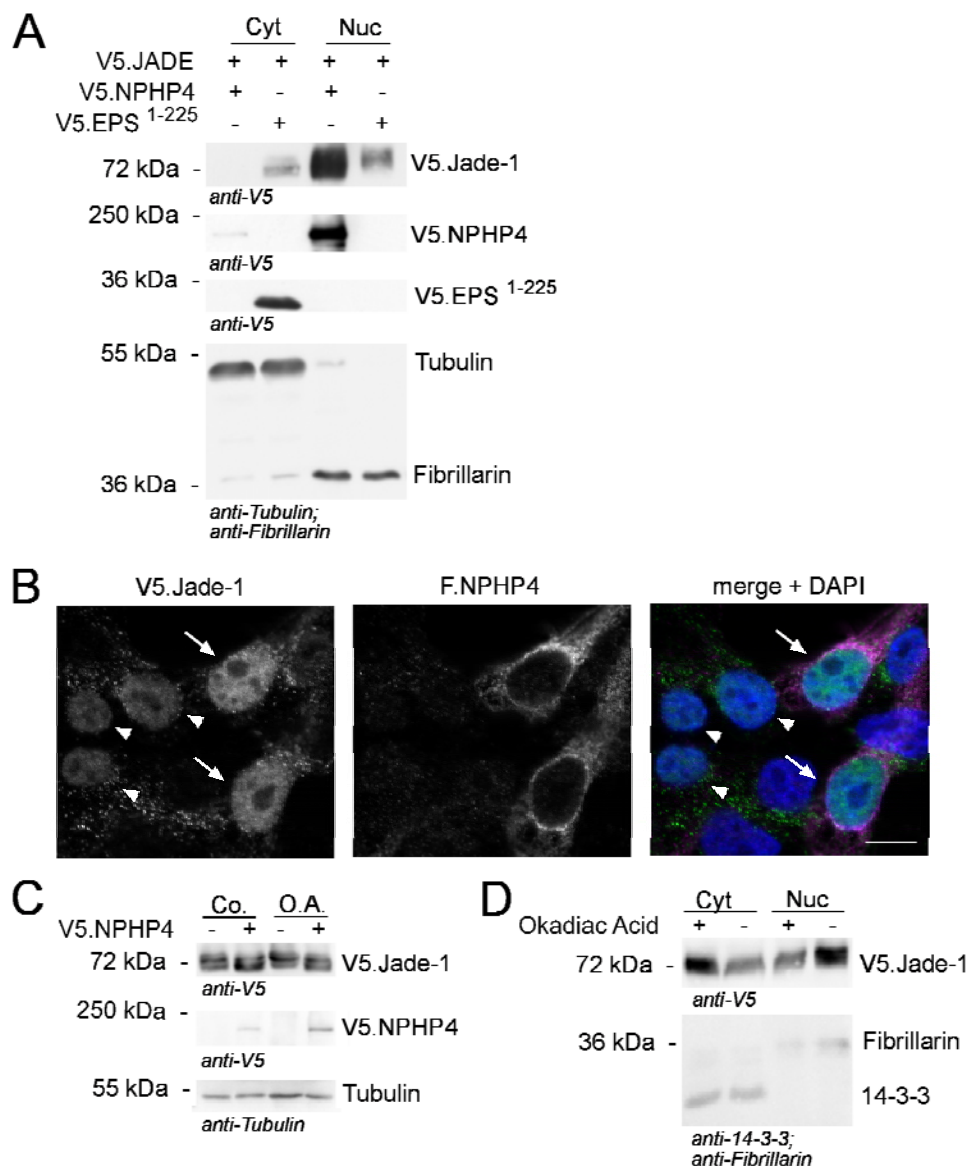


**Figure 12. NPHP4 increases nuclear translocation of Jade-1 in a phosphorylation-dependent manner.**

**A.** Subcellular fractionation was performed 24 hours after transient transfection of V5.Jade-1 together with either V5.NPHP4 or a control protein (V5.EPS<sup>1-225</sup>) in HEK 293T cells. V5.NPHP4 decreased the amount of V5.Jade-1 associating with the cytosolic fraction (Cyt), but increased the amount of V5.Jade-1 associating with the nuclear fraction (Nuc). Over-expressed V5.NPHP4 predominantly associated with the nuclear fraction, in contrast to the control protein V5.EPS<sup>1-225</sup>. Note that when expressed with the control protein, V5.Jade-1 was visualized as a smaller cytosolic band plus a larger nuclear band. In the presence of V5.NPHP4, the smaller band was instead associated with the nuclear fraction. Endogenous tubulin and endogenous fibrillarin marked the cytosolic and nuclear fractions, respectively. The cytosolic fraction was concentrated three times more than the nuclear fraction in order to visualize cytosolic V5.Jade-1. **B.** Immunofluorescence image of HEK 293T cells transiently transfected with low amounts of V5.Jade-1 and F.NPHP4. Cells were fixed in PFA after 24 hours and immunostained with anti-Flag antibody (magenta) or anti-V5 antibody (green). Cells positive for both expressed proteins showed an increased amount of V5.Jade-1 in the nucleus (arrows) compared to cells that only expressed V5.Jade-1 (arrowheads). Note that overexpressed F.NPHP4 does not localize within the nucleus. Flag and V5 staining in nontransfected cells confirmed that nuclear Jade-1 staining was specific (not shown). Scale bar = 10  $\mu$ m. **C.** HEK 293T cells were transiently transfected with V5.Jade-1 plus either V5.NPHP4 or empty vector. After 24 hours, cells were incubated for 45 minutes

in fresh medium containing 1  $\mu$ M water as control (Co.) or okadaic acid (O.A.) and then harvested as a whole cell lysate. V5.NPHP4 stabilized the smaller band of V5.Jade-1 under control conditions but not in the presence of okadaic acid. **D.** HEK 293 cells were transiently transfected with V5.Jade-1. After 24 hours, cells were incubated in fresh medium containing 1  $\mu$ M okadaic acid or water for 45 minutes, and then harvested for cell fractionation. V5.Jade-1 accumulated in the nucleus under control conditions but in the cytosol when incubated with okadaic acid. All western blots are representative of 3 independent experiments. Data has been previously published in Borgal *et al.*, 2012 (218).

#### 6.4 NPHP4 and Jade-1 additively reduce canonical Wnt signaling

Both NPHP4 and Jade-1 have previously been published to negatively regulate the canonical Wnt signaling pathway (193, 198). Furthermore, Jade-1 was demonstrated to ubiquitylate the major canonical Wnt effector  $\beta$ -catenin in the nucleus as well as in the cytosol (198). Since NPHP4 enhances Jade-1 specifically in the nucleus, it was questioned whether NPHP4 could enhance the negative regulation of the canonical Wnt pathway by Jade-1. To test this, V5.NPHP4 and V5.Jade-1 were expressed either separately or together in combination and assessed for their ability to reduce  $\beta$ -catenin-stimulated TOPFlash TCF/LEF reporter activity in a dual-luciferase assay (Fig 13A). In agreement with previous reports, both V5.NPHP4 and V5.Jade-1 were able to reduce the TOPFlash reporter activity in a dose dependent manner. When the transfected amounts of V5.NPHP4 and V5.Jade-1 were titrated so that each individually reduced TOPFlash reporter activity by 50%, the combination of the titrated amounts of these two plasmids additively reduced Wnt reporter activity by a further 50%. Corroborating these results, transfection of the same plasmid ratios additively reduced endogenous protein expression of the canonical Wnt target gene c-myc (Fig 13B). Addition of a control protein to either V5.NPHP4 or V5.Jade-1 did not further reduce Wnt reporter activity by either of these proteins (Fig 13C), and neither V5.NPHP4 nor V5.Jade-1 were able to reduce the heightened reporter activity induced by the non-phosphorylatable S33A mutant  $\beta$ -catenin (Fig 13D).

In order to determine whether there existed a hierarchy of dependence in the ability of Jade-1 and NPHP4 to negatively regulate the canonical Wnt pathway, siRNA knockdown experiments were performed. Knocking down endogenous NPHP4 significantly enhanced the ability of  $\beta$ -catenin to stimulate canonical Wnt reporter activity compared to scrambled siRNA. Furthermore, in the presence of NPHP4 siRNA, the ability of over-expressed V5.Jade-1 to negatively regulate Wnt reporter activity was significantly reduced (Fig 13E). Similarly, knocking down endogenous Jade-1 reduced the ability of V5.NPHP4 to negatively regulate canonical Wnt reporter activity (Fig 13F). However, this effect did not reach significance, indicating that the requirement of NPHP4 by Jade-1 is more potent than the requirement for Jade-1 by NPHP4.

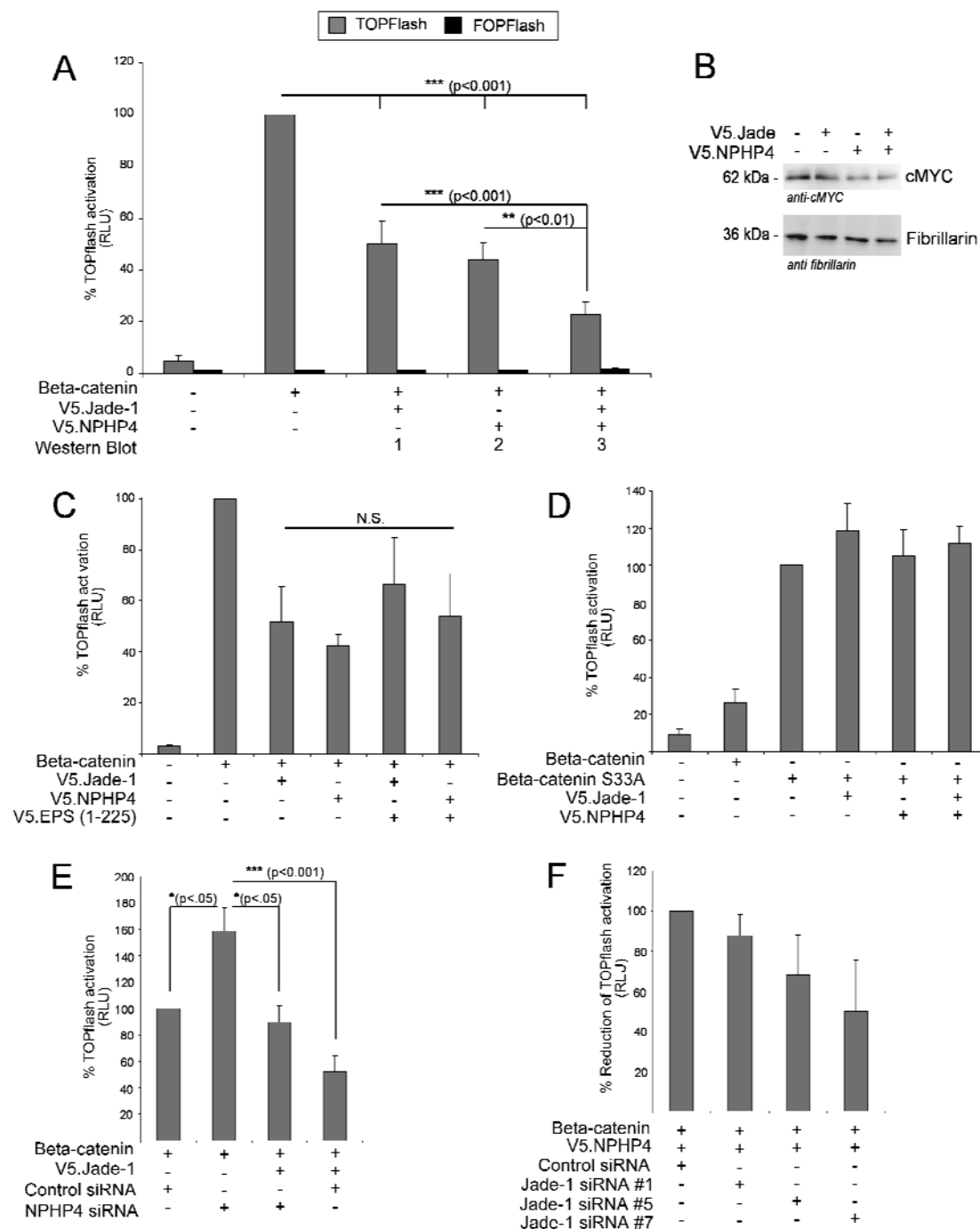


**Figure 13. NPHP4 and Jade-1 additively reduce canonical Wnt activity in a mutually dependent fashion.**

For all canonical Wnt reporter assays, the constitutively active *Renilla* luciferase reporter was used to control transfection efficiency and was mixed with either the TOPflash TCF/LEF reporter plasmid or non-responsive control reporter FOPFlash as indicated. Prior to adding experimental plasmids, F.β-catenin or empty vector were added to this reporter mixture to ensure equal plasmid amounts. In all cases HEK 293T cells were transiently transfected for 24 hours prior to lysis, and Wnt reporter activity was quantified as relative luciferase units (RLU). **A.** Expression of either V5.NPHP4 or V5.Jade-1 plus empty vector was able to reduce β-catenin stimulated TOPflash reporter activity. When the effect by each plasmid was titrated to a 50% reduction of reporter activity, the combination of V5.NPHP4 and V5.Jade-1 together further reduced reporter activity significantly ( $F(3,31) = 66.79$ ,  $p < 0.0001$ ; Tukey's post hoc test as indicated,  $** = p < 0.01$ ,  $*** = p < 0.001$ ). Error bars indicate mean  $\pm$  SE.

Experiments were each done in triplicate for TOPFlash. FOPFlash levels consistently showed no activation (one triplicate was done for each treatment group). **B.** HEK 293T cells were transiently transfected with F.β-catenin and experimental plasmids as indicated, using the same ratios as used for the luciferase experiments. Cells were processed 24 hours later as a whole cell lysates. Expression of V5.NPHP4 and V5.Jade-1 reduced the protein level of Wnt gene target c-myc. **C.** Transient transfection of a control plasmid (V5.EPS<sup>1-225</sup>) in addition to either V5.NPHP4 or V5.Jade-1 did not further reduce Wnt reporter activity. N.S. = not significant as determined by one-way ANOVA between the four experimental conditions ( $F(3,11) = 1.841$ ;  $p = 0.24$ ; error bars indicate mean  $\pm$  SE). **D.** Neither V5.Jade-1 nor V5.NPHP4, alone or in combination, were able to reduce the heightened reporter activity stimulated by the non-phosphorylatable S33A β.catenin mutant (error bars indicate mean  $\pm$  SE). **E.** Transient transfection with F.β-catenin and reporter plasmids, together with either NPHP4 siRNA or control siRNA and either V5.Jade-1 or empty vector. Wnt reporter activity was significantly increased in the presence of NPHP4 siRNA compared to cells receiving control siRNA. This effect was reversed by the addition of V5.Jade-1, although V5.Jade-1 combined with NPHP4 siRNA did not reduce Wnt reporter activity to the extent that V5.Jade-1 combined with control siRNA could ( $F(3,15) = 13.88$ ,  $p < 0.001$ ; Tukey's post hoc test as indicated, \* =  $p < 0.05$ , \*\*\* =  $p < 0.001$ ; error bars indicate mean  $\pm$  SE). **F.** The amount that V5.NPHP4 in the presence of control siRNA was able to reduce F.β-catenin-stimulated TOPFlash reporter activity was normalized to 100% (see "Materials & Methods"), and this value was compared with the reduction in reporter activity due to V5.NPHP4 in the presence of three separate Jade siRNAs. Jade siRNA showed a non-significant trend toward reduced NPHP4 efficacy (error bars indicate mean  $\pm$  SE). Data has been previously published in Borgal *et al.*, 2012 (218).

### 6.5 Genetic interaction of NPHP4 and Jade-1 in zebrafish embryos.

To test whether the biochemical relationship between NPHP4 and Jade-1 had functional relevance *in vivo*, the developing zebrafish embryo was used as a model system. This can be considered an appropriate model to study the function of genes related to human cystic kidney disease because the zebrafish homologs of human cystoproteins localize to primary cilia and morpholino knockdown of these results in pronephric cyst formation in the zebrafish embryo (219, 220). *In vivo* morpholino knockdown of *nphp4* expression has previously been reported to lead to a curved body phenotype in zebrafish (193, 221). This phenotype has been associated with defects in canonical Wnt signaling, ciliary defects, and pronephric cysts (178, 193, 221–224). Injection of an *nphp4* ATG-targeting morpholino confirmed a body curvature phenotype in 92% of injected embryos at 72 hours post fertilization. Injection of either a *jade-1* ATG- or *jade-1* 5'UTR-targeting morpholino also resulted in a curved body phenotype 72 hours post-fertilization, although the prevalence of this phenotype was weaker (56.5% of embryos) using the same ATG-targeting morpholino dose (Fig 14A). When morpholino injection doses were individually titrated so that knockdown of either gene alone yielded almost no body curvature, the combined injection of *nphp4* and *jade-1* morpholinos at this dosage resulted in a body curvature phenotype in 31.5% of injected embryos. This genetic interaction indicates that Jade-1 and NPHP4 are involved in the same functional pathway *in vivo* (Fig 14B).

Furthermore, pronephric cysts were identified in developing embryos 72 hours after *jade-1* 5'UTR morpholino injection (Fig 14C). Taken together these data support a model whereby reduced

expression of the canonical Wnt regulator Jade-1 contributes to kidney cyst formation, and this is exacerbated by reduced expression of the Jade-1 stabilizing protein NPHP4.

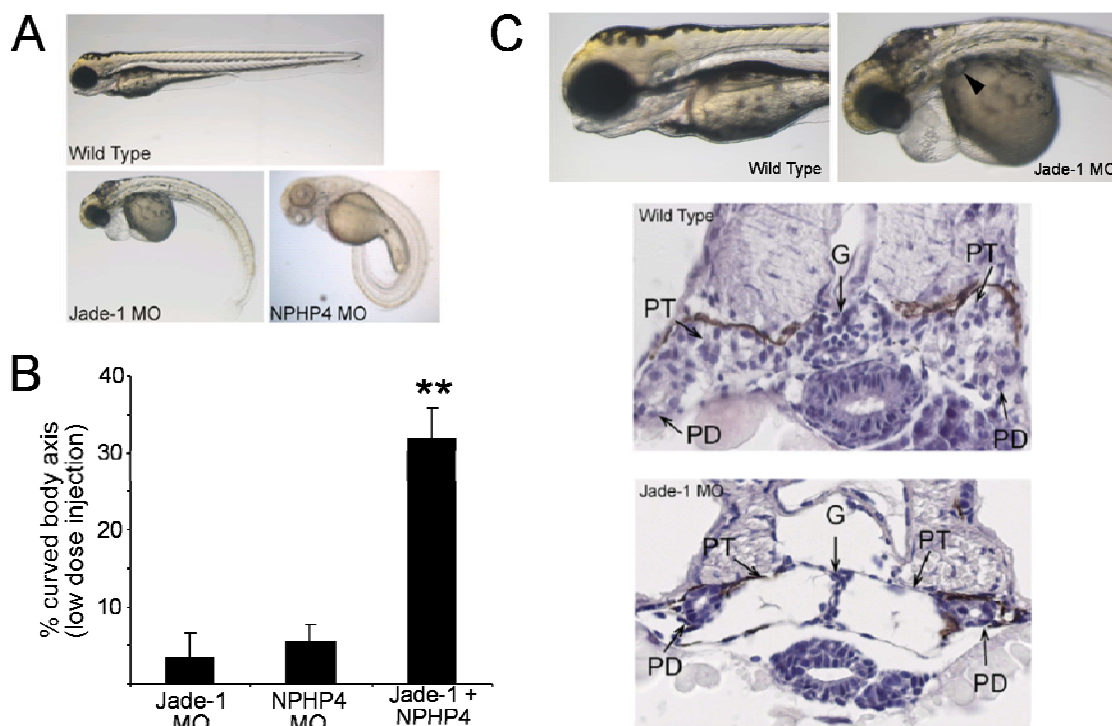


**Figure 14. Genetic interaction of Jade-1 and NPHP4 in the developing zebrafish embryo.**

Morpholinos targeting *jade-1* or *nphp4* were injected into zebrafish embryos at the 1-2 cell stage. Developing embryos were assessed 72 hours post fertilization (hpf) for body curvature, and were scored as positive only if the tail was angled more than 45° from the head-neck axis. This abnormal body curvature phenotype has previously been associated with mutations in cystic kidney causing disease genes, ciliary abnormalities, pronephric cysts, and defective Wnt signaling (see text). **A.** Representative images of 72 hpf embryos injected with *nphp4* or *jade-1* morpholinos as indicated. **B.** Injection doses of *nphp4* and *jade-1* ATG-targeting morpholinos were individually titrated to a concentration low enough to yield almost no obvious phenotype. The combination of these two morpholinos at this low concentration resulted in a dramatic increase in the occurrence of abnormal body curvature ( $F(2,8) = 25.35$ ;  $p < 0.001$ , Tukey's post hoc test describes difference between combination and each individual condition, \*\* =  $p < 0.01$ ; error bars indicate mean  $\pm$  SE). **C.** Injection of the *jade-1* 5'UTR-targeting morpholino resulted in the development of pronephric cysts (arrowhead, upper panel; PT, pronephric tubule; PD, pronephric duct; G, glomerulum). All zebrafish experiments were performed in collaboration with Dr. Sandra Habbig and Dr. Julia Hatzold in the lab of Prof. Matthias Hammerschmidt. Data has been previously published in Borgal *et al.*, 2012 (218).

## 6.6 Classical $\beta$ -catenin kinase CK1 $\alpha$ phosphorylates Jade-1, abolishing negative Wnt regulation

The ability of NPHP4 to stabilize Jade-1 protein levels and augment repression of canonical Wnt activity appears to be dependent on the ability of NPHP4 to alter the phosphorylation status of Jade-1: if phosphatase activity is inhibited by okadaic acid, NPHP4 can no longer stabilize Jade-1 (Fig 12C). To determine whether phosphorylation of Jade-1 also contributes to regulation of canonical Wnt

activity, two candidate kinases were evaluated regarding their impact on Jade-1 phosphorylation status. CK1 $\alpha$  and GSK3 $\beta$  are both integral kinase members of the constitutively active  $\beta$ -catenin destruction complex. When the canonical Wnt pathway is inactive, both of these kinases phosphorylate  $\beta$ -catenin to repress the Wnt signal, but when this Wnt pathway is active these kinases instead phosphorylate membrane-bound LRP5/6, augmenting the Wnt response (170). It was demonstrated that while both F.GSK3 $\beta$  and F.CK1 interact with V5.Jade-1, only F.CK1 $\alpha$  altered the protein expression of V5.Jade-1 (Fig 15A). Specifically, F.CK1 $\alpha$  increased the protein amount of, and interacting predominantly with, a V5.Jade-1 species of increased size suggestive of phosphorylation (Fig 15A). Whole cell lysate experiments confirmed that co-expression of F.NPHP4 stabilized the smaller species of V5.Jade-1 while co-expression of F.CK1 $\alpha$  stabilized the larger species of V5.Jade-1 (Fig 15B). Of interest, co-expression of F.NPHP4 with V5.Jade-1 further repressed the TOPflash Wnt reporter activity as was expected; however, the co-expression of F.CK1 $\alpha$  completely abolished repression of the Wnt reporter by V5.Jade-1 (Fig 15C). Nevertheless V5.Jade-1 was still able to reduce the heightened Wnt reporter activity stimulated by F.CK1 $\alpha$ , although the ability of V5.Jade-1 to do so was significantly reduced (Fig 15D).

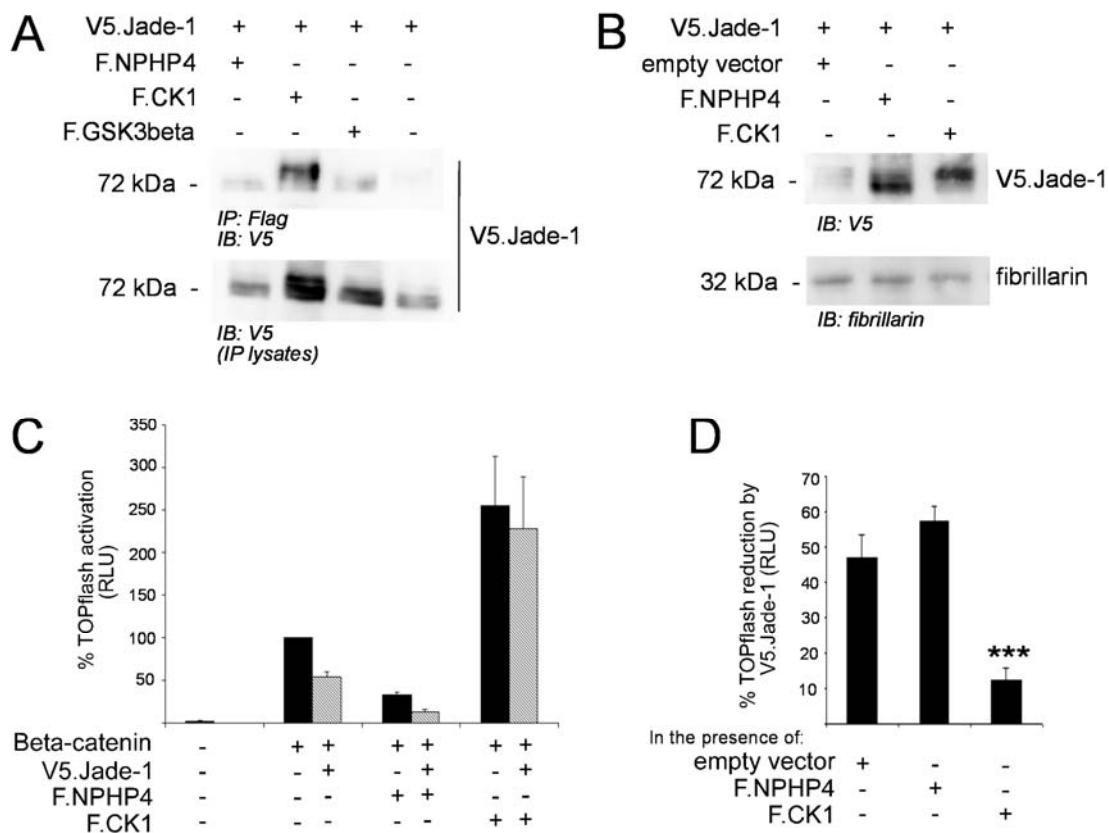


**Figure 15. F.CK1 $\alpha$  increases the expression size of V5.Jade-1 and abolishes repression of canonical Wnt reporter.**

**A.** HEK 293T cells were transiently transfected with V5.Jade-1 and either F.CK1 $\alpha$ , F.GSK3 $\beta$ , F.NPHP4 as a positive control, or F.EPS<sup>1-225</sup> as a negative control. After 24 hours cells the Flag tag was immunoprecipitated and all but the negative control protein were found to interact. Of note, only co-expression with F.CK1 $\alpha$  led to an increase in V5.Jade-1 protein expression size. **B.** HEK 293T cells

were transiently transfected with V5.Jade-1 plus F.NPHP4 or F.CK1 $\alpha$  and processed 24 hours later as a whole cell lysate. Co-expression of F.NPHP4 stabilized the smaller species of V5.Jade-1, while co-expression of F.CK1 $\alpha$  stabilized the larger species of V5.Jade-1. **C.** HEK 293T cells were transiently transfected with TOPflash and *Renilla* luciferase reporter plasmids, as well as F. $\beta$ -catenin and experimental plasmids as indicated. Repression of Wnt reporter activity by V5.Jade-1 was augmented by F.NPHP4 but completely reversed in the presence of F.CK1 $\alpha$  (error bars indicate mean  $\pm$  SE) **D.** Data pairs from each experiment contributing to Figure 12C were analyzed in terms of the percentage that V5.Jade was able to reduce Wnt reporter activity in the presence of co-expressed empty vector, F.NPHP4, or F.CK1 $\alpha$ . In the presence of empty vector or F.NPHP4, V5.Jade-1 reduced Wnt reporter activity by a further 50%; however, in the presence of F.CK1 $\alpha$ , the ability of V5.Jade-1 to reduce Wnt reporter activity was significantly decreased.  $F(2,11)=78.72$ ,  $p<0.0001$ ; Tukey's post hoc test indicates significance from both other conditions:  $***=p<0.001$ ; error bars indicate mean  $\pm$  SE).

The consensus CK1 phosphorylation motif is (pS/pT)-x-x-(S/T), where a serine or threonine residue three positions downstream from a previously phosphorylated serine or threonine residue will be recognized and phosphorylated by CK1 (225). CK1 can also phosphorylate an unprimed consensus sequence of (D/E)-x-x-(S/T), but this must be preceded by multiple acidic residues to reach the same efficiency of a primed substrate (226). Jade-1 has previously been identified in mass spectrometry screens to be phosphorylated on several sites which could correspond to classical CK1 phosphorylation motifs (227, 228; also see Fig 16A). To determine whether the increased size of over-expressed Jade-1 in the presence of F.CK1 $\alpha$  was due to phosphorylation on any of these motifs, mass spectrometry was performed on lysates prepared from HEK 293T cells expressing V5.Jade-1 alone or in combination with F.CK1. In both conditions, several published sites corresponding to the last serine or threonine of a potential CK1 $\alpha$  phosphorylation motif were confirmed to be phosphorylated. Furthermore, one novel site corresponding to a CK1 motif was identified to be phosphorylated only in the presence of F.CK1 $\alpha$  (Fig 16B). However, mutation of any of these sites to a nonpolar alanine did not reduce the ability of over-expressed F.CK1 $\alpha$  to increase the expression size of V5.Jade-1 or alter the repression of  $\beta$ -catenin-stimulated TOPflash reporter activity (data not shown; Fig 16A). To narrow down the possible sites of action, truncation mutants were sub-cloned from V5.Jade-1 and expressed together with either F.CK1 $\alpha$  or F.NPHP4. As suggested by the multitude of CK1 phosphorylation motifs in this region, the Jade-1 N-terminus displayed profound size shifts when co-expressed with F.CK1 $\alpha$ , while the Jade-1 C-terminus was not affected (Fig16C). Of interest, F.NPHP4 also did not affect the C-terminus of V5.Jade-1, but substantially stabilized both the middle and the N-terminal segments (Fig 16D). However, in contrast to F.CK1 co-expression which specifically enhanced the larger band of the N-terminal V5.Jade-1 truncation, co-expression of F.NPHP4 predominantly led to stabilization of the lower sized N-terminal fragment. It is furthermore noteworthy that in the latter case the larger band in the N-terminal truncation was also mildly stabilized, and in the middle segment of V5.Jade-1 the larger band was exclusively stabilized. This could be due to secondary post-translational modifications acting on the partial protein, and indicates that the N-terminal fragment is required for F.NPHP4 to stabilize the smaller form of full length V5.Jade-1.

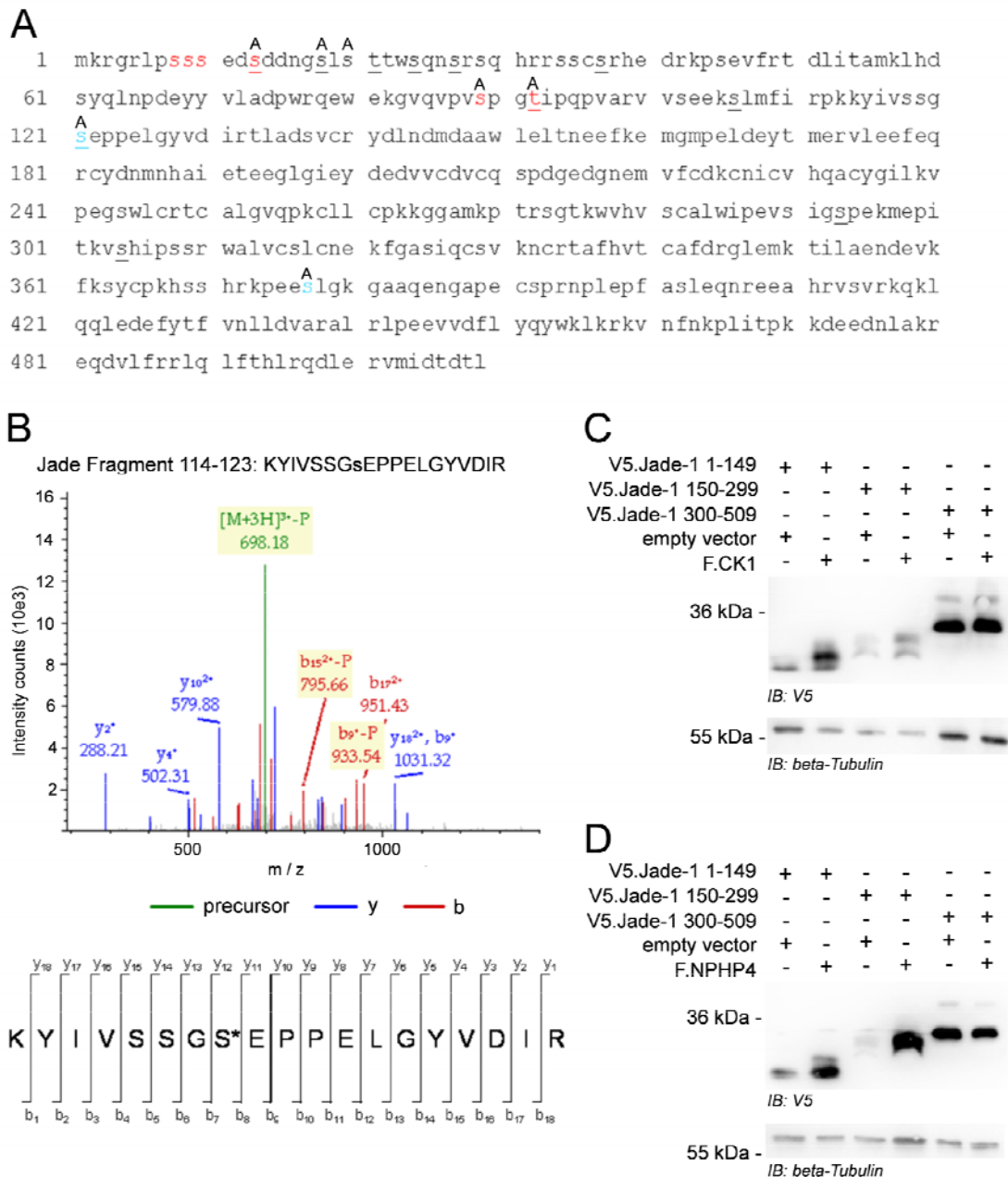


**Figure 16. The Jade-1 N-terminus is regulated by both CK1 $\alpha$  and NPHP4.**

**A.** Amino acid sequence of Jade-1 with all target serines of classical CK1 phosphorylation motifs underlined. Previously published phosphorylation sites identified by mass spectrometry screens are shown in red (227, 228). Novel phosphorylated serines identified by mass spectrometry are shown in blue. The presence of the letter “A” above a given amino acid indicates a point mutation to alanine. All point mutations except serines 18 and 20 had no effect on full-length Jade-1 phosphorylation by CK1 $\alpha$ . **B.** HEK 293T cells were transiently transfected with V5.Jade-1 plus either F.CK1 $\alpha$  or empty vector and were lysed 24 hours later in a buffer containing 8 M Urea and 50 mM ammonium bicarbonate. Peptides were digested using trypsin and phosphopeptides were enriched Fe-NTA immobilized metal affinity chromatography columns before analysis with LTQ Orbitrap XL mass spectrometer. A peak in V5.Jade-1 fragment 114-133 was detected only in lysates containing F.CK1 $\alpha$ . The phosphorylated residue was identified as S121. **C-D.** HEK 293T cells were transiently transfected with truncations of V5.Jade-1 as indicated plus either empty vector or F.CK1 $\alpha$  (C) / F.NPHP4 (D).

Cells were processed 24 hours later as a whole cell lysate. In both cases, the C-term truncation was not affected, but the N-terminal truncation showed stabilization of the larger band when co-expressed with F.CK1 $\alpha$  (C), or the smaller band when co-expressed with F.NPHP4 (D). *All mass spectrometry was performed in collaboration with Dr. Markus Rinschen in the CECAD Proteomics Facility run by Dr. Tobias Lamkemeyer.*

The high concentration of serines in an N-terminal fragment of Jade-1 renders it difficult to identify by mass spectrometry which single residues might be phosphorylated in the presence of CK1 $\alpha$ . Point mutation of CK1-target serines for all canonical sites attempted, including the newly identified site consisting of a CK1 motif where the target serine was phosphorylated only in the presence of F.CK1 $\alpha$ , did not alter the ability of CK1 $\alpha$  to phosphorylate V5.Jade-1. Therefore, point mutation of a putative unprimed CK1 phosphorylation site at S18 was attempted. This site, E-D-S-D-D-N-G-S, fulfills the unprimed CK1 motif requirement that a serine be preceded by multiple acidic residues immediately prior to the -3 position. Of note, the amino acid sequence continued from S18 to S20 is S-L-S, and this sequence is identical to the noncanonical motif reported at the only phosphorylation site that CK1 targets on  $\beta$ -catenin, S45 (225). In the case of  $\beta$ -catenin, CK1 phosphorylates the first serine in this motif and does not require a previous priming event. Of interest, if this site on Jade-1 were to be recognized by CK1 $\alpha$ , it would create an opportunity for sequential phosphorylation by CK1 of canonical motifs T21, S24, and S27. Point mutation of the serine at positions 18 to alanine reduced the size shifting effect of F.CK1 on V5.Jade-1. This effect was most pronounced when both serine 18 and serine 20 were changed to alanines (Fig 17A). Wnt reporter activity modification by the Jade-1 S18AS20A mutant was consistent with predictions based on previous data, although it was less dramatic than suggested by the biochemistry. The F.CK1 $\alpha$ -mediated enhancement  $\beta$ -catenin-stimulated TOPflash reporter activity was significantly reduced in the presence of V5.Jade-1 S18AS20A, but not by wild-type V5.Jade-1 (Fig 17B). Conversely, the F.NPHP4-mediated decrease in TOPflash reporter activity was augmented in the presence of both V5.Jade-1 species (Fig 17C).

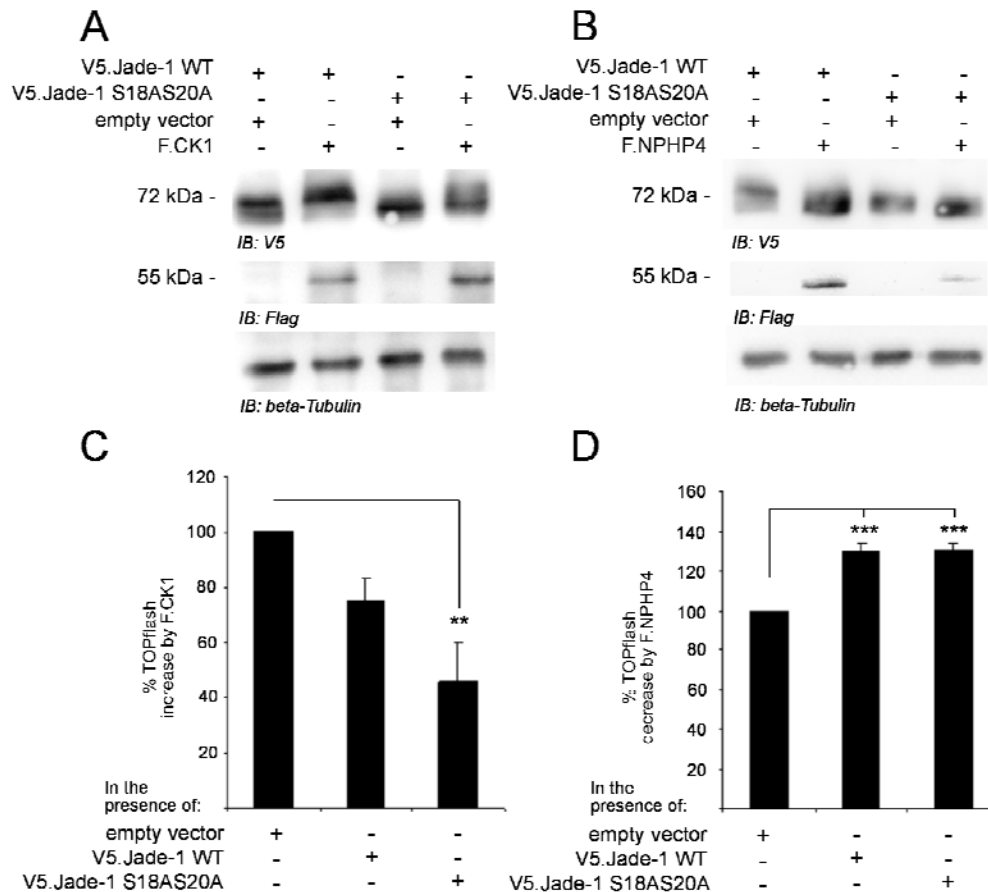


**Figure 17. Point mutations of V5.Jade-1 alter the influence of CK1 $\alpha$  but not NPHP4.**

HEK 293T cells were transiently transfected with the indicated expression vectors and were processed as whole cell lysates after 24 hours. **A.** Co-expression with F.CK1 $\alpha$  increased protein expression size of wild-type V5.Jade-1 but this effect was reduced for the V5.Jade-1 S18AS20A mutant. **B.** Co-expression with F.NPHP4 reduced protein expression size of V5.Jade-1 and stabilizes V5.Jade-1 S18AS20A. Note that in both experiments under basal conditions V5.Jade-1 S18AS20A is reduced in size compared to wild-type V5.Jade-1, indicating a lack of endogenous phosphorylation by CK1. **C & D.** HEK 293T cells were transiently transfected with F. $\beta$ -catenin and TOPflash reporter plasmid, constitutively active *Renilla* luciferase, and experimental plasmids together with either F.CK1 $\alpha$  (C) or F.NPHP4 (D). Cells were lysed after 24 hours and luciferase activity stimulated by F. $\beta$ -catenin alone was set to 100% for each experiment. Data were then normalized for each experiment so that the increase in signal by F.CK1 $\alpha$  in the presence of empty vector (C), or the decrease in signal by F.NPHP4 in the presence of empty vector (D) was set to 100%. **C.** The V5.Jade-1 S18AS20A mutant significantly reduced the ability of F.CK1 $\alpha$  to increase reporter activation, while wild-type V5.Jade-1 expression did not ( $F(2,11)=13.52$ ,  $p=0.006$ ; Tukey's post hoc test as indicated:  $**=p<0.01$ ; error bars indicate mean  $\pm$  SE). **D.** Both V5.Jade-1 species significantly augmented the decrease in reporter activity by F.NPHP4 ( $F(2,11)=52.30$ ,  $p=0.0002$ ; Tukey's post hoc test as indicated:  $***=p<0.001$ ; error bars indicate mean  $\pm$  SE).

The increased Wnt reporter activity in the presence of F.CK1 $\alpha$  was not predicted. CK1 $\alpha$  is a well established member of the  $\beta$ -catenin destruction complex and would be expected to contribute to the phosphorylation and degradation of endogenous or over-expressed  $\beta$ -catenin. However, CK1 induces secondary body axis in *Xenopus* embryos (229) and inhibiting CK1 generates a loss-of-Wnt

mom (more mesoderm) phenotype in *C. elegans* (230), therefore CK1 was originally identified as a transducer of Wnt signaling. More recently CK1 $\alpha$  has been shown to phosphorylate LRP, contributing to the Wnt response (170), therefore the action of CK1 $\alpha$  could be context dependent. However, when the relationship between over-expressed F.CK1 $\alpha$  and F. $\beta$ -catenin was investigated, it was found that protein expression of F.CK1 $\alpha$  was reduced in the presence of F. $\beta$ -catenin (Fig 18A). In contrast, expression of the same level of F. $\beta$ -catenin did not reduce protein expression of V5.Jade-1 (Fig 18B). However, when plasmid transfection amount of F. $\beta$ -catenin was increased by a factor of five, V5.Jade-1 protein expression was reduced in a similar fashion to that of F.CK1 $\alpha$  (Fig 18B). In line with this, over-expression of V5.Jade-1 in a TOPflash reporter assay when F. $\beta$ -catenin plasmid transfection was increased by a factor of five resulted in increased stimulation rather than abrogation of the TOPflash reporter luciferase expression (Fig 18C). These data indicate that over-expressed  $\beta$ -catenin is able to stimulate degradation of negative canonical Wnt regulating proteins, although it does so at different thresholds.

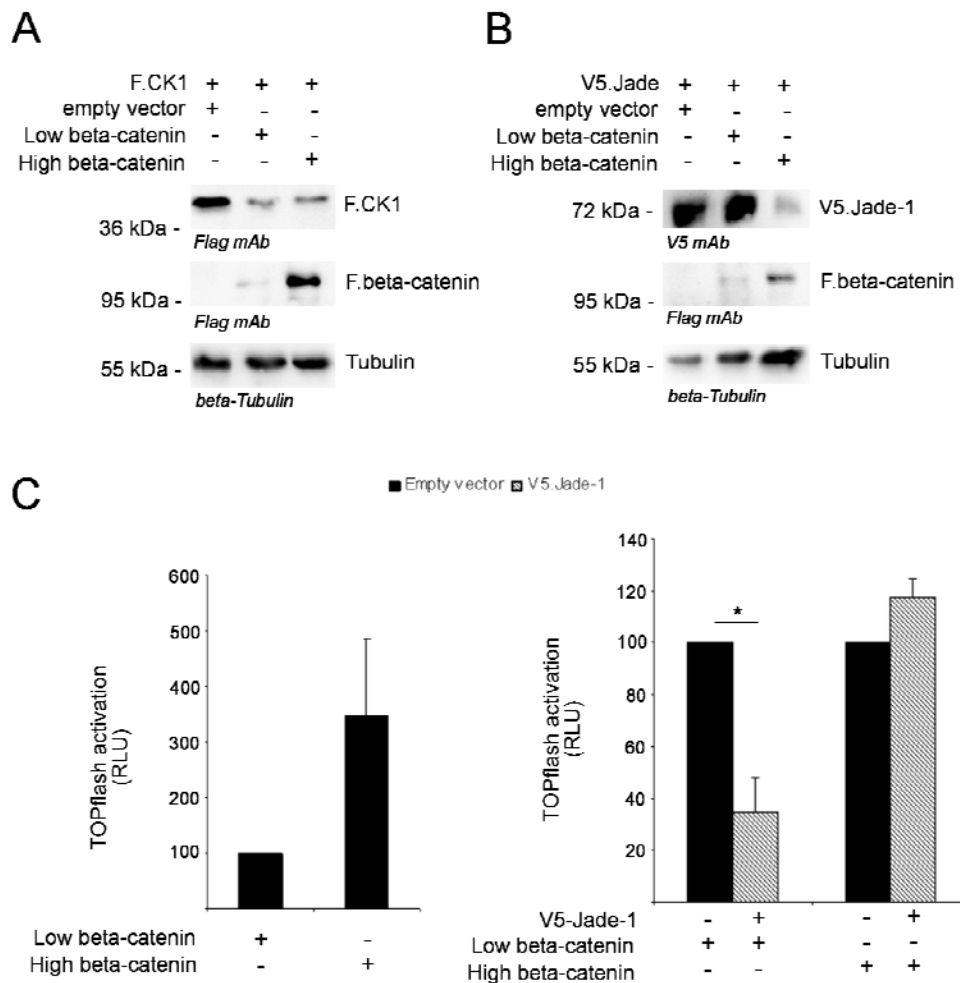


**Figure 18. Increased expression of F. $\beta$ -catenin reduces protein levels of V5.Jade and F.CK1 $\alpha$  at different thresholds.**

**A.** HEK 293T cells were transiently transfected with a master mix of F.CK1 $\alpha$  plus indicated plasmids and processed 24 hours later as a whole cells lysate. Both low and high amounts of transfected F. $\beta$ -

catenin were able to reduce protein expression of F.CK1 $\alpha$ . **B.** HEK 293T cells were transiently transfected with a master mix of V5.Jade-1 plus indicated plasmids and processed 24 later as a whole cells lysate. Only a high amount of transfected F. $\beta$ -catenin was able to reduce protein expression of V5.Jade-1. **C.** HEK 293T cells were transiently transfected with TOPflash reporter plasmid plus constitutively active *Renilla* luciferase, together with experimental plasmids as indicated. A high transfection dose of F. $\beta$ -catenin increased reporter activity substantially (left panel). When reporter activity was set to 100% independently for the high- and low-dose conditions, TOPflash stimulation by low levels of F. $\beta$ -catenin was significantly reduced by V5.Jade-1 expression ( $t(3) = 4.978$ ,  $* = p = 0.01$ ; error bars indicate mean  $\pm$  SE), whereas reporter activity stimulated by high levels of F. $\beta$ -catenin was increased by V5.Jade-1 expression, although this did not reach significance ( $t(3) = 2.309$ ,  $p = 0.1$ ; error bars indicate mean  $\pm$  SE).

### 6.7 Perspectives: CK1-mediated phosphorylation of Jade-1 by PLK1.

Altered Wnt regulation due to Jade-1 phosphorylation by CK1 $\alpha$  could impact a multitude of downstream events. One clue regarding possible biological effects can be derived from the second novel phosphorylation site identified on V5.Jade-1 by mass spectrometry (Fig 16A). Serine 377 of V5.Jade-1 was phosphorylated only in the presence of over-expressed F.CK1 $\alpha$  (Fig 19A), but this site does not correspond to either a primed or unprimed CK1 phosphorylation motif. Instead, the phosphorylation site surrounding serine 377 on V5.Jade-1 was a close match to the consensus phosphorylation motif of Polo-like kinase 1 (PLK1) which is D/E-X-S/T- $\phi$ -X-D/E where  $\phi$  = any hydrophobic residue. The putative phosphorylation motif recognized on V5.Jade-1 was E-E-S-L-G-K, which fulfilled the criteria with the exception that the last residue was basic rather than acidic (Fig 19B).

Of interest, the minimum requirement for a Polobox-domain (PBD) binding motif is a serine immediately preceding a phosphorylated serine or threonine (231). An S-pT motif exists in the N-terminus of Jade-1, where the phosphorylated threonine at T21 could be the target of a CK1 $\alpha$  motif providing the unprimed CK1 $\alpha$  target S18 had previously been phosphorylated (Fig 16B, Fig13A). To determine whether CK1 $\alpha$ -mediated phosphorylation at this site by PLK1 was a possibility, F.PLK1 or a control protein were co-expressed with V5.Jade-1 and the Flag protein was immune-precipitated. V5.Jade-1 co-precipitated with F.PLK1 but not with a control protein (Fig 19C). The Flag-tagged smear corresponding to F.PLK is suggestive of post-translational modification in the presence of V5.Jade-1.

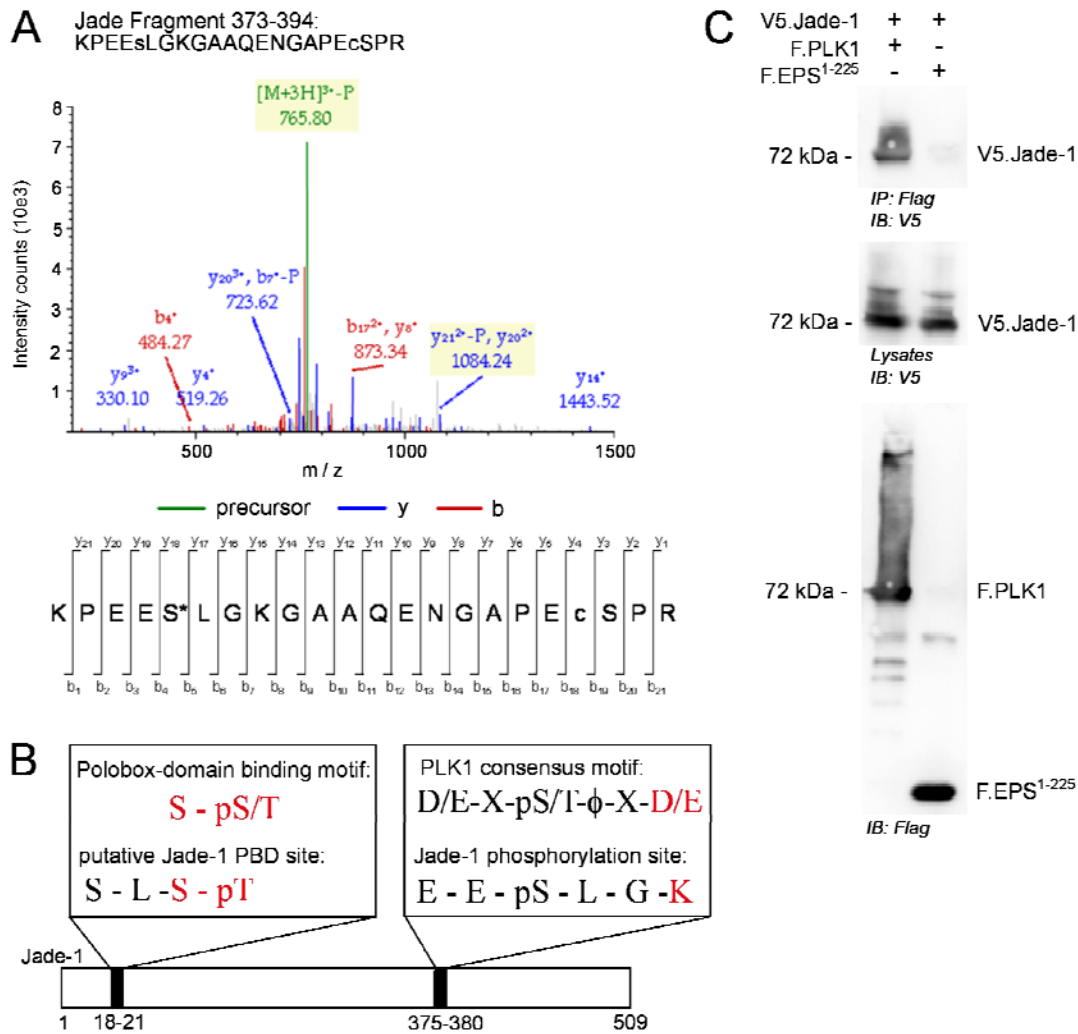


**Figure 19. Jade-1 is phosphorylated in the presence of CK1 on a PLK1-like motif.**

**A.** HEK 293T cells were lysed 24 hours after being transiently transfected with V5.Jade-1 plus either F.CK1 $\alpha$  or empty vector in an 8M Urea buffer with 50mM ammonium bicarbonate. Peptides were digested in trypsin and phosphopeptides were enriched using Fe-NTA immobilized metal affinity chromatography columns before analysis with LTQ Orbitrap XL mass spectrometer. A peak in V5.Jade-1 fragment 373-394 was detected only in lysates containing F.CK1 $\alpha$ . The phosphorylated residue was identified as S377. **B.** The motif containing S377 did not resemble a CK1 phosphorylation motif and instead was similar to a PLK1 consensus motif. The minimum requirement for a polobox-domain binding motif is located at Jade-1 residues 20-21, and the required phosphorylation at T21 matches the target of a canonical CK1 phosphorylation motif. **C.** HEK 293T cells were transiently transfected with V5.Jade-1 and either F.PLK1 or a control protein (F.EPS<sup>1-225</sup>) for 24 hours. Immunoprecipitation was performed using an anti-Flag antibody and V5.Jade-1 co-precipitated with F.PLK1 but not the control protein. All mass spectrometry was performed in collaboration with Dr. Markus Rinschen in the CECAD Proteomics Facility run by Dr. Tobias Lamkemeyer.

## 7 DISCUSSION

A growing body of evidence links renal cyst formation to the dysfunction of cell signaling pathways mediated by the primary cilium, including the canonical Wnt signaling pathway. The current work further links ciliary proteins to canonical Wnt regulation by providing evidence that the canonical Wnt regulator Jade-1 is a part of the nephrocystin protein complex. It has recently been demonstrated that the single-subunit E3 ubiquitin ligase Jade-1 targets cytosolic and nuclear  $\beta$ -catenin, the main effector of canonical Wnt target gene activation, for proteasomal degradation and in doing so negatively regulates canonical Wnt signaling (198). The current work demonstrates that Jade-1 localizes to the centrosome and primary cilium where it interacts with members of the NPH protein complex. Jade-1 protein levels are stabilized by NPHP4, which facilitates Jade-1 nuclear translocation in a phosphatase-dependent manner. Jade-1 and NPHP4 cooperatively restrain  $\beta$ -catenin signaling, and this cooperation is maintained *in vivo*. The classical  $\beta$ -catenin kinase CK1 $\alpha$  phosphorylates Jade-1, which abrogates negative Wnt regulation. A novel Jade-1 phosphorylation site identified in the presence of CK1 $\alpha$  closely resembles a PLK1 phosphorylation motif. PLK1 interacts with Jade-1 and may represent a link between Jade-1, NPH proteins, and the cell cycle. Parts of this work pertaining to nuclear translocation of Jade-1 by NPHP4 have been previously published in Borgal *et al.*, 2012 (218), as indicated in the figure legends.

### 7.1 Jade-1 is a novel member of the nephrocystin protein complex at the ciliary region.

In agreement with previous reports, endogenous Jade-1 localized to both the cytosol and nucleus, excluding nucleoli (196–198). The current work has additionally identified endogenous Jade-1 at the centrosome and within the primary cilium using three independent commercial antibodies. Although Jade-1 was most often visualized as a concentration in the nucleus and at the centrosome, the dynamic nature of this protein was apparent when comparing neighbouring cells from the same experiment. A minority of cells consistently displayed exceptionally intense nuclear or ciliary staining, while other cells were void of nuclear Jade-1 and many cells displayed a peri-nuclear staining pattern. The factors influencing Jade-1 localization are not known, and the variation reported here was not readily explained by any obvious change in cell cycle status or ciliary length.

Despite inter-cellular variation in nuclear or ciliary staining intensities, Jade-1 was consistently observed to be present at the centrosome of interphase cells and mitotic spindle of dividing cells. Jade-1 was verified to be a component of the centrosome complex independent of microtubule transport, and was found to co-localize with transition zone marker NPHP1. Several NPH proteins co-localize at the basal-body or transition zone (14, 23), and are therefore well positioned to interact with Jade-1. To determine whether any of the NPH proteins were candidates to influence the

ability of Jade-1 to negatively regulate canonical Wnt signaling, NPH proteins were screened by co-precipitation for an interaction with V5.Jade-1, and were assessed for their ability to restrain canonical Wnt signaling. V5.Jade-1 was co-precipitated by all NPH proteins tested: F.NPHP1, F.NPHP2, F.NPHP3, F.NPHP4, F.NPHP5, F.NPHP7, F.NPHP8, and F.NPHP9. However, the strength of interaction was variable between proteins as well as between experiments, and analysis of IP lysates indicated that the effect of the different overexpressed NPH proteins could differentially regulate V5.Jade-1. Through the last decade several studies have suggested that NPHP proteins form a common protein complex in which NPHP1 serves as a scaffolding protein (232–234). A recent study based on tandem affinity purification and mass spectrometry confirmed this and reported NPHP1, 4, and 8 to complex separately from NPHP5 and NPHP6 (14). This study also reported that NPHP1, NPHP4, and NPHP8 localize specifically to the transition zone while NPHP2, NPHP3, and NPHP9 localize to the “inversin compartment” at the proximal cilium, and NPHP2, NPHP5, and NPHP6 localize to the basal body. The differential regulation of over-expressed V5.Jade-1 by various over-expressed NPH proteins could reflect a role for each of the NPH proteins in the dynamic expression pattern of endogenous Jade-1. NPHP2, NPHP3, NPHP4 and NPHP7 have previously been identified as negative canonical Wnt regulators (178, 192, 193, 195). Confirming and extending this, all tested NPH proteins restrained rather than amplified canonical Wnt reporter activity. Strikingly, at very low doses NPHP4 and NPHP9 maintained a profound effect. The interaction between V5.Jade-1 and F.NPHP4 was more robust than that observed for V5.Jade-1 and F.NPHP9, which suggested NPHP4 may be an optimal candidate to continue to investigate in terms of Wnt regulation via Jade-1. Since all NPH proteins complex together in vivo and are therefore likely to interact in vitro, further confirmation of endogenous interaction was also sought by co-localization studies described in the next section.

## **7.2 NPHP4 increases nuclear translocation of Jade-1 in a phosphorylation dependent manner.**

The interaction between F.NPHP4 and V5.Jade-1 was confirmed by reciprocal co-immunoprecipitation experiments, and endogenous Jade-1 was further demonstrated to co-precipitate with over-expressed F.NPHP4. Endogenous NPHP4 and Jade-1 were also visualized by immunofluorescence to localize in close proximity at the primary cilium of serum-starved RPE-1 cells. Endogenous NPHP4 immunofluorescence was consistently observed in a peri-nuclear pattern, which demonstrated a striking co-localization with endogenous Jade-1 in cells where Jade-1 was predominantly non-nuclear. Closer examination of lysates from co-precipitation experiments revealed that co-expression of F.NPHP4 decreased V5.Jade-1 in the mostly cytosolic IP lysate but increased V5.Jade-1 protein levels in a whole cell lysate taken from the same experiment. Taken together with

their peri-nuclear co-localization, these data suggested that NPHP4 was in a prime position to stabilize and enhance nuclear translocation of Jade-1.

To validate this, stabilization of V5.Jade-1 by V5.NPHP4 was first confirmed and demonstrated to be specific, as over-expressed V5.NPHP4 did not stabilize the co-expressed control protein V5.GFP. Analysis by qPCR revealed that V5.NPHP4 overexpression did not alter transcription rates of endogenous Jade-1. Instead, over-expression of V5.NPHP4 stabilizes V5.Jade-1 by protecting it from proteasomal degradation, as the stabilization of V5.Jade-1 by the proteasome inhibitor MG132 was not further enhanced in the presence of V5.NPHP4. Over-expressed V5.Jade-1 was consistently visualized in western blot experiments as a double band, and it was the smaller of these two bands that was predominantly stabilized by V5.NPHP4, indicating that NPHP4 might influence the phosphorylation status of Jade-1. Co-expression of V5.NPHP4 and V5.Jade-1 in the presence of the phosphatase inhibitor okadaic acid abrogated the ability of V5.NPHP4 to stabilize V5.Jade-1. Cell fractionation revealed that under standard conditions the smaller V5.Jade-1 species localizes within the cytosol, whereas the larger species is nuclear. Over-expression of V5.NPHP4 causes a shift of the smaller Jade-1 species from the cytosol to the nucleus. Under basal conditions V5.Jade-1 was observed in immunofluorescence and in western blot to localize primarily to the nucleus; however, in the presence of okadaic acid V5.Jade-1 accumulated in the cytosol. Taken together, these data support a scenario whereby NPHP4 leads to the protein stabilization of Jade-1 either by increasing phosphatase activity or by blocking kinase access to phosphorylation sites on Jade-1. The non-phosphorylated form of Jade-1 could then escape proteasomal degradation and instead be able to enter the nucleus where it is again phosphorylated by nuclear kinases.

The perinuclear localization of endogenous NPHP4 renders it optimally localized to influence nuclear trafficking. In cell fraction experiments over-expressed V5.NPHP4 associated with the nuclear fraction in contrast to the cytosolic fractionation of control protein V5.EPS<sup>1-225</sup>. However, like endogenous NPHP4, over-expressed F.NPHP4 was not observed to be nuclear by immunofluorescence staining. These data support a close physical relationship between NPHP4 and the nuclear envelope. Recent parallels have been drawn between the function of the nuclear pore and ciliary/flagellar pore complexes (75, 78), and several classical proteins required for nuclear import and export are described as a part of the ciliary proteome (59). Furthermore, NPH and other ciliopathy proteins have been demonstrated to provide a specific role in the ciliary pore complex at the transition zone (109). The presence of NPHP4 at both the cilium and the perinuclear compartment may reflect similar functions involving the regulation of protein import and/or export at each of these locations. NPHP4 may therefore represent a novel example in a growing list of proteins that function at both the CPC and NPC. The question regarding whether NPC and CPC proteins simply serve the same role at separate locations or whether these proteins represent a specific communication link between the cilium and the nucleus remains to be addressed.

### 7.3 NPHP4 and Jade-1 additively regulate canonical Wnt signaling.

NPHP4 and Jade-1 have previously been independently shown to restrain canonical Wnt signaling (193, 198). The current data demonstrate that these two proteins act cooperatively to do so: the additive reduction in F. $\beta$ -catenin-stimulated TOPflash TCF/LEF reporter activity by V5.NPHP4 and V5.Jade-1 would not have been observed if these proteins influenced  $\beta$ -catenin in a mutually exclusive fashion. To emphasize this, expression of a control protein was not able to augment the effect of either V5.Jade-1 or V5.NPHP4. In addition to reduction of reporter activity, the combined over-expression of V5.Jade-1 and V5.NPHP4 were able to reduce protein expression of the canonical Wnt target gene cMYC. Neither V5.Jade-1 nor V5.NPHP4 were able to reduce reporter activity stimulated by an S33A mutant version of F. $\beta$ -catenin which cannot be phosphorylated, indicating the effect of both proteins depended on their ability to influence the recognition of  $\beta$ -catenin by the proteasome. Of interest, phosphorylated  $\beta$ -catenin accumulates at the basal body while the S33A  $\beta$ -catenin mutant does not (235), which may hint that the regulation of  $\beta$ -catenin by Jade-1 and NPHP4 requires events occurring at this location. Knockdown of endogenous NPHP4 led to significantly enhanced Wnt reporter activity, which could be rescued by over-expression of V5.Jade-1. However, in these conditions V5.Jade-1 was significantly less effective than when co-transfected with scrambled siRNA. This suggests that the ability of Jade-1 to ubiquitinate  $\beta$ -catenin reaches maximum efficiency only in the presence of NPHP4, likely due to protein stabilization and the enhanced opportunity for Jade-1 to ubiquitinate nuclear  $\beta$ -catenin. Knockdown of endogenous Jade-1 reduced the efficiency of V5.NPHP4 in restraining Wnt reporter activity, but there was substantial variability in this effect which indicates that Jade-1 is not the only route through which NPHP4 acts. Indeed, it was recently demonstrated that NPHP4 can also regulate canonical Wnt signaling by decreasing the protein level of the canonical Wnt activator Dsh upstream of  $\beta$ -catenin (193). It is relevant to note that low amounts of Wnt3a can induce a rapid increase in  $\beta$ -catenin without Dsh involvement (236), which opens up the intriguing possibility that NPHP4 moderates Wnt signaling via Jade-1 in situations of low level  $\beta$ -catenin activation but can influence Dsh when  $\beta$ -catenin levels increase. Indeed, the interaction between Jade-1 and  $\beta$ -catenin is reduced when Wnt3a is present (198).

Cooperation between Jade-1 and NPHP4 was supported by the *in vivo* demonstration of a genetic interaction using the developing zebrafish embryo. Morpholino knockdown of each of these proteins led to a curved body phenotype which was similar to that reported after morpholino knockdown of the known Wnt regulator and cystic kidney causing gene *nphp2/inversin* (178). This phenotype was also recently reported by two independent groups after *nphp4* knockdown (193, 221), where *nphp4* morphants were further demonstrated to have ciliary defects and develop pronephric cysts. In accordance with an established link between body curvature, pronephric cysts and ciliary defects (222, 223), pronephric cysts were identified in *jade-1* morphants displaying body axis curvature. The similarity of these phenotypes strongly suggests Wnt deregulation and/or ciliary dysfunction in both the *nphp4* and *jade-1* morphants. Of note, zebrafish body curvature in *nphp4*

morphant embryos was much more frequent than in *jade-1* morphants, mirroring the difference in potency observed in the regulation of Wnt gene activity by NPHP4 *versus* Jade-1 in the reporter assays described above. This difference may be due either to multiple roles in Wnt regulation for NPHP4 or to mechanisms in place to compensate for a loss of Jade-1; either scenario would mean that a loss of NPHP4 would have more dramatic consequences. Taken together, these data support a model whereby NPHP4 acts through multiple mechanisms to regulate canonical Wnt signaling, one of these being the stabilization of the  $\beta$ -catenin ubiquitin ligase Jade-1.

#### **7.4 Phosphorylation of Jade-1 by CK1 $\alpha$ abrogates negative Wnt regulation.**

Stabilization of the smaller of the two V5.Jade-1 species by V5.NPHP4 was consistently observed by western blot, and this stabilization was dependent on phosphatase activity. To determine whether the larger version of V5.Jade-1 could be a result of phosphorylation and whether this phosphorylation played a specific role in Wnt regulation, it was first evaluated whether Jade-1 interacted with any of the classical kinases within the canonical Wnt signaling pathway. Within the destruction complex, CK1 $\alpha$  primes  $\beta$ -catenin for sequential phosphorylation by GSK3 $\beta$ , leading to ubiquitination of cytosolic  $\beta$ -catenin by  $\beta$ -TrCP which targets  $\beta$ -catenin for proteasomal degradation (156, 157). Although V5.Jade-1 co-precipitated with F.GSK3 $\beta$  and F.CK1 $\alpha$ , only co-expression of F.CK1 $\alpha$  resulted in an increase in V5.Jade-1 protein expression size. Indeed, F.CK1 $\alpha$  appeared to stably interact only with this larger version of V5.Jade-1. While the phosphatase-dependent stabilization of Jade-1 by NPHP4 further repressed Wnt gene activation, expression of F.CK1 $\alpha$  increased Wnt reporter activity. Co-expression of V5.Jade-1 in this condition was still able to restrain the F.CK1 $\alpha$ -mediated enhancement of Wnt reporter activity; however, the ability of V5.Jade-1 to do so was markedly reduced. F.CK1 $\alpha$  did not reduce protein expression of V5.Jade-1, indicating instead that phosphorylation of Jade-1 by CK1 $\alpha$  abrogates the ability of Jade-1 to ubiquitinate  $\beta$ -catenin.

##### **7.4.1 CK1 $\alpha$ phosphorylates Jade-1 and $\beta$ -catenin using the same motif**

Mass spectrometry confirmed the presence of several previously published phosphorylated serines and identified two novel Jade-1 phosphorylation sites which were only detected when Jade-1 was co-expressed with CK1 $\alpha$ . However, point mutation of any of these serines to alanine did not alter the ability of F.CK1 $\alpha$  to phosphorylate V5.Jade-1. Truncations of V5.Jade-1 expressed in the presence or absence of F.CK1 $\alpha$  or F.NPHP4 revealed that in both cases the N-terminus was modified while the C-terminus was completely unaltered. The N-terminus of Jade-1 contains many classical CK1 phosphorylation motifs, several of which are positioned so that the phosphorylation of the target serine by CK1 creates the subsequent CK1 phosphorylation motif. CK1 has previously been demonstrated to be a kinase capable of sequential phosphorylation of target proteins (237); however, the initial serine

in such a cascade must be previously phosphorylated. In the case of Jade-1, the initial serine in a cascade of three sequential CK1 $\alpha$  phosphorylation motifs corresponds to an unprimed CK1 $\alpha$  consensus motif, meaning that CK1 $\alpha$  would be capable of priming its own sequential phosphorylation of Jade-1. The serine in this unprimed CK1 $\alpha$  motif, S18, follows a congregation of acidic residues which are required for unprimed CK1 $\alpha$  phosphorylation (226). Of note, the sequence following S18 is S - L - S, which is identical to the noncanonical unprimed motif that CK1 $\alpha$  phosphorylates on  $\beta$ -catenin to prime sequential phosphorylation by GSK3 $\beta$  within the destruction complex (225). This sequence is also contained within the adenomatous polyposis coli (APC) protein, which is a member of the  $\beta$ -catenin destruction complex. Unprimed phosphorylation of S1505 on APC by CK1 initiates a cascade of phosphorylation by CK1 and GSK3 $\beta$  that releases  $\beta$ -catenin from binding within the destruction complex (238). Point mutation of the S18 and S20 residues on Jade-1 abolished the CK1 $\alpha$ -induced size shift of Jade-1. Co-expression of the S18AS20A mutant also impaired the ability of CK1 $\alpha$  over-expression to increase canonical Wnt reporter activity more than co-expression of wild-type Jade-1 was able to. However, CK1 $\alpha$  was still able to increase Wnt reporter activity in these conditions, indicating that the action of phosphorylating Jade-1 is not the only contributor to this effect or that endogenous Jade-1 can still play a major role.

It is interesting to note that the same motif that is phosphorylated by CK1 $\alpha$  on  $\beta$ -catenin is also phosphorylated by CK1 $\alpha$  on Jade-1, with opposing effects: phosphorylation of S45 on  $\beta$ -catenin negatively regulates canonical Wnt signaling by priming cytosolic  $\beta$ -catenin for ubiquitination and subsequent degradation, whereas phosphorylation of the S18-S20 sequence on Jade-1 abrogates the ability of Jade-1 to contribute to  $\beta$ -catenin ubiquitination. Physiologically, these CK1 $\alpha$ -mediated phosphorylation events might be separated temporally or spatially. Jade-1 has been reported to ubiquitinate nuclear and cytosolic  $\beta$ -catenin, whereas CK1 $\alpha$  is mainly considered to regulate  $\beta$ -catenin via its cytosolic role in the destruction complex (156, 157), although a larger CK1 $\alpha$  splice variant may have a nuclear role (239) and many destruction complex components are also found in the nucleus (240). The influence of CK1 $\alpha$  may therefore depend on other cellular events governing access of this kinase to each substrate. Temporal regulation may depend on the activation status of Wnt signaling and the  $\beta$ -catenin destruction complex. A prime example of temporal regulation within the Wnt pathway is given by the classical Wnt kinases CK1 $\alpha$  and GSK3 $\beta$ . Phosphorylation of cytosolic  $\beta$ -catenin requires CK1 $\alpha$  and GSK3 $\beta$  to work cooperatively within the destruction complex. When a Wnt ligand binds to a Fz receptor, the entire destruction complex is relocated to bind with LRP5/6 and Fz at the plasma membrane, where CK1 $\alpha$  and GSK3 $\beta$  are required to phosphorylate LRP5/6 and enable the LRP-mediated Wnt response (170, 171, 241). The role of CK1 $\alpha$  in facilitating Wnt signaling appears to be limited to this immediate event: it complexes with LRP and axin at 30 minutes but not 2 hours after Wnt stimulation (242). Binding of a Wnt ligand recruits E-cadherin and p120-catenin to the LRP/Fz complex, creating a Wnt “signalosome” that is capable of phosphorylating Dsh and initiating the canonical Wnt signaling cascade. After the initial 30 minutes of signalosome function,

CK1 $\alpha$  phosphorylates E-cadherin and this releases p120-catenin from the Wnt signalosome, preventing continued Dsh-2 phosphorylation and contributing to “turning off” the Wnt pathway (242). This series of events means that CK1 $\alpha$ , a kinase that constitutively acts to restrain inappropriate  $\beta$ -catenin activation, responds to a Wnt signaling event by temporally regulated opposing responses: initially CK1 $\alpha$  contributes to signal propagation but it subsequently disables a prolonged response.

#### 7.4.2 Exogenous $\beta$ -catenin causes CK1 $\alpha$ and Jade-1 degradation at different thresholds

This duplicity of CK1 $\alpha$  function might help to explain results showing that CK1 $\alpha$  knockdown decreased Wnt3a-induced TOPflash reporter activity despite increasing  $\beta$ -catenin protein level (242). The current results show a converse contradiction: over-expression of CK1 $\alpha$  increased TOPflash reporter Wnt gene activity. Based on the above discussion, without Wnt stimulation and LRP/Fz signalosome activation CK1 $\alpha$  should be predominantly active at the destruction complex and act as a negative regulator. Further investigation of the current results yielded surprising data showing that exogenous  $\beta$ -catenin decreased expression of F.CK1 $\alpha$ . The reduction of a negative regulator would therefore allow for increased reporter activity; however, because some of the over-expressed CK1 $\alpha$  was nevertheless present, it is likely that the presence of high levels of  $\beta$ -catenin stimulated other cellular events which heightened reporter activity not only through repressing CK1 $\alpha$  expression.

Recent mathematical modeling combined with experimental confirmation in *Xenopus* embryos has demonstrated Wnt gene transcription is sensitive to fold-change rather than absolute  $\beta$ -catenin levels, and can buffer response to  $\beta$ -catenin fluctuation of up to four-fold which would be present in naturally occurring noise (243). When exogenous  $\beta$ -catenin was increased five-fold, V5.Jade-1 was also decreased. These results suggest that an increase in cellular  $\beta$ -catenin not only initiates events leading to its destruction, such as increased rate of destruction complex turnover, but that it also stimulates events leading to the degradation of its negative regulators and the system targets different proteins depending on threshold levels of activation. For example, downregulation of protein levels of CK1 $\alpha$  required only a low amount of  $\beta$ -catenin, and led to a dramatic increase in Wnt reporter activity, whereas downregulation of Jade-1 required a 5-fold increase in over-expressed  $\beta$ -catenin, and resulted in a comparatively mild signal augmentation. The difference in thresholds for these events may contribute to the temporal regulation necessary for operational transients of  $\beta$ -catenin activation to occur.

In general, a pattern has emerged over the last decade of research whereby Wnt signal itself has been shown to initiate its own downregulation. On a genetic level, Wnt signaling increases transcription rate of the secreted Wnt inhibitor Dickkopf 1 (244, 245) and the destruction complex rate-limiting factor Axin2 (246, 247). On a protein level, not only does the signalosome inactivate itself as described above, but also the destruction complex increases turnover rate in response to higher concentrations of  $\beta$ -catenin: in these conditions non-phosphorylated APC is also able to bind  $\beta$ -

catenin, although this is with reduced affinity compared to phosphorylated APC in low  $\beta$ -catenin conditions thereby increasing the rate of  $\beta$ -catenin turnover at the destruction complex (248). While the multiple mechanisms in place to restrain  $\beta$ -catenin signaling have been extensively studied, the mechanisms that  $\beta$ -catenin uses to overcome these are less well understood. Perhaps, the evolution of this pathway to use the same players in different contexts ensures negative regulators were “otherwise engaged” for a specific amount of time so that an effective signal can be achieved when required. This activation then triggers multiple system termination processes; a phenomenon which is telling in terms of how important it is that the pathway does not remain in a prolonged active state. Indeed, disruption of this process is well known to contribute to multiple forms of carcinoma (155, 249, 250). If heightened Wnt signaling has the potential for disaster, why has activation of this pathway in adults been maintained by evolution? Several lines of evidence exist to suggest that isolated re-activation of Wnt signaling is as critical for tissue maintenance in adults as gradient-based signaling is during tissue development in embryogenesis. A paradigm involving isolated and strictly controlled signaling activity may help to explain the complex roles of CK1 $\alpha$ , Jade-1 and NPHP4.

## **7.5 Requirement and regulation of Wnt/ $\beta$ -catenin signaling in the adult kidney: possible roles for Jade-1 and nephrocystin proteins.**

### **7.5.1 Wnt signaling defects during development do not explain cyst formation in NPH**

In order to determine the roles for Jade-1 and NPH proteins in regulating canonical Wnt activity in healthy *versus* diseased adult tissue, the contributing factors regulating each of the Wnt signaling pathways during embryogenesis and in adulthood must be understood. Although much is yet to be discovered, the requirement for canonical Wnt/ $\beta$ -catenin signaling during kidney development is well known. Wnt9b and Wnt4 act sequentially through  $\beta$ -catenin signaling to induce uretic branching and generate epithelial renal vesicles within the metanephric mesenchyme (251–253). However,  $\beta$ -catenin signaling must subsequently be attenuated in order to complete epithelial development (251, 254). In mice,  $\beta$ -catenin signaling is downregulated in the first week of age and disappears completely by 3 weeks of age (179), which is accompanied by changes in gene expression including Wnt targets (255). As the current data has shown the NPH proteins to be involved in negative canonical Wnt regulation, it is possible that this switch critically relies on the NPH protein complex. However, kidneys in NPH are normal at birth, and cysts generally do not form until after the first several years of life. Therefore, the requirement of NPH complex function might be more critical in regulating events occurring after development.

After birth, directed cell movements contribute to the convergent extension required for elongation of kidney tubules. The intercalation of cells during convergent extension requires Wnt signaling via the  $\beta$ -catenin independent PCP pathway (167, 256). PCP signaling also contributes to

oriented cell division, disruption of which is associated with cyst formation as cells no longer divide along the plane of the tubule (162, 257–259). However, disruption of oriented cell division does not precede initial cyst expansion (163), and spindle orientation in dividing cells is random prior to birth despite decreasing cell number in tubule circumference (167), which indicates that pathological tubule expansion might result primarily from deficits in Wnt/PCP-controlled directed convergent extension (256). However, as mentioned above, in contrast to developmental cystic kidney diseases such as ARPKD, disruption of the required developmental switch between canonical Wnt and planar cell polarity signaling does not offer a ready explanation for inherited diseases in which kidney cysts are seen later in life, such as ADPKD or NPH. Cyst formation later in life might instead reflect a failure to maintain, rather than to form, polarized kidney tubules.

### 7.5.2 The Wnt signaling pathways are required for injury repair

The data in the current work demonstrate a complex relationship between  $\beta$ -catenin and its negative regulators Jade-1, CK1 $\alpha$ , and NPHP4. Each of these negative regulators can modify the efficiency of another, acting in concert or in competition. Furthermore, the efficiency of Jade-1 and CK1 $\alpha$  to regulate  $\beta$ -catenin is dependent upon the amount of free  $\beta$ -catenin present, whilst NPHP4 did not appear to be affected by this. In order to clarify a biological role for these proteins, it appears that the cellular status regarding amount of free  $\beta$ -catenin must be taken into consideration. Although free  $\beta$ -catenin is kept at low levels in differentiated epithelia, activation of Wnt signaling during kidney tubule maintenance events might create “windows” of  $\beta$ -catenin activity which change the role of proteins regulating, or regulated by, the Wnt pathways. It is therefore important to understand the events contributing to  $\beta$ -catenin signaling activity in adult renal epithelia, in order to understand how a mutation altering the function of the NPH protein complex might disrupt this.

Throughout life, renal tubules are constantly subject to damage by obstructive, ischemic or toxic insults, and must be able to proliferate to replace lost cells. Current models suggest cyst expansion could occur due to disrupted injury repair in the kidney (260, 261). Indeed, conditional knockout of the *Pkd1* gene causes adult mice to slowly develop focal kidney cysts over four months, but these mice show severe cyst progression only 4–10 weeks after nephrotoxic or ischemic renal injury (187, 262). In these mice, canonical Wnt activators were abnormally upregulated while negative regulators were downregulated compared to wild-type injured mice or knockouts without injury (187), indicating that cyst formation involves excessive canonical Wnt signaling. However, a similar phenotype was observed in *Ahil* knockout mice (263). Loss of the *AHIL* in humans causes Joubert syndrome, a ciliopathy associated with NPH. *Ahil*-null mice are born with normal kidneys but develop NPH at around 5 months of age, which is accelerated dramatically after nephrotoxic or ischemic renal injury. Surprisingly Jbn, the protein product of the *Ahil* gene, was required for activation of the canonical Wnt pathway, and this Wnt activation was required for repair after renal injury. Of interest,

in wild-type animals canonical Wnt reporter activity was specifically enhanced at the cortico-medullary boundary after injury, which is the region prone to cyst formation in NPH. While this data seemingly contradicts the canonical Wnt overactivation reported in *Pkd1* mutant mice, it mirrors the contradictory reports that either gain- or loss-of-function of  $\beta$ -catenin signaling can lead to renal cyst formation (158–161) and fits into a model whereby Wnt/ $\beta$ -catenin signaling is necessary for initial proliferation following renal injury but must be down-regulated to allow for PCP signaling required for differentiation of replacement cells (261). Data exists to suggest that injury-induced proliferating cells are de-differentiated tubular epithelial cells undergoing epithelial-mesenchymal-epithelial cycling (264). In support of this, fate-mapping of tubular repair *in vivo* demonstrated that de-differentiated epithelial cells are responsible for tubule repair (265) but revealed that these cells only share some features with fibroblasts and do not exit the tubule to contribute to the interstitial fibrotic response, which is due instead to pericyte-derived myofibroblasts also upregulated after injury (266). Although many of the processes contributing to these events are not yet known, evidence exists to support the requirement of both Wnt/ $\beta$ -catenin and Wnt/PCP signaling in injury repair (187, 259, 267–272).

### **7.5.3 Different mechanisms of canonical Wnt activation during injury repair and development: roles for cystoproteins at the primary cilium and cell-to-cell contacts.**

The localization of many NPH proteins to both the primary cilium and cell-to-cell contacts suggests that these cellular regions might play an important role in the ability of epithelial cells to initiate signaling pathways in response to injury. In this work, Jade-1 was demonstrated to also localize to primary cilia and to interact with several members of the NPH protein complex. Jade-1 therefore may optimally contribute to the negative regulation of canonical Wnt signaling only in cells containing a functional NPH protein complex within a mature cilium. Primary cilia play an important role in the regulation of Wnt signaling and may be involved in changing the cell's response from canonical Wnt to PCP (178, 182, 186, 273). Conditional knockout of *Kif3a* causes a loss of cilia in both adult and developing mice; however, like the models described above, severe cyst progression occurred only in young mice or after injury in adults (271). This data supports the idea that the “developmental profile” of the tubular epithelium contributes to cyst formation. However, if cells undergoing repair must revert to a developmental status capable of division and subsequently differentiate into a mature tubular cell, then it is curious that a genetic mutation interrupting this process would not interrupt the similar sequence of events occurring during development. In this context, the developmental role of the primary cilium might differ from its role during injury repair in adulthood. For example, urine flow disruption due to renal obstruction would reduce ciliary mechanosensation, which leads to proteolytic cleavage of the polycystin-1 C-term fragment that translocates to the nucleus and upregulates  $\beta$ -catenin signaling (260). It has recently been shown that overexpression of the polycystin-1 C-term fragment degrades Jade-1 (274), which supports the current

data showing that high exogenous  $\beta$ -catenin degrades Jade-1. As the renal epithelium recovers from injury, renal cilia double in length which is normalized after injury is resolved (275, 276). This might render the cilium more sensitive to flow and restore Jade-1 levels by decreasing polycystin-1 cleavage. Bending of a longer cilium might also to enhance calcium influx (132, 133), possibly dependent on upregulation of the ciliary polycystin-1 / polystin -2 calcium channel (139). Of interest, the injury-induced ciliary length increase in mice is preceded by increased mRNA expression of *Invs* and *Pkd1* (276). *PKD1* encodes polycystin-1 which is required for correct localization of polycystin-2 (141), and *INVS* encodes NPHP2, known to be important for calcium-mediated Dsh regulation (178). Increased cellular calcium influx has been shown to play an important role in downregulating  $\beta$ -catenin activation via Protein-kinase-C (277) or via NPHP2/Dsh (178). During development, primary cilia might not be as critical in regulating calcium influx. Short cilia in *Tg737* mutant mice impaired flow-induced calcium influx at 2 weeks of age but not at 1 week of age (138), indicating that before post-natal day 14 primary cilia are not required to regulate calcium levels. Notably, an atypical dihydropyridine-activated  $\text{Ca}^{2+}$  channel was apically localized in collecting duct cells and elicited a response in newborn but not adult rats (278).

Injury repair also differs greatly from developmental processes in that cell-to-cell contacts must be not only established but first disassembled to allow for cell division. As several NPH proteins localize to cell-to-cell contacts as well as to primary cilia there is likely to be crosstalk between these two locations. Also relevant to injury repair,  $\beta$ -catenin is an adhesion molecule which binds E-cadherin at cell-to-cell contacts in addition to its effector role in the canonical Wnt signaling. Dissociation of the zonula adherens by ATP depletion was used to model ischemic injury in Opossum Kidney cells and resulted in  $\beta$ -catenin release from adherens junctions and concomitant accumulation in the nucleus (279). A loss of cell-to-cell contacts also decreases Hippo signaling pathway activation (280, 281), which leads to increased nuclear  $\beta$ -catenin due to two known mechanisms: first, the shift of Hippo effector TAZ to the nucleus decreases inhibitory cytosolic binding between TAZ and Dsh, allowing Dsh phosphorylation and subsequent inhibition of the  $\beta$ -catenin destruction complex (282); and second, the shift of Hippo effector YAP to the nucleus decreases inhibitory cytosolic binding with  $\beta$ -catenin, allowing nuclear translocation of  $\beta$ -catenin (283). Genetic mutation which disrupts an aspect of these processes might mitigate  $\beta$ -catenin signaling needed for repair, but might not effect Wnt ligand stimulated  $\beta$ -catenin signaling needed during development. Injury-specific responses also include increased expression of hepatocyte growth factor (HGF) in renal tubular cells, with the HGF target c-met upregulated specifically at the site of injury (284). HGF signaling increases nuclear  $\beta$ -catenin accumulation independently of external Wnt signaling (285). In the bladder, injury stimulates Shh expression in basal cells which elicits stromal Wnt2 and Wnt4 expression stimulating proliferation in stromal and urothelial cells; this response was dependent on Gli1 which was not needed for normal development (286). As Shh signaling requires functional primary cilia, a genetic mutation disrupting ciliary function could impede this mechanism should a similar injury response

occur in the renal tubules. After ischemic renal injury, invading macrophages secrete Wnt7b which is critical to drive dividing cells through the G2 checkpoint during the repair process (272). Of interest, G2/M arrest after kidney injury causes tubulointerstitial fibrosis (287), a hallmark symptom of NPH. The injury-induced presence of secreted ligands suggests that neighbouring healthy cells must be able to resist Wnt/ $\beta$ -catenin- or HGF/ $\beta$ -catenin-stimulated cell division. In contrast to sub-confluent cells, confluent epithelial cells do not upregulate Rac or AKT activity in response to HGF stimulation, and this results in a decreased  $\beta$ -catenin signaling response due to a lack of AKT-mediated GSK3 $\beta$  inhibition (288). Established adherens junction complexes in confluent cells may also play a key role by stabilizing membrane bound E-cadherin allowing for its interaction with  $\beta$ -catenin (289), which reduces the potential for  $\beta$ -catenin signaling (290, 291) and regulates proliferation via the Hippo signaling pathway (292). Loss of contact inhibition in tumour cells leads to increased proliferation via  $\beta$ -catenin signaling caused by impaired adherens junctions and increased Rac activity (293, 294). An isolated lack of confluency in injured tubular cells may therefore help to create a localized response to a secreted ligand. A mutation impairing the ability of confluent cells to resist this signal would compromise injury repair by expanding the area of cell proliferation.

#### 7.5.4 Re-establishing polarity after injury: roles for cystoproteins and the primary cilium

The current data highlights a negative canonical Wnt regulating role for NPH proteins, which suggests that opposed to the lack of Wnt signaling due to NPH-causing Jbn dysfunction, NPH proteins may be more critical in events allowing PCP signaling to occur, including “turning off” canonical Wnt signaling after injury. Again, evidence exists to support that there may be injury-specific mechanisms in place regulating PCP that differ from a whole tissue processes used during development. For instance, the Wnt receptor Fz3, which is important in Wnt/calcium and Wnt/PCP signaling, relocates from the tight junctions to the apical plasma membrane after renal injury (270). Cystic kidneys of *Pkd1* knockout mice retain upregulated Fz3 at the apical membrane of collecting duct cells and specifically in primary cilia (259), perhaps suggesting a failure to restore Fz3 to the tight junctions. Altered PCP in mouse *Pkd1* pre-cystic kidneys is also indicated by increased variability in centrosome positioning after injury, which the authors suggest reflect a lack of ciliary communication, since *Ift20* ciliary knockout mice also show mislocalized centrosomes in non-dividing cells (295). Indeed, mitotic spindle orientation shows increased randomization in precystic tubules of Kif3a knockout mice lacking primary cilia (271). As loss of the essential vertebrate PCP gene *Fat4* also causes misoriented cell division and cystic kidneys (257), it is apparent that disruption of PCP signaling as well as canonical Wnt signaling can contribute to cyst formation which may be particularly relevant after injury. The exact roles that ciliary proteins including NPHP4 or Jade-1 might play in this process are unknown.

The primary cilium is important in regulation of each of the Wnt signaling pathways, and many cystoproteins, including NPH proteins, share a common localization at this organelle. However, the role of NPH proteins in injury repair is largely unexplored. Possibly, the primary cilium is important in mediating cellular responses due to its small size which could allow a sustained second messenger signal compared to within the soma where such a signal would be quickly diluted (131). Alternatively, the primary cilium could enhance the speed of response, due to the proximity of molecules in the ciliary lumen compared to the cell soma. In the context of injury repair, NPH proteins might be required to fulfill a role as ciliary “gate-keepers”, limiting or selectively enhancing signal transmission to the rest of the cell, or to mediate cross-talk with pathways monitoring the status of cell contacts or the cell cycle. Based on their association with actin as well as microtubule-based structures, it has been proposed that “the nephrocystins integrate signals related to cell adhesion with those controlling cell cycle progression through the cilia sensor”(233). Relevant to PCP *versus*  $\beta$ -catenin signaling events, NPHP1 and NPHP4 mRNA is significantly upregulated during polarization, while knock-down of these proteins delays tight junction and cilia formation in MDCK cells (296). As mentioned, the current data as well as previous publications demonstrate that many of the NPH proteins also play a role in the negative regulation of canonical Wnt signaling (178, 192, 193, 195). Taken together, these data indicate that during a repair scenario NPH proteins might play an important role in the final stages rather than initiation of these events.

In light of this, it is interesting to consider the current data showing that high expression of  $\beta$ -catenin decreases expression of its negative regulator Jade-1, while expression of NPHP4 is able to stabilize this Jade-1 and decrease  $\beta$ -catenin signaling. In interphase cells, phosphorylated  $\beta$ -catenin accumulates at the centrosome while  $\beta$ -catenin localizes within the ciliary lumen (182). Jade-1 also accumulates at the centrosome, and its role in ubiquitinating this pool of  $\beta$ -catenin could be mediated by many of the NPH proteins. The Wnt co-receptor LRP6 is not detected in the healthy adult kidney cortex but is detected robustly in this region following injury (272), and the competence of LRP6 to respond to Wnt ligands reaches a maximum during the G2/M phase of cell division (154). An initial increase in  $\beta$ -catenin during this time could destabilize CK1 $\alpha$  and disrupt destruction complex function, which could further increase  $\beta$ -catenin expression to a level where Jade-1 protein is also decreased. Whether this might occur at the centrosome or also at the nucleus is unknown. In either case, as discussed above even as cells initiate a response to  $\beta$ -catenin signaling termination signals are activated. In this light it is of interest that CK1 $\alpha$  accumulates at the centrosome when cells enter prophase (297), which could have the effect of either phosphorylating  $\beta$ -catenin to reduce a Wnt response, or phosphorylating Jade-1 and LRP6 to enhance it. The balance between these two possibilities might be tipped by NPHP4, which is shown by the current data to modify the same N-terminal fragment of Jade-1 in the opposite fashion as does CK1 $\alpha$ . NPHP4 localizes to centrosome in confluent cells (233), and might play a role when cells reach confluence in “turning off” an injury-induced Wnt response. In subconfluent cells, NPHP4 is dispersed throughout the cytoplasm, and it

might play an earlier role during this time in enhancing Jade-1 nuclear translocation. As Jade-1 can also ubiquitinate non-phosphorylated  $\beta$ -catenin (198), the ability of cytosolic NPHP4 to enhance this might be particularly important during injury repair.

Accumulation of CK1 $\alpha$  at the centrosome just prior to cell division has opened one other interesting possibility for Jade-1 function. CK1 $\alpha$  phosphorylation of Jade-1 creates a binding site for PLK1, which allows the phosphorylation of Jade-1 at a site which is similar to the PLK1 consensus phosphorylation motif. PLK1 is an important kinase for cell cycle progression, and was recently shown to co-localize with NPHP1 at the transition zone and to be activated during ciliary disassembly (298). PLK1 has further been demonstrated to complex with Dsh and activate Aurora-A kinase during Wnt-mediated ciliary disassembly (299). Results from the current work demonstrate that PLK1 also interacts with Jade-1, and the Plk-associated protein smears in these experiments suggest that PLK1 may be ubiquitinated by Jade-1. Downstream effects of this CK1 $\alpha$ -mediated Jade-1 /PLK1 interaction are unknown, but the timing of CK1 $\alpha$  accumulation at the centrosome suggests that Jade-1 could be important in regulating PLK1-mediated ciliary disassembly. PLK1-mediated phosphorylation of Dsh has also been shown to be required for spindle orientation (300), opening an alternative possibility of Jade-1 and CK1 $\alpha$  involvement in this event. Both of these PLK1-mediated spindle orientation and ciliary disassembly are relevant to renal injury repair, and it will be exciting to tease apart further roles for these proteins in these events.

## 7.6 Conclusion

Cystic kidneys are a common occurrence in several different diseases and represent a major burden on the health care system. Although much remains to be elucidated, it is obvious that renal injury can markedly exacerbate cyst progression, and that repair pathways involve Wnt/ $\beta$ -catenin, Wnt/PCP, and Wnt/calcium signaling. Both primary cilia and the integrity of cell-contacts play a role in each of these pathways, and it is likely no coincidence that protein products of ciliopathy-causing genes localize to both of these regions. If failure to repair renal injury is a key instigator of cyst formation, this would account for the wide variety of protein dysfunction which can lead to a similar renal cystic phenotype. Conversely, so many ways by which to interfere with this process would account for the variations in the exact cystic phenotype seen as a result of different gene mutations. The requirement for an environmental co-factor would furthermore account for variation in time of disease onset between patients with the same genetic mutation.

The current work explores a detailed relationship between  $\beta$ -catenin regulation by Jade-1 and the NPH protein complex. As the data indicate, the regulation of  $\beta$ -catenin by these proteins depends on the amount of free  $\beta$ -catenin and results in a complex interplay between the negative Wnt regulators NPHP4, CK1 $\alpha$ , and Jade-1. The efficacy of  $\beta$ -catenin regulation by these proteins may very well be temporally regulated and dependent on the status of cell division and the maturation of the

---

primary cilium. While much knowledge has been gained in the last decades regarding ciliopathy research, detailed understanding of the role that these organelles play in healthy and diseased tissue will be required to fully understand ciliopathy-related diseases. Understanding the molecular mechanisms underlying injury repair will provide powerful new tools to treat these diseases as well as other diseases which may result from aberrant injury repair. Understanding the molecular mechanisms controlling Wnt signaling, cell adhesion, and cell division will also be of critical importance in designing next generation therapies for diseases caused by deregulation of these processes such as cancer.

## 8 PUBLICATIONS

### 8.1 Publications in Academic Journals

L. Borgal, S. Habbig, J. Hatzold, M. C. Liebau, C. Dafinger, I. Sacarea, M. Hammerschmidt, T. Benzing, B. Schermer, 2012. The ciliary protein nephrocystin-4 translocates the canonical Wnt regulator Jade-1 to the nucleus to negatively regulate  $\beta$ -catenin signaling. *J Biol Chem.* 287 (39): 25370-80.

L. Borgal, M. Hong, D. Sadi & I. Mendez, 2007. Differential effects of glial cell line-derived neurotrophic factor on A9 and A10 dopamine neuron survival in vitro. *Neuroscience.* 147 (3): 712-9.

### 8.2 Publications in International Academic Conferences

L. Borgal, M. Rinschen, T. Benzing, B. Schermer, 2012. Nuclear translocation of the canonical Wnt-regulator Jade-1 is phosphorylation-dependent. The American Society for Cell Biology Annual Meeting, San Francisco. *Mol. Biol. Cell* 23 (suppl). Abstract No. 2301.

(oral presentation)

L. Borgal, S. Habbig, M. C. Liebau, C. Dafinger, R. Mueller, T. Benzing, B. Schermer, 2011. The Cilia-associated Protein NPHP4 Translocates Canonical Wnt-regulator Jade-1 to the Nucleus. American Society of Nephrology, Philadelphia. Abstract No. FR-OR249

L. Borgal, S. Habbig, J. Hatzold, M.C. Liebau, C. Dafinger, T. Benzing, M. Hammerschmidt, B. Schermer, 2011. The ciliary protein NPHP4 translocates canonical Wnt regulator Jade-1 to the nucleus. The EMBO Meeting, Vienna. Abstract No. C141

L. Borgal, D. Sadi & I. Mendez, 2003. Complex sensorimotor recovery of 6-OHDA lesioned hemiparkinsonian rats with low dose intrastriatal FVM grafts. *Experimental Neurology.* 181(1):86.

L. Borgal, M. McLeod, M. Lewington, D. Sadi, I. Mendez, 2004. Effect of local liposomal tacrolimus on cell survival and behavioural recovery following double co-grafts of VM and GDNF-C17.2 cells in the 6-OHDA rat model of Parkinson's disease. *Experimental Neurology.* 187(1): 225.

## 9 REFERENCES

1. Guay-Woodford, L. M. (2006) Renal cystic diseases: diverse phenotypes converge on the cilium/centrosome complex. *Pediatr. Nephrol.*, 21, 1369–1376.
2. Wilson, P. D. (2004) Polycystic kidney disease. *N. Engl. J. Med.*, 350, 151–164.
3. Gordon, C. E. (2012) *Harrison's Principles of Internal Medicine 18th ed*, 18th Ed., The McGraw-Hill Companies, Inc.
4. Wilson, P. D., and Goilav, B. (2007) Cystic disease of the kidney. *Annu Rev Pathol*, 2, 341–368.
5. Salomon, R., Saunier, S., and Niaudet, P. (2009) Nephronophthisis. *Pediatr. Nephrol*, 24, 2333–2344.
6. Hildebrandt, F., and Zhou, W. (2007) Nephronophthisis-associated ciliopathies. *J. Am. Soc. Nephrol.*, 18, 1855–1871.
7. Hurd, T. W., and Hildebrandt, F. (2011) Mechanisms of nephronophthisis and related ciliopathies. *Nephron Exp. Nephrol.*, 118, e9–14.
8. Bredrup, C., Saunier, S., Oud, M. M., Fiskerstrand, T., Hoischen, A., Brackman, D., Leh, S. M., Midtbø, M., Filhol, E., Bole-Feysot, C., Nitschké, P., et al. (2011) Ciliopathies with skeletal anomalies and renal insufficiency due to mutations in the IFT-A gene WDR19. *Am. J. Hum. Genet.*, 89, 634–643.
9. Chaki, M., Airik, R., Ghosh, A. K., Giles, R. H., Chen, R., Slaats, G. G., Wang, H., Hurd, T. W., Zhou, W., Cluckey, A., Gee, H. Y., et al. (2012) Exome capture reveals ZNF423 and CEP164 mutations, linking renal ciliopathies to DNA damage response signaling. *Cell*, 150, 533–548.
10. Davis, E. E., Zhang, Q., Liu, Q., Diplas, B. H., Davey, L. M., Hartley, J., Stoetzel, C., Szymanska, K., Ramaswami, G., Logan, C. V., Muzny, D. M., et al. (2011) TTC21B contributes both causal and modifying alleles across the ciliopathy spectrum. *Nat. Genet.*, 43, 189–196.
11. Zaghoul, N. A., and Katsanis, N. (2010) Functional modules, mutational load and human genetic disease. *Trends Genet.*, 26, 168–176.
12. Zaghoul, N. A., Liu, Y., Gerdes, J. M., Gascue, C., Oh, E. C., Leitch, C. C., Bromberg, Y., Binkley, J., Leibel, R. L., Sidow, A., Badano, J. L., et al. (2010) Functional analyses of variants reveal a significant role for dominant negative and common alleles in oligogenic Bardet-Biedl syndrome. *Proc. Natl. Acad. Sci. U.S.A.*, 107, 10602–10607.
13. Hildebrandt, F., and Otto, E. (2005) Cilia and centrosomes: a unifying pathogenic concept for cystic kidney disease? *Nat. Rev. Genet.*, 6, 928–940.
14. Sang, L., Miller, J. J., Corbit, K. C., Giles, R. H., Brauer, M. J., Otto, E. A., Baye, L. M., Wen, X., Scales, S. J., Kwong, M., Huntzicker, E. G., et al. (2011) Mapping the NPHP-JBTS-MKS protein network reveals ciliopathy disease genes and pathways. *Cell*, 145, 513–528.

15. Pazour, G. J. (2004) Intraflagellar transport and cilia-dependent renal disease: the ciliary hypothesis of polycystic kidney disease. *J. Am. Soc. Nephrol.*, 15, 2528–2536.
16. Zhang, Q., Taulman, P. D., and Yoder, B. K. (2004) Cystic kidney diseases: all roads lead to the cilium. *Physiology (Bethesda)*, 19, 225–230.
17. Omran, H., Fernandez, C., Jung, M., Häffner, K., Fargier, B., Villaquiran, A., Waldherr, R., Gretz, N., Brandis, M., Rüschenhoff, F., Reis, A., et al. (2000) Identification of a New Gene Locus for Adolescent Nephronophthisis, on Chromosome 3q22 in a Large Venezuelan Pedigree. *The American Journal of Human Genetics*, 66, 118–127.
18. Moyer, J. H., Lee-Tischler, M. J., Kwon, H. Y., Schrick, J. J., Avner, E. D., Sweeney, W. E., Godfrey, V. L., Cacheiro, N. L., Wilkinson, J. E., and Woychik, R. P. (1994) Candidate gene associated with a mutation causing recessive polycystic kidney disease in mice. *Science*, 264, 1329–1333.
19. Barr, M. M., and Sternberg, P. W. (1999) A polycystic kidney-disease gene homologue required for male mating behaviour in *C. elegans*. *Nature*, 401, 386–389.
20. Pazour, G. J., Dickert, B. L., Vucica, Y., Seeley, E. S., Rosenbaum, J. L., Witman, G. B., and Cole, D. G. (2000) Chlamydomonas IFT88 and its mouse homologue, polycystic kidney disease gene *tg737*, are required for assembly of cilia and flagella. *J. Cell Biol.*, 151, 709–718.
21. Yoder, B. K., Hou, X., and Guay-Woodford, L. M. (2002) The polycystic kidney disease proteins, polycystin-1, polycystin-2, polaris, and cystin, are co-localized in renal cilia. *J. Am. Soc. Nephrol.*, 13, 2508–2516.
22. Reiter, J. F., Blacque, O. E., and Leroux, M. R. (2012) The base of the cilium: roles for transition fibres and the transition zone in ciliary formation, maintenance and compartmentalization. *EMBO Rep.*, 13, 608–618.
23. Czarnecki, P. G., and Shah, J. V. (2012) The ciliary transition zone: from morphology and molecules to medicine. *Trends in Cell Biology*, 22, 201–210.
24. Badano, J. L., Mitsuma, N., Beales, P. L., and Katsanis, N. (2006) The ciliopathies: an emerging class of human genetic disorders. *Annu Rev Genomics Hum Genet*, 7, 125–148.
25. Fliegauf, M., Benzing, T., and Omran, H. (2007) When cilia go bad: cilia defects and ciliopathies. *Nat. Rev. Mol. Cell Biol*, 8, 880–893.
26. Chang, B., Khanna, H., Hawes, N., Jimeno, D., He, S., Lillo, C., Parapuram, S. K., Cheng, H., Scott, A., Hurd, R. E., Sayer, J. A., et al. (2006) In-frame deletion in a novel centrosomal/ciliary protein CEP290/NPHP6 perturbs its interaction with RPGR and results in early-onset retinal degeneration in the *rd16* mouse. *Hum. Mol. Genet.*, 15, 1847–1857.
27. Otto, E. A., Loeys, B., Khanna, H., Hellemans, J., Sudbrak, R., Fan, S., Muerb, U., O’Toole, J. F., Helou, J., Attanasio, M., Utsch, B., et al. (2005) Nephrocystin-5, a ciliary IQ domain protein, is mutated in Senior-Loken syndrome and interacts with RPGR and calmodulin. *Nat. Genet.*, 37, 282–288.
28. Roepman, R., Letteboer, S. J. F., Arts, H. H., van Beersum, S. E. C., Lu, X., Krieger, E., Ferreira, P. A., and Cremers, F. P. M. (2005) Interaction of nephrocystin-4 and RPGRIP1 is disrupted by nephronophthisis or Leber congenital amaurosis-associated mutations. *Proc. Natl. Acad. Sci. U.S.A.*, 102, 18520–18525.

29. Insinna, C., and Besharse, J. C. (2008) Intraflagellar transport and the sensory outer segment of vertebrate photoreceptors. *Dev. Dyn.*, 237, 1982–1992.
30. Hildebrandt, F., Attanasio, M., and Otto, E. (2009) Nephronophthisis: disease mechanisms of a ciliopathy. *J Am Soc Nephrol*, 20, 23–35.
31. Garcia-Gonzalo, F. R., Corbit, K. C., Sirerol-Piquer, M. S., Ramaswami, G., Otto, E. A., Noriega, T. R., Seol, A. D., Robinson, J. F., Bennett, C. L., Josifova, D. J., García-Verdugo, J. M., et al. (2011) A transition zone complex regulates mammalian ciliogenesis and ciliary membrane composition. *Nat. Genet.*, 43, 776–784.
32. Watnick, T., and Germino, G. (2003) From cilia to cyst. *Nat. Genet.*, 34, 355–356.
33. Donaldson, J. C., Dise, R. S., Ritchie, M. D., and Hanks, S. K. (2002) Nephrocystin-conserved domains involved in targeting to epithelial cell-cell junctions, interaction with filamins, and establishing cell polarity. *J. Biol. Chem.*, 277, 29028–29035.
34. Huan, Y., and van Adelsberg, J. (1999) Polycystin-1, the PKD1 gene product, is in a complex containing E-cadherin and the catenins. *J. Clin. Invest.*, 104, 1459–1468.
35. Nürnberger, J., Bacallao, R. L., and Phillips, C. L. (2002) Inversin forms a complex with catenins and N-cadherin in polarized epithelial cells. *Mol. Biol. Cell*, 13, 3096–3106.
36. Attanasio, M., Uhlenhaut, N. H., Sousa, V. H., O’Toole, J. F., Otto, E., Anlag, K., Klugmann, C., Treier, A.-C., Helou, J., Sayer, J. A., Seelow, D., et al. (2007) Loss of GLIS2 causes nephronophthisis in humans and mice by increased apoptosis and fibrosis. *Nat. Genet*, 39, 1018–1024.
37. Brown, N. E., and Murcia, N. S. (2003) Delayed cystogenesis and increased ciliogenesis associated with the re-expression of polaris in Tg737 mutant mice. *Kidney Int.*, 63, 1220–1229.
38. O’Toole, J. F., Liu, Y., Davis, E. E., Westlake, C. J., Attanasio, M., Otto, E. A., Seelow, D., Nurnberg, G., Becker, C., Nuutinen, M., Kärppä, M., et al. (2010) Individuals with mutations in XPNPEP3, which encodes a mitochondrial protein, develop a nephronophthisis-like nephropathy. *J. Clin. Invest.*, 120, 791–802.
39. Pedersen, L. B., Schrøder, J. M., Satir, P., and Christensen, S. T. (2011) The ciliary cytoskeleton. *Compr. Physiol.*, 2, 779-803.
40. Wheatley, D. N. (2005) Landmarks in the first hundred years of primary (9+0) cilium research. *Cell Biol. Int.*, 29, 333–339.
41. Sorokin, S. (1962) Centrioles and the formation of rudimentary cilia by fibroblasts and smooth muscle cells. *J. Cell Biol.*, 15, 363–377.
42. Pazour, G. J., and Witman, G. B. (2003) The vertebrate primary cilium is a sensory organelle. *Curr. Opin. Cell Biol.*, 15, 105–110.
43. Tucker, R. W., Pardee, A. B., and Fujiwara, K. (1979) Centriole ciliation is related to quiescence and DNA synthesis in 3T3 cells. *Cell*, 17, 527–535.
44. Pan, J., Seeger-Nukpezah, T., and Golemis, E. A. (2012) The role of the cilium in normal and abnormal cell cycles: emphasis on renal cystic pathologies. *Cellular and molecular life sciences: CMLS*, doi. 10.1007/s00018-012-1052-z

45. Kim, S., and Tsiokas, L. (2011) Cilia and cell cycle re-entry: more than a coincidence. *Cell Cycle*, 10, 2683–2690.
46. Qin, H., Wang, Z., Diener, D., and Rosenbaum, J. (2007) Intraflagellar transport protein 27 is a small G protein involved in cell-cycle control. *Curr Biol*, 17, 193–202.
47. Robert, A., Margall-Ducos, G., Guidotti, J.-E., Brégerie, O., Celati, C., Bréchet, C., and Desdouets, C. (2007) The intraflagellar transport component IFT88/polaris is a centrosomal protein regulating G1-S transition in non-ciliated cells. *J Cell Sci*, 120, 628–37.
48. Pugacheva, E. N., Jablonski, S. A., Hartman, T. R., Henske, E. P., and Golemis, E. A. (2007) HEF1-dependent Aurora A activation induces disassembly of the primary cilium. *Cell*, 129, 1351–63.
49. Li, A., Saito, M., Chuang, J.-Z., Tseng, Y.-Y., Dedesma, C., Tomizawa, K., Kaitsuka, T., and Sung, C.-H. (2011) Ciliary transition zone activation of phosphorylated Tctex-1 controls ciliary resorption, S-phase entry and fate of neural progenitors. *Nat Cell Biol*, 13, 402–411.
50. Jacoby, M., Cox, J. J., Gayral, S., Hampshire, D. J., Ayub, M., Blockmans, M., Pernot, E., Kisseleva, M. V., Compère, P., Schiffmann, S. N., Gergely, F., et al. (2009) INPP5E mutations cause primary cilium signaling defects, ciliary instability and ciliopathies in human and mouse. *Nat. Genet.*, 41, 1027–1031.
51. Bielas, S. L., Silhavy, J. L., Brancati, F., Kisseleva, M. V., Al-Gazali, L., Sztriha, L., Bayoumi, R. A., Zaki, M. S., Abdel-Aleem, A., Rosti, R. O., Kayserili, H., et al. (2009) Mutations in INPP5E, encoding inositol polyphosphate-5-phosphatase E, link phosphatidyl inositol signaling to the ciliopathies. *Nat. Genet.*, 41, 1032–1036.
52. Piao, T., Luo, M., Wang, L., Guo, Y., Li, D., Li, P., Snell, W. J., and Pan, J. (2009) A microtubule depolymerizing kinesin functions during both flagellar disassembly and flagellar assembly in *Chlamydomonas*. *Proc. Natl. Acad. Sci. U.S.A.*, 106, 4713–4718.
53. Kim, S., Zaghoul, N. A., Bubenshchikova, E., Oh, E. C., Rankin, S., Katsanis, N., Obara, T., and Tsiokas, L. (2011) Nde1-mediated inhibition of ciliogenesis affects cell cycle re-entry. *Nat Cell Biol*, 13, 351–360.
54. Spalluto, C., Wilson, D. I., and Hearn, T. (2012) Nek2 localises to the distal portion of the mother centriole/basal body and is required for timely cilium disassembly at the G2/M transition. *Eur. J. Cell Biol.*, 91, 675–686.
55. Ward, C. J., Yuan, D., Masyuk, T. V., Wang, X., Punyashthiti, R., Whelan, S., Bacallao, R., Torra, R., LaRusso, N. F., Torres, V. E., and Harris, P. C. (2003) Cellular and subcellular localization of the ARPKD protein; fibrocystin is expressed on primary cilia. *Hum. Mol. Genet.*, 12, 2703–2710.
56. Iwanaga, T., Miki, T., and Takahashi-Iwanaga, H. (2011) Restricted expression of somatostatin receptor 3 to primary cilia in the pancreatic islets and adenohypophysis of mice. *Biomed. Res.*, 32, 73–81.
57. Iwanaga, T., Hozumi, Y., and Takahashi-Iwanaga, H. (2011) Immunohistochemical demonstration of dopamine receptor D2R in the primary cilia of the mouse pituitary gland. *Biomed. Res.*, 32, 225–235.

58. Berbari, N. F., Lewis, J. S., Bishop, G. A., Askwith, C. C., and Mykytyn, K. (2008) Bardet-Biedl syndrome proteins are required for the localization of G protein-coupled receptors to primary cilia. *Proc. Natl. Acad. Sci. U.S.A.*, 105, 4242–4246.
59. Ishikawa, H., Thompson, J., Yates, J. R., 3rd, and Marshall, W. F. (2012) Proteomic analysis of mammalian primary cilia. *Curr. Biol.*, 22, 414–419.
60. Gerdes, J. M., Davis, E. E., and Katsanis, N. (2009) The vertebrate primary cilium in development, homeostasis, and disease. *Cell*, 137, 32–45.
61. Gherman, A., Davis, E. E., and Katsanis, N. (2006) The ciliary proteome database: an integrated community resource for the genetic and functional dissection of cilia. *Nat. Genet.*, 38, 961–962.
62. Sorokin, S. P. (1968) Reconstructions of centriole formation and ciliogenesis in mammalian lungs. *J. Cell. Sci.*, 3, 207–230.
63. Piel, M., Meyer, P., Khodjakov, A., Rieder, C. L., and Bornens, M. (2000) The respective contributions of the mother and daughter centrioles to centrosome activity and behavior in vertebrate cells. *J. Cell Biol.*, 149, 317–330.
64. Kobayashi, T., and Dynlacht, B. D. (2011) Regulating the transition from centriole to basal body. *J. Cell Biol.*, 193, 435–444.
65. Paintrand, M., Moudjou, M., Delacroix, H., and Bornens, M. (1992) Centrosome organization and centriole architecture: their sensitivity to divalent cations. *J. Struct. Biol.*, 108, 107–128.
66. Gilula, N. B., and Satir, P. (1972) The ciliary necklace. A ciliary membrane specialization. *J. Cell Biol.*, 53, 494–509.
67. Graser, S., Stierhof, Y.-D., Lavoie, S. B., Gassner, O. S., Lamla, S., Le Clech, M., and Nigg, E. A. (2007) Cep164, a novel centriole appendage protein required for primary cilium formation. *J. Cell Biol.*, 179, 321–30.
68. Craige, B., Tsao, C.-C., Diener, D. R., Hou, Y., Lechtreck, K.-F., Rosenbaum, J. L., and Witman, G. B. (2010) CEP290 tethers flagellar transition zone microtubules to the membrane and regulates flagellar protein content. *J. Cell Biol.*, 190, 927–940.
69. Anderson, R. G. (1972) The three-dimensional structure of the basal body from the rhesus monkey oviduct. *J. Cell Biol.*, 54, 246–265.
70. Nachury, M. V., Seeley, E. S., and Jin, H. (2010) Trafficking to the ciliary membrane: how to get across the periciliary diffusion barrier? *Annu. Rev. Cell Dev. Biol.*, 26, 59–87.
71. Vieira, O. V., Gaus, K., Verkade, P., Fullekrug, J., Vaz, W. L. C., and Simons, K. (2006) FAPP2, cilium formation, and compartmentalization of the apical membrane in polarized Madin-Darby canine kidney (MDCK) cells. *Proc. Natl. Acad. Sci. U.S.A.*, 103, 18556–18561.
72. Rosenbaum, J. L., and Witman, G. B. (2002) Intraflagellar transport. *Nat. Rev. Mol. Cell Biol.*, 3, 813–825.
73. Pedersen, L. B., and Rosenbaum, J. L. (2008) Chapter 2 Intraflagellar Transport (IFT) Role in Ciliary Assembly, Resorption and Signalling. *Curr. Top. Dev. Biol.*, 85, 23–61.

74. Obado, S. O., and Rout, M. P. (2012) Ciliary and nuclear transport: different places, similar routes? *Dev. Cell*, 22, 693–694.
75. Dishinger, J. F., Kee, H. L., Jenkins, P. M., Fan, S., Hurd, T. W., Hammond, J. W., Truong, Y. N.-T., Margolis, B., Martens, J. R., and Verhey, K. J. (2010) Ciliary entry of the kinesin-2 motor KIF17 is regulated by importin-beta2 and RanGTP. *Nat. Cell Biol.*, 12, 703–710.
76. Nair, K. S., Hanson, S. M., Mendez, A., Gurevich, E. V., Kennedy, M. J., Shestopalov, V. I., Vishnivetskiy, S. A., Chen, J., Hurley, J. B., Gurevich, V. V., and Slepak, V. Z. (2005) Light-dependent redistribution of arrestin in vertebrate rods is an energy-independent process governed by protein-protein interactions. *Neuron*, 46, 555–567.
77. Calvert, P. D., Schiesser, W. E., and Pugh, E. N. (2010) Diffusion of a soluble protein, photoactivatable GFP, through a sensory cilium. *J Gen Physiol*, 135, 173–196.
78. Kee, H. L., Dishinger, J. F., Lynne Blasius, T., Liu, C.-J., Margolis, B., and Verhey, K. J. (2012) A size-exclusion permeability barrier and nucleoporins characterize a ciliary pore complex that regulates transport into cilia. *Nat. Cell Biol.*, 14, 431–437.
79. Ward, H. H., Brown-Glaberman, U., Wang, J., Morita, Y., Alper, S. L., Bedrick, E. J., Gattone, V. H., 2nd, Deretic, D., and Wandinger-Ness, A. (2011) A conserved signal and GTPase complex are required for the ciliary transport of polycystin-1. *Molecular Biology of the Cell*, 22, 3289–3305.
80. Deretic, D., Schmerl, S., Hargrave, P. A., Arendt, A., and McDowell, J. H. (1998) Regulation of sorting and post-Golgi trafficking of rhodopsin by its C-terminal sequence QVS(A)PA. *Proc. Natl. Acad. Sci. U.S.A.*, 95, 10620–10625.
81. Geng, L., Okuhara, D., Yu, Z., Tian, X., Cai, Y., Shibazaki, S., and Somlo, S. (2006) Polycystin-2 traffics to cilia independently of polycystin-1 by using an N-terminal RVxP motif. *J. Cell. Sci.*, 119, 1383–1395.
82. Pazour, G. J., and Bloodgood, R. A. (2008) Chapter 5 targeting proteins to the ciliary membrane. *Curr Top Dev Biol*, 85, 115–49.
83. Berbari, N. F., Johnson, A. D., Lewis, J. S., Askwith, C. C., and Mykytyn, K. (2008) Identification of ciliary localization sequences within the third intracellular loop of G protein-coupled receptors. *Mol. Biol. Cell*, 19, 1540–1547.
84. Follit, J. A., Li, L., Vucica, Y., and Pazour, G. J. (2010) The cytoplasmic tail of fibrocystin contains a ciliary targeting sequence. *J Cell Biol*, 188, 21–28.
85. Kozminski, K. G., Johnson, K. A., Forscher, P., and Rosenbaum, J. L. (1993) A motility in the eukaryotic flagellum unrelated to flagellar beating. *Proc. Natl. Acad. Sci. U.S.A.*, 90, 5519–5523.
86. Kozminski, K. G., Beech, P. L., and Rosenbaum, J. L. (1995) The Chlamydomonas kinesin-like protein FLA10 is involved in motility associated with the flagellar membrane. *J Cell Biol*, 131, 1517–1527.
87. Johnson, K. A., and Rosenbaum, J. L. (1992) Polarity of flagellar assembly in Chlamydomonas. *J Cell Biol*, 119, 1605–1611.

88. Pazour, G. J., Wilkerson, C. G., and Witman, G. B. (1998) A Dynein Light Chain Is Essential for the Retrograde Particle Movement of Intraflagellar Transport (IFT). *J Cell Biol*, 141, 979–992.
89. Cole, D. G., Diener, D. R., Himelblau, A. L., Beech, P. L., Fuster, J. C., and Rosenbaum, J. L. (1998) Chlamydomonas Kinesin-II–dependent Intraflagellar Transport (IFT): IFT Particles Contain Proteins Required for Ciliary Assembly in *Caenorhabditis elegans* Sensory Neurons. *J Cell Biol*, 141, 993–1008.
90. Pazour, G. J., Dickert, B. L., and Witman, G. B. (1999) The DHC1b (DHC2) isoform of cytoplasmic dynein is required for flagellar assembly. *J. Cell Biol.*, 144, 473–481.
91. Pedersen, L. B., Geimer, S., and Rosenbaum, J. L. (2006) Dissecting the molecular mechanisms of intraflagellar transport in *chlamydomonas*. *Curr. Biol.*, 16, 450–459.
92. Signor, D., Wedaman, K. P., Orozco, J. T., Dwyer, N. D., Bargmann, C. I., Rose, L. S., and Scholey, J. M. (1999) Role of a class DHC1b dynein in retrograde transport of IFT motors and IFT raft particles along cilia, but not dendrites, in chemosensory neurons of living *Caenorhabditis elegans*. *J. Cell Biol.*, 147, 519–530.
93. Iomini, C., Babaev-Khaimov, V., Sassaroli, M., and Piperno, G. (2001) Protein Particles in *Chlamydomonas* Flagella Undergo a Transport Cycle Consisting of Four Phases. *J Cell Biol*, 153, 13–24.
94. Pan, X., Ou, G., Civelekoglu-Scholey, G., Blacque, O. E., Endres, N. F., Tao, L., Mogilner, A., Leroux, M. R., Vale, R. D., and Scholey, J. M. (2006) Mechanism of transport of IFT particles in *C. elegans* cilia by the concerted action of kinesin-II and OSM-3 motors. *J Cell Biol*, 174, 1035–1045.
95. Snow, J. J., Ou, G., Gunnarson, A. L., Walker, M. R. S., Zhou, H. M., Brust-Mascher, I., and Scholey, J. M. (2004) Two anterograde intraflagellar transport motors cooperate to build sensory cilia on *C. elegans* neurons. *Nat. Cell Biol.*, 6, 1109–1113.
96. Jenkins, P. M., Hurd, T. W., Zhang, L., McEwen, D. P., Brown, R. L., Margolis, B., Verhey, K. J., and Martens, J. R. (2006) Ciliary Targeting of Olfactory CNG Channels Requires the CNGB1b Subunit and the Kinesin-2 Motor Protein, KIF17. *Current Biology*, 16, 1211–1216.
97. Insinna, C., Pathak, N., Perkins, B., Drummond, I., and Besharse, J. C. (2008) The homodimeric kinesin, Kif17, is essential for vertebrate photoreceptor sensory outer segment development. *Developmental Biology*, 316, 160–170.
98. Scholey, J. M. (2008) Intraflagellar transport motors in cilia: moving along the cell’s antenna. *J Cell Biol*, 180, 23–29.
99. Silverman, M. A., and Leroux, M. R. (2009) Intraflagellar transport and the generation of dynamic, structurally and functionally diverse cilia. *Trends Cell Biol.*, 19, 306–316.
100. Vashishtha, M., Walther, Z., and Hall, J. L. (1996) The kinesin-homologous protein encoded by the *Chlamydomonas* FLA10 gene is associated with basal bodies and centrioles. *J. Cell. Sci.*, 109 ( Pt 3), 541–549.
101. Deane, J. A., Cole, D. G., Seeley, E. S., Diener, D. R., and Rosenbaum, J. L. (2001) Localization of intraflagellar transport protein IFT52 identifies basal body transitional fibers as the docking site for IFT particles. *Curr. Biol.*, 11, 1586–1590.

102. Baldari, C. T., and Rosenbaum, J. (2010) Intraflagellar transport: it's not just for cilia anymore. *Current Opinion in Cell Biology*, 22, 75–80.
103. Follit, J. A., Tuft, R. A., Fogarty, K. E., and Pazour, G. J. (2006) The intraflagellar transport protein IFT20 is associated with the Golgi complex and is required for cilia assembly. *Mol Biol Cell*, 17, 3781–92.
104. Rosenbaum, J. L., Moulder, J. E., and Ringo, D. L. (1969) FLAGELLAR ELONGATION AND SHORTENING IN CHLAMYDOMONAS The Use of Cycloheximide and Colchicine to Study the Synthesis and Assembly of Flagellar Proteins. *J Cell Biol*, 41, 600–619.
105. Qin, H., Diener, D. R., Geimer, S., Cole, D. G., and Rosenbaum, J. L. (2004) Intraflagellar transport (IFT) cargo: IFT transports flagellar precursors to the tip and turnover products to the cell body. *J. Cell Biol.*, 164, 255–266.
106. Reiter, J. F., and Mostov, K. (2006) Vesicle transport, cilium formation, and membrane specialization: the origins of a sensory organelle. *Proc. Natl. Acad. Sci. U.S.A.*, 103, 18383–18384.
107. Jékely, G., and Arendt, D. (2006) Evolution of intraflagellar transport from coated vesicles and autogenous origin of the eukaryotic cilium. *Bioessays*, 28, 191–198.
108. Jauregui, A. R., Nguyen, K. C. Q., Hall, D. H., and Barr, M. M. (2008) The *Caenorhabditis elegans* nephrocystins act as global modifiers of cilium structure. *J. Cell Biol*, 180, 973–988.
109. Williams, C. L., Li, C., Kida, K., Inglis, P. N., Mohan, S., Semenec, L., Bialas, N. J., Stupay, R. M., Chen, N., Blacque, O. E., Yoder, B. K., et al. (2011) MKS and NPHP modules cooperate to establish basal body/transition zone membrane associations and ciliary gate function during ciliogenesis. *J. Cell Biol*, 192, 1023–1041.
110. Omran, H. (2010) NPHP proteins: gatekeepers of the ciliary compartment. *J Cell Biol*, 190, 715–717.
111. Jiang, S.-T., Chiou, Y.-Y., Wang, E., Chien, Y.-L., Ho, H.-H., Tsai, F.-J., Lin, C.-Y., Tsai, S.-P., and Li, H. (2009) Essential role of nephrocystin in photoreceptor intraflagellar transport in mouse. *Hum Mol Genet*, 18, 1566–77.
112. Murga-Zamalloa, C. A., Desai, N. J., Hildebrandt, F., and Khanna, H. (2010) Interaction of ciliary disease protein retinitis pigmentosa GTPase regulator with nephronophthisis-associated proteins in mammalian retinas. *Mol. Vis.*, 16, 1373–1381.
113. Murga-Zamalloa, C. A., Atkins, S. J., Peranen, J., Swaroop, A., and Khanna, H. (2010) Interaction of retinitis pigmentosa GTPase regulator (RPGR) with RAB8A GTPase: implications for cilia dysfunction and photoreceptor degeneration. *Hum. Mol. Genet.*, 19, 3591–3598.
114. Singla, V., and Reiter, J. F. (2006) The primary cilium as the cell's antenna: signaling at a sensory organelle. *Science*, 313, 629–633.
115. Bronshtein, A. A., and Minor, A. V. (1977) [Regeneration of olfactory flagella and restoration of the electroolfactogram following application of triton X-100 to the olfactory mucosa of frogs]. *Tsitologiya*, 19, 33–39.

116. Menco, B. P. M. (2005) The fine-structural distribution of G-protein receptor kinase 3, beta-arrestin-2, Ca<sup>2+</sup>/calmodulin-dependent protein kinase II and phosphodiesterase PDE1C2, and a Cl(-)-cotransporter in rodent olfactory epithelia. *J. Neurocytol.*, 34, 11–36.
117. Krieger, J., Schleicher, S., Strotmann, J., Wanner, I., Boekhoff, I., Raming, K., De Geus, P., and Breer, H. (1994) Probing olfactory receptors with sequence-specific antibodies. *Eur. J. Biochem.*, 219, 829–835.
118. Ishikawa, H., and Marshall, W. F. (2011) Ciliogenesis: building the cell's antenna. *Nat. Rev. Mol. Cell Biol.*, 12, 222–234.
119. Marshall, W. F., and Nonaka, S. (2006) Cilia: tuning in to the cell's antenna. *Curr Biol*, 16, R604–14.
120. Händel, M., Schulz, S., Stanarius, A., Schreff, M., Erdtmann-Vourliotis, M., Schmidt, H., Wolf, G., and Höllt, V. (1999) Selective targeting of somatostatin receptor 3 to neuronal cilia. *Neuroscience*, 89, 909–926.
121. Brailov, I., Bancila, M., Brisorgueil, M. J., Miquel, M. C., Hamon, M., and Vergé, D. (2000) Localization of 5-HT(6) receptors at the plasma membrane of neuronal cilia in the rat brain. *Brain Res.*, 872, 271–275.
122. Shah, A. S., Ben-Shahar, Y., Moninger, T. O., Kline, J. N., and Welsh, M. J. (2009) Motile Cilia of Human Airway Epithelia Are Chemosensory. *Science*, 325, 1131–1134.
123. Bloodgood, R. A. (2010) Sensory reception is an attribute of both primary cilia and motile cilia. *J. Cell. Sci.*, 123, 505–509.
124. Huangfu, D., Liu, A., Rakeman, A. S., Murcia, N. S., Niswander, L., and Anderson, K. V. (2003) Hedgehog signalling in the mouse requires intraflagellar transport proteins. *Nature*, 426, 83–87.
125. Liu, A., Wang, B., and Niswander, L. A. (2005) Mouse intraflagellar transport proteins regulate both the activator and repressor functions of Gli transcription factors. *Development*, 132, 3103–3111.
126. Corbit, K. C., Aanstad, P., Singla, V., Norman, A. R., Stainier, D. Y. R., and Reiter, J. F. (2005) Vertebrate Smoothed functions at the primary cilium. *Nature*, 437, 1018–21.
127. Haycraft, C. J., Banizs, B., Aydin-Son, Y., Zhang, Q., Michaud, E. J., and Yoder, B. K. (2005) Gli2 and Gli3 localize to cilia and require the intraflagellar transport protein polaris for processing and function. *PLoS Genet.*, 1, e53.
128. Hu, Q., Milenkovic, L., Jin, H., Scott, M. P., Nachury, M. V., Spiliotis, E. T., and Nelson, W. J. (2010) A septin diffusion barrier at the base of the primary cilium maintains ciliary membrane protein distribution. *Science*, 329, 436–439.
129. Schneider, L., Clement, C. A., Teilmann, S. C., Pazour, G. J., Hoffmann, E. K., Satir, P., and Christensen, S. T. (2005) PDGFR $\alpha$  Signaling Is Regulated through the Primary Cilium in Fibroblasts. *Current Biology*, 15, 1861–1866.
130. Wong, S. T., Trinh, K., Hacker, B., Chan, G. C. K., Lowe, G., Gaggar, A., Xia, Z., Gold, G. H., and Storm, D. R. (2000) Disruption of the Type III Adenylyl Cyclase Gene Leads to Peripheral and Behavioral Anosmia in Transgenic Mice. *Neuron*, 27, 487–497.

131. Bishop, G. A., Berbari, N. F., Lewis, J., and Mykytyn, K. (2007) Type III adenylyl cyclase localizes to primary cilia throughout the adult mouse brain. *J. Comp. Neurol.*, 505, 562–571.
132. Praetorius, H. A., and Spring, K. R. (2001) Bending the MDCK cell primary cilium increases intracellular calcium. *J. Membr. Biol.*, 184, 71–79.
133. Schwartz, E. A., Leonard, M. L., Bizios, R., and Bowser, S. S. (1997) Analysis and modeling of the primary cilium bending response to fluid shear. *Am. J. Physiol.*, 272, F132–138.
134. Praetorius, H. A., Frøkiaer, J., and Leipziger, J. (2005) Transepithelial pressure pulses induce nucleotide release in polarized MDCK cells. *Am. J. Physiol. Renal Physiol.*, 288, F133–141.
135. Praetorius, H. A., and Spring, K. R. (2003) Removal of the MDCK cell primary cilium abolishes flow sensing. *J Membr Biol*, 191, 69–76.
136. Siroky, B. J., Ferguson, W. B., Fuson, A. L., Xie, Y., Fintha, A., Komlosi, P., Yoder, B. K., Schwiebert, E. M., Guay-Woodford, L. M., and Bell, P. D. (2006) Loss of primary cilia results in de-regulated and unabated apical calcium entry in ARPKD collecting duct cells. *Am. J. Physiol. Renal Physiol.*, 290, F1320–1328.
137. Hovater, M. B., Olteanu, D., Hanson, E. L., Cheng, N.-L., Siroky, B., Fintha, A., Komlosi, P., Liu, W., Satlin, L. M., Bell, P. D., Yoder, B. K., et al. (2008) Loss of apical monocilia on collecting duct principal cells impairs ATP secretion across the apical cell surface and ATP-dependent and flow-induced calcium signals. *Purinergic Signal.*, 4, 155–170.
138. Liu, W., Murcia, N. S., Duan, Y., Weinbaum, S., Yoder, B. K., Schwiebert, E., and Satlin, L. M. (2005) Mechanoregulation of intracellular Ca<sup>2+</sup> concentration is attenuated in collecting duct of monocilium-impaired orpk mice. *Am. J. Physiol. Renal Physiol.*, 289, F978–988.
139. Nauli, S. M., Alenghat, F. J., Luo, Y., Williams, E., Vassilev, P., Li, X., Elia, A. E. H., Lu, W., Brown, E. M., Quinn, S. J., Ingber, D. E., et al. (2003) Polycystins 1 and 2 mediate mechanosensation in the primary cilium of kidney cells. *Nat. Genet.*, 33, 129–137.
140. Nauli, S. M., Rossetti, S., Kolb, R. J., Alenghat, F. J., Consugar, M. B., Harris, P. C., Ingber, D. E., Loghman-Adham, M., and Zhou, J. (2006) Loss of polycystin-1 in human cyst-lining epithelia leads to ciliary dysfunction. *J. Am. Soc. Nephrol.*, 17, 1015–1025.
141. Hanaoka, K., Qian, F., Boletta, A., Bhunia, A. K., Piontek, K., Tsiokas, L., Sukhatme, V. P., Guggino, W. B., and Germino, G. G. (2000) Co-assembly of polycystin-1 and -2 produces unique cation-permeable currents. *Nature*, 408, 990–994.
142. Xu, C., Rossetti, S., Jiang, L., Harris, P. C., Brown-Glaberman, U., Wandinger-Ness, A., Bacallao, R., and Alper, S. L. (2007) Human ADPKD primary cyst epithelial cells with a novel, single codon deletion in the PKD1 gene exhibit defective ciliary polycystin localization and loss of flow-induced Ca<sup>2+</sup> signaling. *Am. J. Physiol. Renal Physiol.*, 292, F930–945.
143. Yamaguchi, T., Nagao, S., Wallace, D. P., Belibi, F. A., Cowley, B. D., Pelling, J. C., and Grantham, J. J. (2003) Cyclic AMP activates B-Raf and ERK in cyst epithelial cells from autosomal-dominant polycystic kidneys. *Kidney International*, 63, 1983–1994.
144. Yamaguchi, T., Wallace, D. P., Magenheimer, B. S., Hempson, S. J., Grantham, J. J., and Calvet, J. P. (2004) Calcium Restriction Allows cAMP Activation of the B-Raf/ERK Pathway, Switching Cells to a cAMP-dependent Growth-stimulated Phenotype. *J. Biol. Chem.*, 279, 40419–40430.

145. Shillingford, J. M., Murcia, N. S., Larson, C. H., Low, S. H., Hedgepeth, R., Brown, N., Flask, C. A., Novick, A. C., Goldfarb, D. A., Kramer-Zucker, A., Walz, G., et al. (2006) The mTOR pathway is regulated by polycystin-1, and its inhibition reverses renal cystogenesis in polycystic kidney disease. *PNAS*, 103, 5466–5471.
146. Fischer, D.-C., Jacoby, U., Pape, L., Ward, C. J., Kuwertz-Broeking, E., Renken, C., Nizze, H., Querfeld, U., Rudolph, B., Mueller-Wiefel, D. E., Bergmann, C., et al. (2009) Activation of the AKT/mTOR pathway in autosomal recessive polycystic kidney disease (ARPKD). *Nephrol. Dial. Transplant.*, 24, 1819–1827.
147. Walz, G., Budde, K., Mannaa, M., Nürnberger, J., Wanner, C., Sommerer, C., Kunzendorf, U., Banas, B., Hörl, W. H., Obermüller, N., Arns, W., et al. (2010) Everolimus in Patients with Autosomal Dominant Polycystic Kidney Disease. *New England Journal of Medicine*, 363, 830–840.
148. Serra, A. L., Poster, D., Kistler, A. D., Krauer, F., Raina, S., Young, J., Rentsch, K. M., Spanaus, K. S., Senn, O., Kristanto, P., Scheffel, H., et al. (2010) Sirolimus and kidney growth in autosomal dominant polycystic kidney disease. *N. Engl. J. Med.*, 363, 820–829.
149. Torres, V. E., Chapman, A. B., Devuyst, O., Gansevoort, R. T., Grantham, J. J., Higashihara, E., Perrone, R. D., Krasa, H. B., Ouyang, J., and Czerwiec, F. S. (2012) Tolvaptan in Patients with Autosomal Dominant Polycystic Kidney Disease. *N. Engl. J. Med.*,
150. Abdul-Majeed, S., and Nauli, S. M. (2011) Calcium-mediated mechanisms of cystic expansion. *Biochim. Biophys. Acta*, 1812, 1281–1290.
151. Hikasa, H., and Sokol, S. Y. (2012) Wnt Signaling in Vertebrate Axis Specification. *Cold Spring Harb Perspect Biol*, doi: 10.1101/cshperspect.a007955
152. Ulloa, F., and Martí, E. (2010) Wnt won the war: antagonistic role of Wnt over Shh controls dorso-ventral patterning of the vertebrate neural tube. *Dev. Dyn*, 239, 69–76.
153. Barker, N. (2008) The canonical Wnt/beta-catenin signalling pathway. *Methods Mol. Biol*, 468, 5–15.
154. Niehrs, C., and Acebron, S. P. (2012) Mitotic and mitogenic Wnt signalling. *The EMBO Journal*, 31, 2705–2713.
155. Clevers, H. (2006) Wnt/beta-catenin signaling in development and disease. *Cell*, 127, 469–80.
156. Clevers, H., and Nusse, R. (2012) Wnt/ $\beta$ -catenin signaling and disease. *Cell*, 149, 1192–1205.
157. MacDonald, B. T., Tamai, K., and He, X. (2009) Wnt/beta-catenin signaling: components, mechanisms, and diseases. *Dev. Cell*, 17, 9–26.
158. Saadi-Kheddouci, S., Berrebi, D., Romagnolo, B., Cluzeaud, F., Peuchmaur, M., Kahn, A., Vandewalle, A., and Perret, C. (2001) Early development of polycystic kidney disease in transgenic mice expressing an activated mutant of the beta-catenin gene. *Oncogene*, 20, 5972–5981.
159. Qian, C.-N., Knol, J., Igarashi, P., Lin, F., Zylstra, U., Teh, B. T., and Williams, B. O. (2005) Cystic renal neoplasia following conditional inactivation of *apc* in mouse renal tubular epithelium. *J. Biol. Chem*, 280, 3938–3945.

160. Marose, T. D., Merkel, C. E., McMahon, A. P., and Carroll, T. J. (2008) Beta-catenin is necessary to keep cells of ureteric bud/Wolffian duct epithelium in a precursor state. *Dev. Biol.*, 314, 112–126.
161. Pinson, K. I., Brennan, J., Monkley, S., Avery, B. J., and Skarnes, W. C. (2000) An LDL-receptor-related protein mediates Wnt signalling in mice. *Nature*, 407, 535–538.
162. Fischer, E., Legue, E., Doyen, A., Nato, F., Nicolas, J.-F., Torres, V., Yaniv, M., and Pontoglio, M. (2006) Defective planar cell polarity in polycystic kidney disease. *Nat. Genet.*, 38, 21–23.
163. Nishio, S., Tian, X., Gallagher, A. R., Yu, Z., Patel, V., Igarashi, P., and Somlo, S. (2010) Loss of oriented cell division does not initiate cyst formation. *J. Am. Soc. Nephrol.*, 21, 295–302.
164. Grumolato, L., Liu, G., Mong, P., Mudbhary, R., Biswas, R., Arroyave, R., Vijayakumar, S., Economides, A. N., and Aaronson, S. A. (2010) Canonical and noncanonical Wnts use a common mechanism to activate completely unrelated coreceptors. *Genes Dev.*, 24, 2517–2530.
165. Maye, P., Zheng, J., Li, L., and Wu, D. (2004) Multiple Mechanisms for Wnt11-mediated Repression of the Canonical Wnt Signaling Pathway. *J. Biol. Chem.*, 279, 24659–24665.
166. Kiefer, S. M., Robbins, L., and Rauchman, M. (2012) Conditional expression of wnt9b in six2-positive cells disrupts stomach and kidney function. *PLoS ONE*, 7, e43098.
167. Karner, C. M., Chirumamilla, R., Aoki, S., Igarashi, P., Wallingford, J. B., and Carroll, T. J. (2009) Wnt9b signaling regulates planar cell polarity and kidney tubule morphogenesis. *Nat. Genet.*, 41, 793–799.
168. Gerdes, J. M., and Katsanis, N. (2008) Ciliary function and wnt signal modulation. *Curr Top Dev Biol*, 85, 175–95.
169. Chien, A. J., Conrad, W. H., and Moon, R. T. (2009) A Wnt survival guide: from flies to human disease. *J. Invest. Dermatol.*, 129, 1614–1627.
170. Dale, T. (2006) Kinase cogs go forward and reverse in the Wnt signaling machine. *Nat. Struct. Mol. Biol.*, 13, 9–11.
171. Li, V. S. W., Ng, S. S., Boersema, P. J., Low, T. Y., Karthaus, W. R., Gerlach, J. P., Mohammed, S., Heck, A. J. R., Maurice, M. M., Mahmoudi, T., and Clevers, H. (2012) Wnt signaling through inhibition of  $\beta$ -catenin degradation in an intact Axin1 complex. *Cell*, 149, 1245–1256.
172. Gao, C., and Chen, Y.-G. (2010) Dishevelled: The hub of Wnt signaling. *Cell. Signal*, 22, 717–727.
173. Cliffe, A., Hamada, F., and Bienz, M. (2003) A role of Dishevelled in relocating Axin to the plasma membrane during wingless signaling. *Curr. Biol*, 13, 960–966.
174. Bilic, J., Huang, Y.-L., Davidson, G., Zimmermann, T., Cruciat, C.-M., Bienz, M., and Niehrs, C. (2007) Wnt induces LRP6 signalosomes and promotes dishevelled-dependent LRP6 phosphorylation. *Science*, 316, 1619–1622.
175. Kohn, A. D., and Moon, R. T. (2005) Wnt and calcium signaling: beta-catenin-independent pathways. *Cell Calcium*, 38, 439–446.

176. Sheldahl, L. C., Slusarski, D. C., Pandur, P., Miller, J. R., Kühl, M., and Moon, R. T. (2003) Dishevelled activates Ca<sup>2+</sup> flux, PKC, and CamKII in vertebrate embryos. *J Cell Biol*, 161, 769–777.
177. Miller, R. K., and McCrea, P. D. (2010) Wnt to build a tube: contributions of Wnt signaling to epithelial tubulogenesis. *Dev. Dyn*, 239, 77–93.
178. Simons, M., Gloy, J., Ganner, A., Bullerkotte, A., Bashkurov, M., Krönig, C., Schermer, B., Benzing, T., Cabello, O. A., Jenny, A., Mlodzik, M., et al. (2005) Inversin, the gene product mutated in nephronophthisis type II, functions as a molecular switch between Wnt signaling pathways. *Nat. Genet*, 37, 537–543.
179. Iglesias, D. M., Hueber, P.-A., Chu, L., Campbell, R., Patenaude, A.-M., Dziarmaga, A. J., Quinlan, J., Mohamed, O., Dufort, D., and Goodyer, P. R. (2007) Canonical WNT signaling during kidney development. *Am J Physiol Renal Physiol*, 293, F494–F500.
180. Sugiyama, N., Tsukiyama, T., Yamaguchi, T. P., and Yokoyama, T. (2011) The canonical Wnt signaling pathway is not involved in renal cyst development in the kidneys of inv mutant mice. *Kidney International*, 79, 957–965.
181. Bellavia, S., Dahan, K., Terryn, S., Cosyns, J.-P., Devuyst, O., and Pirson, Y. (2010) A homozygous mutation in INVS causing juvenile nephronophthisis with abnormal reactivity of the Wnt/beta-catenin pathway. *Nephrol. Dial. Transplant.*, 25, 4097–4102.
182. Corbit, K. C., Shyer, A. E., Dowdle, W. E., Gauden, J., Singla, V., Chen, M.-H., Chuang, P.-T., and Reiter, J. F. (2008) Kif3a constrains beta-catenin-dependent Wnt signalling through dual ciliary and non-ciliary mechanisms. *Nat Cell Biol*, 10, 70–6.
183. Ocbina, P. J. R., Tuson, M., and Anderson, K. V. (2009) Primary cilia are not required for normal canonical Wnt signaling in the mouse embryo. *PLoS ONE*, 4, e6839.
184. Lin, F., Hiesberger, T., Cordes, K., Sinclair, A. M., Goldstein, L. S. B., Somlo, S., and Igarashi, P. (2003) Kidney-specific inactivation of the KIF3A subunit of kinesin-II inhibits renal ciliogenesis and produces polycystic kidney disease. *Proc. Natl. Acad. Sci. U.S.A.*, 100, 5286–5291.
185. Huang, P., and Schier, A. F. (2009) Dampened Hedgehog signaling but normal Wnt signaling in zebrafish without cilia. *Development*, 136, 3089–3098.
186. Gerdes, J. M., Liu, Y., Zaghoul, N. A., Leitch, C. C., Lawson, S. S., Kato, M., Beachy, P. A., Beales, P. L., DeMartino, G. N., Fisher, S., Badano, J. L., et al. (2007) Disruption of the basal body compromises proteasomal function and perturbs intracellular Wnt response. *Nat Genet*, 39, 1350–60.
187. Happé, H., Leonhard, W. N., van der Wal, A., van de Water, B., Lantinga-van Leeuwen, I. S., Breuning, M. H., de Heer, E., and Peters, D. J. M. (2009) Toxic tubular injury in kidneys from Pkd1-deletion mice accelerates cystogenesis accompanied by dysregulated planar cell polarity and canonical Wnt signaling pathways. *Hum. Mol. Genet*, 18, 2532–2542.
188. Kim, I., Ding, T., Fu, Y., Li, C., Cui, L., Li, A., Lian, P., Liang, D., Wang, D. W., Guo, C., Ma, J., et al. (2009) Conditional mutation of Pkd2 causes cystogenesis and upregulates beta-catenin. *J. Am. Soc. Nephrol*, 20, 2556–2569.
189. Greer, Y. E., and Rubin, J. S. (2011) Casein kinase 1 delta functions at the centrosome to mediate Wnt-3a-dependent neurite outgrowth. *J. Cell Biol.*, 192, 993–1004.

190. Fumoto, K., Kadono, M., Izumi, N., and Kikuchi, A. (2009) Axin localizes to the centrosome and is involved in microtubule nucleation. *EMBO Rep*, 10, 606–613.
191. Wallingford, J. B., and Mitchell, B. (2011) Strange as it may seem: the many links between Wnt signaling, planar cell polarity, and cilia. *Genes Dev.*, 25, 201–213.
192. Bergmann, C., Fliegauf, M., Brüche, N. O., Frank, V., Olbrich, H., Kirschner, J., Schermer, B., Schmedding, I., Kispert, A., Kränzlin, B., Nürnberg, G., et al. (2008) Loss of nephrocystin-3 function can cause embryonic lethality, Meckel-Gruber-like syndrome, situs inversus, and renal-hepatic-pancreatic dysplasia. *Am. J. Hum. Genet.*, 82, 959–970.
193. Burcklé, C., Gaudé, H.-M., Vesque, C., Silbermann, F., Salomon, R., Jeanpierre, C., Antignac, C., Saunier, S., and Schneider-Maunoury, S. (2011) Control of the Wnt pathways by nephrocystin-4 is required for morphogenesis of the zebrafish pronephros. *Hum Mol Genet*, 20, 2611–2627.
194. Mahuzier, A., Gaudé, H.-M., Grampa, V., Anselme, I., Silbermann, F., Leroux-Berger, M., Delacour, D., Ezan, J., Montcouquiol, M., Saunier, S., Schneider-Maunoury, S., et al. (2012) Dishevelled stabilization by the ciliopathy protein Rpgrip11 is essential for planar cell polarity. *J Cell Biol*, 198, 927–940.
195. Kim, Y.-S., Kang, H. S., and Jetten, A. M. (2007) The Krüppel-like zinc finger protein Glis2 functions as a negative modulator of the Wnt/beta-catenin signaling pathway. *FEBS Lett*, 581, 858–64.
196. Panchenko, M. V., Zhou, M. I., and Cohen, H. T. (2004) von Hippel-Lindau partner Jade-1 is a transcriptional co-activator associated with histone acetyltransferase activity. *J Biol Chem*, 279, 56032–41.
197. Zhou, M. I., Wang, H., Ross, J. J., Kuzmin, I., Xu, C., and Cohen, H. T. (2002) The von Hippel-Lindau tumor suppressor stabilizes novel plant homeodomain protein Jade-1. *J Biol Chem*, 277, 39887–98.
198. Chitalia, V. C., Foy, R. L., Bachschmid, M. M., Zeng, L., Panchenko, M. V., Zhou, M. I., Bharti, A., Seldin, D. C., Lecker, S. H., Dominguez, I., and Cohen, H. T. (2008) Jade-1 inhibits Wnt signalling by ubiquitinating beta-catenin and mediates Wnt pathway inhibition by pVHL. *Nat Cell Biol*, 10, 1208–16.
199. Esteban, M. A., Harten, S. K., Tran, M. G., and Maxwell, P. H. (2006) Formation of primary cilia in the renal epithelium is regulated by the von Hippel-Lindau tumor suppressor protein. *J Am Soc Nephrol*, 17, 1801–6.
200. Schermer, B., Ghenoiu, C., Bartram, M., Müller, R. U., Kotsis, F., Höhne, M., Kühn, W., Rapka, M., Nitschke, R., Zentgraf, H., Fliegauf, M., et al. (2006) The von Hippel-Lindau tumor suppressor protein controls ciliogenesis by orienting microtubule growth. *J Cell Biol*, 175, 547–54.
201. Thoma, C. R., Frew, I. J., Hoerner, C. R., Montani, M., Moch, H., and Krek, W. (2007) pVHL and GSK3beta are components of a primary cilium-maintenance signalling network. *Nat Cell Biol*, 9, 588–95.
202. Elbashir, S. M., Harborth, J., Lendeckel, W., Yalcin, A., Weber, K., and Tuschl, T. (2001) Duplexes of 21-nucleotide RNAs mediate RNA interference in cultured mammalian cells. *Nature*, 411, 494–498.

203. Braman, J., Papworth, C., and Greener, A. (1996) Site-directed mutagenesis using double-stranded plasmid DNA templates. *Methods Mol. Biol.*, 57, 31–44.
204. Brody, J. R., and Kern, S. E. (2004) History and principles of conductive media for standard DNA electrophoresis. *Anal. Biochem.*, 333, 1–13.
205. Chen, I., and Dubnau, D. (2004) DNA uptake during bacterial transformation. *Nat. Rev. Microbiol.*, 2, 241–249.
206. Bertani, G. (2004) Lysogeny at Mid-Twentieth Century: P1, P2, and Other Experimental Systems. *J. Bacteriol.*, 186, 595–600.
207. Phelan, M. C. (2006) Techniques for mammalian cell tissue culture. *Curr Protoc Hum Genet*, Appendix 3, Appendix 3G.
208. Benzing, T., Gerke, P., Höpker, K., Hildebrandt, F., Kim, E., and Walz, G. (2001) Nephrocystin interacts with Pyk2, p130(Cas), and tensin and triggers phosphorylation of Pyk2. *Proc. Natl. Acad. Sci. U.S.A.*, 98, 9784–9789.
209. Schermer, B., Höpker, K., Omran, H., Ghenoiu, C., Fliegau, M., Fekete, A., Horvath, J., Köttgen, M., Hackl, M., Zschiedrich, S., Huber, T. B., et al. (2005) Phosphorylation by casein kinase 2 induces PACS-1 binding of nephrocystin and targeting to cilia. *EMBO J*, 24, 4415–24.
210. Rosenberg, I. M. (2004) *Protein Analysis and Purification: Benchtop Techniques*, (2<sup>nd</sup> ed). Birkhäuser, Boston.
211. Haaijman, J. J. (1988) Immunofluorescence: quantitative considerations. *Acta Histochem. Suppl.*, 35, 77–83.
212. Gould, S. J., and Subramani, S. (1988) Firefly luciferase as a tool in molecular and cell biology. *Analytical Biochemistry*, 175, 5–13.
213. Chomczynski, P., and Sacchi, N. (1987) Single-step method of RNA isolation by acid guanidinium thiocyanate-phenol-chloroform extraction. *Anal. Biochem.*, 162, 156–159.
214. Nasevicius, A., and Ekker, S. C. (2000) Effective targeted gene ‘knockdown’ in zebrafish. *Nature Genetics*, 26, 216–220.
215. Lillie, R. D., and Fullmer, H. M. (1976) *Histopathologic Technique and Practical Histochemistry* (4th ed). McGraw-Hill Book Co., New York.
216. Rinschen, M. M., Yu, M.-J., Wang, G., Boja, E. S., Hoffert, J. D., Pisitkun, T., and Knepper, M. A. (2010) Quantitative phosphoproteomic analysis reveals vasopressin V2-receptor-dependent signaling pathways in renal collecting duct cells. *Proc Natl Acad Sci U S A*, 107, 3882–3887.
217. Wiens, C. J., Tong, Y., Esmail, M. A., Oh, E., Gerdes, J. M., Wang, J., Tempel, W., Rattner, J. B., Katsanis, N., Park, H.-W., and Leroux, M. R. (2010) Bardet-Biedl syndrome-associated small GTPase ARL6 (BBS3) functions at or near the ciliary gate and modulates Wnt signaling. *J. Biol. Chem*, 285, 16218–16230.
218. Borgal, L., Habbig, S., Hatzold, J., Liebau, M. C., Dafinger, C., Sacarea, I., Hammerschmidt, M., Benzing, T., and Schermer, B. (2012) The ciliary protein nephrocystin-4 translocates the

- canonical Wnt regulator Jade-1 to the nucleus to negatively regulate  $\beta$ -catenin signaling. *J. Biol. Chem.*, 287, 25370–25380.
219. Drummond, I. A. (2005) Kidney development and disease in the zebrafish. *J. Am. Soc. Nephrol*, 16, 299–304.
220. Drummond, I. A., and Davidson, A. J. (2010) Zebrafish kidney development. *Methods Cell Biol*, 100, 233–260.
221. Slanchev, K., Pütz, M., Schmitt, A., Kramer-Zucker, A., and Walz, G. (2011) Nephrocystin-4 is required for pronephric duct-dependent cloaca formation in zebrafish. *Hum Mol Genet*, 20, 3119–3128.
222. DiBella, L. M., Park, A., and Sun, Z. (2009) Zebrafish Tsc1 reveals functional interactions between the cilium and the TOR pathway. *Hum. Mol. Genet.*, 18, 595–606.
223. Sun, Z., Amsterdam, A., Pazour, G. J., Cole, D. G., Miller, M. S., and Hopkins, N. (2004) A genetic screen in zebrafish identifies cilia genes as a principal cause of cystic kidney. *Development*, 131, 4085–4093.
224. Drummond, I. A., Majumdar, A., Hentschel, H., Elger, M., Solnica-Krezel, L., Schier, A. F., Neuhaus, S. C., Stemple, D. L., Zwartkruis, F., Rangini, Z., Driever, W., et al. (1998) Early development of the zebrafish pronephros and analysis of mutations affecting pronephric function. *Development*, 125, 4655–4667.
225. Marin, O., Bustos, V. H., Cesaro, L., Meggio, F., Pagano, M. A., Antonelli, M., Allende, C. C., Pinna, L. A., and Allende, J. E. (2003) A noncanonical sequence phosphorylated by casein kinase 1 in beta-catenin may play a role in casein kinase 1 targeting of important signaling proteins. *Proc. Natl. Acad. Sci. U.S.A*, 100, 10193–10200.
226. Pulgar, V., Marin, O., Meggio, F., Allende, C. C., Allende, J. E., and Pinna, L. A. (1999) Optimal sequences for non-phosphate-directed phosphorylation by protein kinase CK1 (casein kinase-1)--a re-evaluation. *Eur. J. Biochem.*, 260, 520–526.
227. Olsen, J. V., Blagoev, B., Gnad, F., Macek, B., Kumar, C., Mortensen, P., and Mann, M. (2006) Global, in vivo, and site-specific phosphorylation dynamics in signaling networks. *Cell*, 127, 635–648.
228. Cantin, G. T., Yi, W., Lu, B., Park, S. K., Xu, T., Lee, J.-D., and Yates, J. R. (2008) Combining protein-based IMAC, peptide-based IMAC, and MudPIT for efficient phosphoproteomic analysis. *J. Proteome Res*, 7, 1346–1351.
229. Gao, Z.-H., Seeling, J. M., Hill, V., Yochum, A., and Virshup, D. M. (2002) Casein kinase I phosphorylates and destabilizes the beta-catenin degradation complex. *Proc. Natl. Acad. Sci. U.S.A.*, 99, 1182–1187.
230. Peters, J. M., McKay, R. M., McKay, J. P., and Graff, J. M. (1999) Casein kinase I transduces Wnt signals. *Nature*, 401, 345–350.
231. Elia, A. E. H., Rellos, P., Haire, L. F., Chao, J. W., Ivins, F. J., Hoepker, K., Mohammad, D., Cantley, L. C., Smerdon, S. J., and Yaffe, M. B. (2003) The molecular basis for phosphodependent substrate targeting and regulation of Plks by the Polo-box domain. *Cell*, 115, 83–95.

232. Otto, E. A., Schermer, B., Obara, T., O'Toole, J. F., Hiller, K. S., Mueller, A. M., Ruf, R. G., Hoefele, J., Beekmann, F., Landau, D., Foreman, J. W., et al. (2003) Mutations in *INVS* encoding inversin cause nephronophthisis type 2, linking renal cystic disease to the function of primary cilia and left-right axis determination. *Nat. Genet.*, 34, 413–420.
233. Mollet, G., Silbermann, F., Delous, M., Salomon, R., Antignac, C., and Saunier, S. (2005) Characterization of the nephrocystin/nephrocystin-4 complex and subcellular localization of nephrocystin-4 to primary cilia and centrosomes. *Hum. Mol. Genet.*, 14, 645–656.
234. Olbrich, H., Fliegau, M., Hoefele, J., Kispert, A., Otto, E., Volz, A., Wolf, M. T., Sasmaz, G., Trauer, U., Reinhardt, R., Sudbrak, R., et al. (2003) Mutations in a novel gene, *NPHP3*, cause adolescent nephronophthisis, tapeto-retinal degeneration and hepatic fibrosis. *Nat. Genet.*, 34, 455–459.
235. Huang, P., Senga, T., and Hamaguchi, M. (2007) A novel role of phospho-beta-catenin in microtubule regrowth at centrosome. *Oncogene*, 26, 4357–4371.
236. Bryja, V., Schulte, G., and Arenas, E. (2007) Wnt-3a utilizes a novel low dose and rapid pathway that does not require casein kinase 1-mediated phosphorylation of Dvl to activate beta-catenin. *Cell. Signal*, 19, 610–616.
237. Okamura, H., Garcia-Rodriguez, C., Martinson, H., Qin, J., Virshup, D. M., and Rao, A. (2004) A conserved docking motif for CK1 binding controls the nuclear localization of NFAT1. *Mol. Cell. Biol.*, 24, 4184–4195.
238. Ferrarese, A., Marin, O., Bustos, V. H., Venerando, A., Antonelli, M., Allende, J. E., and Pinna, L. A. (2007) Chemical dissection of the APC Repeat 3 multistep phosphorylation by the concerted action of protein kinases CK1 and GSK3. *Biochemistry*, 46, 11902–11910.
239. Burzio, V., Antonelli, M., Allende, C. C., and Allende, J. E. (2002) Biochemical and cellular characteristics of the four splice variants of protein kinase CK1alpha from zebrafish (*Danio rerio*). *J. Cell. Biochem.*, 86, 805–814.
240. Willert, K., and Jones, K. A. (2006) Wnt signaling: is the party in the nucleus? *Genes Dev.*, 20, 1394–1404.
241. Zeng, X., Tamai, K., Doble, B., Li, S., Huang, H., Habas, R., Okamura, H., Woodgett, J., and He, X. (2005) A dual-kinase mechanism for Wnt co-receptor phosphorylation and activation. *Nature*, 438, 873–877.
242. Del Valle-Pérez, B., Arqués, O., Vinyoles, M., de Herreros, A. G., and Duñach, M. (2011) Coordinated action of CK1 isoforms in canonical Wnt signaling. *Mol. Cell. Biol.*, 31, 2877–2888.
243. Goentoro, L., and Kirschner, M. W. (2009) Evidence that fold-change, and not absolute level, of beta-catenin dictates Wnt signaling. *Mol. Cell*, 36, 872–884.
244. Niida, A., Hiroko, T., Kasai, M., Furukawa, Y., Nakamura, Y., Suzuki, Y., Sugano, S., and Akiyama, T. (2004) *DKK1*, a negative regulator of Wnt signaling, is a target of the beta-catenin/TCF pathway. *Oncogene*, 23, 8520–8526.
245. González-Sancho, J. M., Aguilera, O., García, J. M., Pendás-Franco, N., Peña, C., Cal, S., García de Herreros, A., Bonilla, F., and Muñoz, A. (2005) The Wnt antagonist *DICKKOPF-1* gene is a downstream target of beta-catenin/TCF and is downregulated in human colon cancer. *Oncogene*, 24, 1098–1103.

246. Lustig, B., Jerchow, B., Sachs, M., Weiler, S., Pietsch, T., Karsten, U., van de Wetering, M., Clevers, H., Schlag, P. M., Birchmeier, W., and Behrens, J. (2002) Negative feedback loop of Wnt signaling through upregulation of conductin/axin2 in colorectal and liver tumors. *Mol. Cell. Biol.*, 22, 1184–1193.
247. Jho, E., Zhang, T., Domon, C., Joo, C.-K., Freund, J.-N., and Costantini, F. (2002) Wnt/beta-catenin/Tcf signaling induces the transcription of Axin2, a negative regulator of the signaling pathway. *Mol. Cell. Biol.*, 22, 1172–1183.
248. Ha, N.-C., Tonzuka, T., Stamos, J. L., Choi, H.-J., and Weis, W. I. (2004) Mechanism of phosphorylation-dependent binding of APC to beta-catenin and its role in beta-catenin degradation. *Mol. Cell.*, 15, 511–521.
249. Valenta, T., Hausmann, G., and Basler, K. (2012) The many faces and functions of  $\beta$ -catenin. *The EMBO Journal*, 31, 2714–2736.
250. Jamieson, C., Sharma, M., and Henderson, B. R. (2012) Wnt signaling from membrane to nucleus:  $\beta$ -catenin caught in a loop. *Int. J. Biochem. Cell Biol.*, 44, 847–850.
251. Park, J.-S., Valerius, M. T., and McMahon, A. P. (2007) Wnt/beta-catenin signaling regulates nephron induction during mouse kidney development. *Development*, 134, 2533–2539.
252. Carroll, T. J., Park, J.-S., Hayashi, S., Majumdar, A., and McMahon, A. P. (2005) Wnt9b plays a central role in the regulation of mesenchymal to epithelial transitions underlying organogenesis of the mammalian urogenital system. *Dev. Cell*, 9, 283–292.
253. Stark, K., Vainio, S., Vassileva, G., and McMahon, A. P. (1994) Epithelial transformation of metanephric mesenchyme in the developing kidney regulated by Wnt-4. *Nature*, 372, 679–683.
254. Schmidt-Ott, K. M., and Barasch, J. (2008) WNT/beta-catenin signaling in nephron progenitors and their epithelial progeny. *Kidney Int.*, 74, 1004–1008.
255. Piontek, K., Menezes, L. F., Garcia-Gonzalez, M. A., Huso, D. L., and Germino, G. G. (2007) A critical developmental switch defines the kinetics of kidney cyst formation after loss of Pkd1. *Nat. Med.*, 13, 1490–1495.
256. Carroll, T. J., and Das, A. (2011) Planar cell polarity in kidney development and disease. *Organogenesis*, 7, 180–190.
257. Saburi, S., Hester, I., Fischer, E., Pontoglio, M., Eremina, V., Gessler, M., Quaggin, S. E., Harrison, R., Mount, R., and McNeill, H. (2008) Loss of Fat4 disrupts PCP signaling and oriented cell division and leads to cystic kidney disease. *Nat. Genet.*, 40, 1010–1015.
258. Bonnet, C. S., Aldred, M., von Ruhland, C., Harris, R., Sandford, R., and Cheadle, J. P. (2009) Defects in cell polarity underlie TSC and ADPKD-associated cystogenesis. *Hum. Mol. Genet.*, 18, 2166–2176.
259. Luyten, A., Su, X., Gondela, S., Chen, Y., Rompani, S., Takakura, A., and Zhou, J. (2010) Aberrant regulation of planar cell polarity in polycystic kidney disease. *J. Am. Soc. Nephrol.*, 21, 1521–1532.
260. Weimbs, T. (2006) Regulation of mTOR by Polycystin-1: is Polycystic Kidney Disease a Case of Futile Repair? *Cell Cycle*, 5, 2425–2429.

261. Lancaster, M. A., and Gleeson, J. G. (2010) Cystic kidney disease: the role of Wnt signaling. *Trends Mol Med*, 16, 349–360.
262. Takakura, A., Contrino, L., Zhou, X., Bonventre, J. V., Sun, Y., Humphreys, B. D., and Zhou, J. (2009) Renal injury is a third hit promoting rapid development of adult polycystic kidney disease. *Hum. Mol. Genet.*, 18, 2523–2531.
263. Lancaster, M. A., Louie, C. M., Silhavy, J. L., Sintasath, L., Decambre, M., Nigam, S. K., Willert, K., and Gleeson, J. G. (2009) Impaired Wnt-beta-catenin signaling disrupts adult renal homeostasis and leads to cystic kidney ciliopathy. *Nat. Med.*, 15, 1046–1054.
264. Ishibe, S., and Cantley, L. G. (2008) Epithelial-mesenchymal-epithelial cycling in kidney repair. *Curr. Opin. Nephrol. Hypertens*, 17, 379–385.
265. Humphreys, B. D., Valerius, M. T., Kobayashi, A., Mugford, J. W., Soeung, S., Duffield, J. S., McMahon, A. P., and Bonventre, J. V. (2008) Intrinsic epithelial cells repair the kidney after injury. *Cell Stem Cell*, 2, 284–291.
266. Humphreys, B. D., Lin, S.-L., Kobayashi, A., Hudson, T. E., Nowlin, B. T., Bonventre, J. V., Valerius, M. T., McMahon, A. P., and Duffield, J. S. (2010) Fate tracing reveals the pericyte and not epithelial origin of myofibroblasts in kidney fibrosis. *Am. J. Pathol.*, 176, 85–97.
267. Surendran, K., Schiavi, S., and Hruska, K. A. (2005) Wnt-dependent beta-catenin signaling is activated after unilateral ureteral obstruction, and recombinant secreted frizzled-related protein 4 alters the progression of renal fibrosis. *J. Am. Soc. Nephrol*, 16, 2373–2384.
268. Hermens, J.-S., Thelen, P., Ringert, R.-H., and Seseke, F. (2007) Alterations of selected genes of the Wnt signal chain in rat kidneys with spontaneous congenital obstructive uropathy. *J Pediatr Urol*, 3, 86–95.
269. Terada, Y., Tanaka, H., Okado, T., Shimamura, H., Inoshita, S., Kuwahara, M., and Sasaki, S. (2003) Expression and function of the developmental gene Wnt-4 during experimental acute renal failure in rats. *J. Am. Soc. Nephrol.*, 14, 1223–1233.
270. Li, L., Zepeda-Orozco, D., Patel, V., Truong, P., Karner, C. M., Carroll, T. J., and Lin, F. (2009) Aberrant planar cell polarity induced by urinary tract obstruction. *Am. J. Physiol. Renal Physiol.*, 297, F1526–1533.
271. Patel, V., Li, L., Cobo-Stark, P., Shao, X., Somlo, S., Lin, F., and Igarashi, P. (2008) Acute kidney injury and aberrant planar cell polarity induce cyst formation in mice lacking renal cilia. *Hum. Mol. Genet.*, 17, 1578–1590.
272. Lin, S.-L., Li, B., Rao, S., Yeo, E.-J., Hudson, T. E., Nowlin, B. T., Pei, H., Chen, L., Zheng, J. J., Carroll, T. J., Pollard, J. W., et al. (2010) Macrophage Wnt7b is critical for kidney repair and regeneration. *Proc. Natl. Acad. Sci. U.S.A.*, 107, 4194–4199.
273. Lancaster, M. A., Schroth, J., and Gleeson, J. G. (2011) Subcellular spatial regulation of canonical Wnt signalling at the primary cilium. *Nat. Cell Biol*, 13, 702–709.
274. Foy, R. L., Chitalia, V. C., Panchenko, M. V., Zeng, L., Lopez, D., Lee, J. W., Rana, S. V., Boletta, A., Qian, F., Tsiokas, L., Piontek, K. B., et al. (2012) Polycystin-1 regulates the stability and ubiquitination of transcription factor Jade-1. *Hum. Mol. Genet.*,

275. Wang, L., Weidenfeld, R., Verghese, E., Ricardo, S. D., and Deane, J. A. (2008) Alterations in renal cilium length during transient complete ureteral obstruction in the mouse. *J Anat*, 213, 79–85.
276. Verghese, E., Weidenfeld, R., Bertram, J. F., Ricardo, S. D., and Deane, J. A. (2008) Renal cilia display length alterations following tubular injury and are present early in epithelial repair. *Nephrol. Dial. Transplant.*, 23, 834–841.
277. Gwak, J., Cho, M., Gong, S.-J., Won, J., Kim, D.-E., Kim, E.-Y., Lee, S. S., Kim, M., Kim, T. K., Shin, J.-G., and Oh, S. (2006) Protein-kinase-C-mediated  $\beta$ -catenin phosphorylation negatively regulates the Wnt/ $\beta$ -catenin pathway. *J Cell Sci*, 119, 4702–4709.
278. Valencia, L., Bidet, M., Martial, S., Sanchez, E., Melendez, E., Tauc, M., Poujeol, C., Martin, D., Namorado, M. D. C., Reyes, J. L., and Poujeol, P. (2001) Nifedipine-activated  $\text{Ca}^{2+}$  permeability in newborn rat cortical collecting duct cells in primary culture. *Am J Physiol Cell Physiol*, 280, C1193–C1203.
279. Price, V. R., Reed, C. A., Lieberthal, W., and Schwartz, J. H. (2002) ATP depletion of tubular cells causes dissociation of the zonula adherens and nuclear translocation of beta-catenin and LEF-1. *J. Am. Soc. Nephrol*, 13, 1152–1161.
280. Boggiano, J. C., and Fehon, R. G. (2012) Growth control by committee: intercellular junctions, cell polarity, and the cytoskeleton regulate Hippo signaling. *Dev. Cell*, 22, 695–702.
281. Sopko, R., and McNeill, H. (2009) The skinny on Fat: an enormous cadherin that regulates cell adhesion, tissue growth, and planar cell polarity. *Curr. Opin. Cell Biol.*, 21, 717–723.
282. Varelas, X., Miller, B. W., Sopko, R., Song, S., Gregorieff, A., Fellouse, F. A., Sakuma, R., Pawson, T., Hunziker, W., McNeill, H., Wrana, J. L., et al. (2010) The Hippo pathway regulates Wnt/beta-catenin signaling. *Dev. Cell*, 18, 579–591.
283. Imajo, M., Miyatake, K., Iimura, A., Miyamoto, A., and Nishida, E. (2012) A molecular mechanism that links Hippo signalling to the inhibition of Wnt/ $\beta$ -catenin signalling. *The EMBO Journal*,
284. Joannidis, M., Spokes, K., Nakamura, T., Faletto, D., and Cantley, L. G. (1994) Regional expression of hepatocyte growth factor/c-met in experimental renal hypertrophy and hyperplasia. *Am. J. Physiol*, 267, F231–236.
285. Monga, S. P. S., Mars, W. M., Padiaditakis, P., Bell, A., Mulé, K., Bowen, W. C., Wang, X., Zarnegar, R., and Michalopoulos, G. K. (2002) Hepatocyte growth factor induces Wnt-independent nuclear translocation of beta-catenin after Met-beta-catenin dissociation in hepatocytes. *Cancer Res*, 62, 2064–2071.
286. Shin, K., Lee, J., Guo, N., Kim, J., Lim, A., Qu, L., Mysorekar, I. U., and Beachy, P. A. (2011) Hedgehog/Wnt feedback supports regenerative proliferation of epithelial stem cells in bladder. *Nature*, 472, 110–114.
287. Yang, L., Besschetnova, T. Y., Brooks, C. R., Shah, J. V., and Bonventre, J. V. (2010) Epithelial cell cycle arrest in G2/M mediates kidney fibrosis after injury. *Nat. Med*, 16, 535–543, 1p following 143.
288. Ishibe, S., Haydu, J. E., Togawa, A., Marlier, A., and Cantley, L. G. (2006) Cell Confluence Regulates Hepatocyte Growth Factor-Stimulated Cell Morphogenesis in a  $\beta$ -Catenin-Dependent Manner. *Mol Cell Biol*, 26, 9232–9243.

289. Bryant, D. M., and Stow, J. L. (2004) The ins and outs of E-cadherin trafficking. *Trends in Cell Biology*, 14, 427–434.
290. Noles, S. R., and Chenn, A. (2007) Cadherin inhibition of beta-catenin signaling regulates the proliferation and differentiation of neural precursor cells. *Mol. Cell. Neurosci.*, 35, 549–558.
291. Sasaki, C. Y., Lin, H., Morin, P. J., and Longo, D. L. (2000) Truncation of the extracellular region abrogates cell contact but retains the growth-suppressive activity of E-cadherin. *Cancer Res.*, 60, 7057–7065.
292. Kim, N.-G., Koh, E., Chen, X., and Gumbiner, B. M. (2011) E-cadherin mediates contact inhibition of proliferation through Hippo signaling-pathway components. *Proc Natl Acad Sci U S A*, 108, 11930–11935.
293. Zhou, L., Ercolano, E., Ammoun, S., Schmid, M. C., Barczyk, M. A., and Hanemann, C. O. (2011) Merlin-deficient human tumors show loss of contact inhibition and activation of Wnt/ $\beta$ -catenin signaling linked to the PDGFR/Src and Rac/PAK pathways. *Neoplasia*, 13, 1101–1112.
294. Bosco, E. E., Nakai, Y., Hennigan, R. F., Ratner, N., and Zheng, Y. (2010) NF2-deficient cells depend on the Rac1-canonical Wnt signaling pathway to promote the loss of contact inhibition of proliferation. *Oncogene*, 29, 2540–2549.
295. Jonassen, J. A., Agustin, J. S., Follit, J. A., and Pazour, G. J. (2008) Deletion of IFT20 in the mouse kidney causes misorientation of the mitotic spindle and cystic kidney disease. *J Cell Biol*, 183, 377–384.
296. Delous, M., Hellman, N. E., Gaudé, H.-M., Silbermann, F., Le Bivic, A., Salomon, R., Antignac, C., and Saunier, S. (2009) Nephrocystin-1 and nephrocystin-4 are required for epithelial morphogenesis and associate with PALS1/PATJ and Par6. *Hum. Mol. Genet*, 18, 4711–4723.
297. Brockman, J. L., Gross, S. D., Sussman, M. R., and Anderson, R. A. (1992) Cell cycle-dependent localization of casein kinase I to mitotic spindles. *PNAS*, 89, 9454–9458.
298. Seeger-Nukpezah, T., Liebau, M. C., Höpker, K., Lamkemeyer, T., Benzing, T., Golemis, E. A., and Schermer, B. (2012) The centrosomal kinase Plk1 localizes to the transition zone of primary cilia and induces phosphorylation of nephrocystin-1. *PLoS ONE*, 7, e38838.
299. Lee, K. H., Johmura, Y., Yu, L.-R., Park, J.-E., Gao, Y., Bang, J. K., Zhou, M., Veenstra, T. D., Yeon Kim, B., and Lee, K. S. (2012) Identification of a novel Wnt5a-CK1 $\epsilon$ -Dvl2-Plk1-mediated primary cilia disassembly pathway. *EMBO J.*, 31, 3104–3117.
300. Kikuchi, K., Niikura, Y., Kitagawa, K., and Kikuchi, A. (2010) Dishevelled, a Wnt signalling component, is involved in mitotic progression in cooperation with Plk1. *EMBO J.*, 29, 3470–3483.

## 10 ACKNOWLEDGEMENTS

I would like to gratefully acknowledge all those who have helped me achieve this goal. First and foremost, I would like to thank Priv-Doz. Dr. Bernhard Schermer for inspiring me to begin my research in ciliary biology. Your constant enthusiasm, encouragement, and expertise are invaluable. I am also grateful for the encouragement of Prof. Dr. Thomas Benzing, whose wealth of experience and wisdom provided a solid direction through the course of my work. I would like to thank Prof. Dr. Michael Melkonian and Priv-Doz. Dr. Roman Thomas, for your time and your insight during our Thesis Committee Meetings, and thank in advance Prof. Dr. Günter Schwarz and Dr. Leonie Kokkelink for their time and effort in their respective roles as Chair and Assessor during my oral thesis defense.

I am grateful for the collaborations held with Dr. Sandra Habbig, Dr. Julia Hatzold, and Prof. Dr. Matthias Hammerschmidt, as well as Dr. Markus Rinschen and Dr. Tobias Lamkemeyer, without all of whom the research pertaining to zebrafish and mass spectrometry would not have been possible.

I extend my gratitude to Prof. Dr. Stefan Herzig and Dr. Marion Rozowski for the guidance and support I have received from the Graduate Program in Pharmacology and Experimental Therapeutics.

I would like to thank and acknowledge each team member of the Nephrolab Cologne for all discussions and encouragement. I would particularly like to acknowledge my office-mates Claudia Dafinger, Sybille Köhler, and Dr. Linus Völker for many technical discussions, constant encouragement and „navigational“ solutions.

Finally, a very warm thank you to my parents, George & Shirley Borgal, for their love and support in all I do, and to my fiancé Richard Vout, for never wavering in his encouragement and patience.

## 11 ERKLÄRUNG

Ich versichere, dass ich die von mir vorgelegte Dissertation selbständig angefertigt, die benutzten Quellen und Hilfsmittel vollständig angegeben und die Stellen der Arbeit – einschließlich Tabellen, Karten und Abbildung –, die anderen Werken im Wortlaut oder dem Sinn nach entnommen sind, in jedem Einzelfall als Entlehnung kenntlich gemacht habe; dass diese Dissertation noch keiner anderen Fakultät oder Universität zur Prüfung vorgelegen hat; dass sie – abgesehen von unten angegebenen Teilpublikationen – noch nicht veröffentlicht worden ist sowie, dass ich eine solche Veröffentlichung vor Abschluss des Promotionsverfahrens nicht vornehmen werde. Die Bestimmungen der Promotionsordnung sind mir bekannt. Die von mir vorgelegte Dissertation ist von Prof. Dr. rer. Nat. Michael Melkonian, Prof. Dr. Thomas Benzing, und Priv-Doz. Dr. med. Bernhard Schermer betreut worden.

Lori Borgal,      Köln den 19.11.2012

## 12 CURRICULUM VITAE

### Persönliche Angaben

Name: Borgal  
Vorname: Lori  
Geboren: 01.04.1981 in Halifax, Canada  
Nationalität: Canadian / Kanadische

### Promotion

Jan 2009-Jan 2013      Promotion an der Universität zu Köln  
  
Internationales Graduiertenprogramm in Pharmakologie und  
Experimenteller Therapeutika, Universität zu Köln  
  
Titel der Dissertation: Wnt Regulation in Cystic Kidney  
Diseases: Roles for Jade-1, NPHP4, and CK1 $\alpha$ .  
  
Betreuer: Prof.Dr. Michael Melkonian; Prof. Dr. Thomas  
Benzing; Priv-Doz. Dr. Bernhard Schermer

### Akademische Ausbildung

09/2004-09/2006      Master of Science, Dalhousie University, Halifax Canada  
  
Titel der Masterarbeit: Combined Effects of Rehabilitation and  
Neurotrophic Environment on Graft Function in the  
Hemiparkinsonian Rat Model.  
  
Betreuer: Dr. Ivar Mendez  
  
09/1999-09/2003      Bachelor of Science, Dalhousie University, Halifax Canada  
  
Titel der Bachelorarbeit: Complex Sensorimotor Recovery of 6-  
OHDA Lesioned Hemiparkinsonian Rats with Low Dose  
Intrastriatal FVM Grafts  
  
Betreuer: Dr. Ivar Mendez

### Schulische Ausbildung

09/1996-06/1999      Queen Elizabeth High School, Halifax Canada  
09/1986-06/1996      Oxford Elementary & Junior High School, Halifax Canada